



A University of Sussex PhD thesis

Available online via Sussex Research Online:

<http://sro.sussex.ac.uk/>

This thesis is protected by copyright which belongs to the author.

This thesis cannot be reproduced or quoted extensively from without first obtaining permission in writing from the Author

The content must not be changed in any way or sold commercially in any format or medium without the formal permission of the Author

When referring to this work, full bibliographic details including the author, title, awarding institution and date of the thesis must be given

Please visit Sussex Research Online for more information and further details

Biological Evaluation of Ferrocene Derivatives



Supojjane Sansook

Supervisor Prof John Spencer

Submitted to the University of Sussex in part fulfilment of the requirements
of the degree of Doctor of Philosophy

March 2017

Declaration

I hereby declare that this thesis is my own work and effort and that it has not been submitted anywhere for any award of another degree. I also undertake that any quotation or paraphrase from the published work of other people has been acknowledged. This work was supervised by Prof John Spencer.

Supojjane Sansook

Acknowledgements

Firstly, I would like to express my sincere thankfulness to my advisor Prof John Spencer for the continuous support of my Ph.D. study, for his encouragement, patience, motivation, guidance and enormous knowledge. His supervision helped me all the time of research and writing of my thesis.

I am very grateful to my 2nd supervisor, Dr. Hazel Cox for useful discussions and her kindness in this research. I would like to also thank Dr. Cory A. Ocasio (Tony) for conducting the biological data and docking study assistance.

I am grateful to my lab colleagues Rhiannon Jones, Jose Gascon, Adam Close, Gavin Roffe, Raysa Khan, Melvyn Ansell, Ella Lineham, Arathy Jose, Mohammad Baqer and Bradley Springett, for their encouragement and helpful suggestion in this research. I would like to thank all of my friends in Sussex for their support and enjoyable time here including Pop, Natt, Mai, Kom, Tik, Por, Yoo, Eak, Toey, Tae, Priow, Bond, Aom, Andy Siska, Colleen, Amber, Troy, Kristen, Tyler, Irene, Hayley, Jess, Katie, Dan, Dave and Tom.

I would like to acknowledge Dr. Alla. K. Abdul-Sada for carrying out all of the mass spectrometry. Dr. Iain. J. Day for his assistance in the use of NMR spectrometers. Dr. G. J. Tizzard (the NCS UK National Crystallography Service, University of Southampton) for carrying out all X-Ray crystallographic measurements. The EPSRC National Mass Spectrometry Service of the University of Swansea. Dr. Stephen Boyer (the Elemental Analysis service at the London Metropolitan University) for the completion of all elemental analyses, as well as our collaborations Prof .Régis Millet from Lille France, Prof Claudio Luparello from Italy and Prof. James E. Bradner from USA.

I would like to thanks staff in chemistry department, University of Sussex for their friendship, kindness and help have been valuable to me.

I am grateful to the Royal Thai Government, Thailand for financial support.

Finally, I would like to thanks my parents, family and friends in Thailand for their priceless support and love.

List of symbols and abbreviations

AAK1	adaptor-associated protein kinase1
AEA	N-arachidonoylethanolamine
2-AG	2-Arachidonoylglycerol
Asp	aspartic acid
BMP2K	bone morphogenic protein-2-inducible kinase
Boc	<i>tert</i> -butyloxycarbonyl
CA	carbonic anhydrase
CB ₁	cannabinoid receptor type 1
CB ₂	cannabinoid receptor type 2
CNS	central nervous system
CTLCL	cutaneous T-cell lymphoma
d	doublet
DIPEA	N,N-Diisopropylethylamine, C ₈ H ₁₉ N
DMF	dimethylformamide, C ₃ H ₇ NO
DMSO	dimethyl sulfoxide, C ₂ H ₆ OS
DNA	deoxyribonucleic acid
DSS	dextran sulfate sodium
DYRK	dual specificity tyrosine-phosphorylation-regulated kinase
EC ₅₀	half maximal effective concentration
EDTA	ethylenediaminetetraacetic acid
EGFR	epidermal growth factor receptor
EtOAc	ethyl acetate, C ₄ H ₈ O ₂
FAAH	fatty acid amide hydrolase
FDA	Food and Drug Administration
FT-IR	fourier transform infrared spectroscopy
GAK	cyclin G-associated kinase

GC ₅₀	Growth Control 50%
Gly	glycine
GPCRs	G protein–coupled receptors
GSH	glutathione
h	hour
HATs	histone acetyltransferases
HBTU	3-[Bis(dimethylamino)methylumyl]-3 <i>H</i> -benzotriazol-1-oxide hexafluorophosphate
HCl	hydrochloric acid
HDACs	histone deacetylases
His	histidine
HOBt	hydroxybenzotriazole
HRMS	high-resolution mass spectrometry
IBS	irritable bowel syndrome
IC ₅₀	half maximal inhibitory concentration
JAHA	<i>N</i> ¹ -hydroxy- <i>N</i> ⁸ -ferrocenyloctanediamide
LC-MS	liquid chromatography–mass spectrometry
m	multiplet
MeOH	methanol, CH ₄ O
MHz	megahertz
mL	milliliter
mM	millimolar
MRI	magnetic resonance imaging
m/z	mass to charge ratio
NADH	nicotinamide adenine dinucleotide
nm	nanometre
nM	nanomolar
NMR	nuclear magnetic resonance
ppm	parts per million
RNA	ribonucleic acid

ROS	reactive oxygen species
rpm	revolutions per minute
RT	room temperature
RTK	receptor tyrosine kinase
s	singlet
SAHA	suberoylanilide hydroxamic acid
SAR	structure activity relationship
SNP	sodium nitroprusside
STK16	serine/threonine-protein kinase16
t	triplet
TLC	thin layer chromatography
TMS	tetramethylsilane
VEGFR3	vascular endothelial growth factor receptor3
ZBG	zinc binding group
μg	microgram
μL	microlitre
μM	micromolar

Abstract

Organometallic complexes containing transition metals, such as Ru(II), Os(II), Ir(III), have been moderately and recently used in medicinal chemistry as anticancer, antimalarial, antimicrobial or diagnostic agents. Current trends have led researchers to explore and define new synthetic methods in the quest for the design of new drugs and reduce the inherent associated toxic side-effects by using metal based compounds. Ferrocene based derivatives have been subjected to study for their biological and medicinal applications. Examples include ferrocenophane polyphenol, ferrocenyl quinone methides, ferrocenyl-aminoquinoline-carboxamide and a ferrocene-substituted hydroxytamoxifen, which has been proved as a potential new breast cancer therapeutic. Ferroquine displays antimalarial activity and ferrocifen is a tamoxifen-ferrocene anticancer agent. During the course of our research, we have focused on synthesizing and studying the biological activity of novel organometallic compounds containing the corresponding ferrocene moiety. We aimed to make, at least, 3 different families of compounds, which were cannabinoid receptor (CB₁/CB₂ receptor agonists), histone deacetylase (HDAC) selective inhibitors and general kinase inhibitors.

Firstly, a review covering the state-of-the-art in bioorganometallic chemistry will be presented. Secondly, we started with the synthesis of a small library of compounds containing the following groups: ferrocenylamine, 4-oxo-1, 4-dihydropyridine and dihydroquinoline. We used aminoferrocene as a bioisostere of the adamantylamine group where previous studies of compounds containing the latter group had showed it to effectively interact with the cannabinoid receptors, CB₁ and CB₂. Some of our compounds displayed good to excellent potency in the nM range against the CB₁ and CB₂ receptors.

Thirdly, we embarked to synthesise HDAC inhibitors knowing their potential as anti-cancer drugs and trying to obtain, wherever possible, enzyme isoform selectivity. One of the well-known HDAC inhibitors is suberoylanilide hydroxamic acid (SAHA). Vorinostat, as it is also known, has received Food and Drug Administration approval for treating patients with cutaneous T-cell lymphoma. The compound developed in our group by replacing ferrocene for the phenyl ring in SAHA, called JAHA, is another example of a highly potent HDAC inhibitor. Our research led to compounds where the hydroxamic

acid moiety in JAHA has been replaced by a benzamide group. This transformation has produced a significant effect in delivering a potent HDAC3 selective HDAC inhibitor. This is supported by biological studies and a molecular modelling rationalisation.

Next, a series of oxindole based analogues have been synthesized by the Knoevenagel condensation reaction of: 5-(pentafluorosulfanyl)-1,3-dihydro-indol-2-one and 6-(pentafluorosulfanyl)-1,3-dihydro-indol-2-one compound with: ferrocenecarboxaldehyde and pyrrole-2-carboxaldehyde. The compounds thereby synthesised have been studied against a panel of kinases, and kinase inhibitory data will be discussed and presented.

In a Future directions section, we will describe the synthesis of FAAH (fatty acid amide hydrolase) inhibitors based on an aminoferrocene backbone.

Table of Contents

Declaration	i
Acknowledgements	ii
List of symbols and abbreviations	iv
Abstract	vii
Table of contents	ix
1. Introduction	1
<i>1.1 Uses of iron complexes in medicinal chemistry</i>	<i>1</i>
<i>1.2 Background on ferrocene</i>	<i>2</i>
<i>1.2.1 Chemistry of ferrocene</i>	<i>3</i>
<i>1.3 Bioisosteres in medicinal chemistry</i>	<i>4</i>
<i>1.3.1 Classical bioisosteres</i>	<i>4</i>
<i>1.3.1.1 monovalent atoms or groups</i>	<i>4</i>
<i>1.3.1.2 divalent atoms or groups</i>	<i>5</i>
<i>1.3.1.3 trivalent atoms or groups</i>	<i>5</i>
<i>1.3.1.4 tetrasubstituted atoms</i>	<i>5</i>
<i>1.3.1.5 ring equivalents</i>	<i>5</i>
<i>1.3.2 Non-classical bioisosteres</i>	<i>5</i>
<i>1.4 Applications of ferrocene in medicinal chemistry</i>	<i>6</i>
<i>1.5 Other metal complexes in medicinal chemistry</i>	<i>21</i>
<i>1.6 Conclusion</i>	<i>29</i>
<i>1.7 References</i>	<i>30</i>
2. Synthesis of CB₂ agonists and FAAH inhibitors containing a ferrocene unit	36
<i>2.1 Overview</i>	<i>36</i>
<i>2.2 Introduction</i>	<i>36</i>

2.3 Results and Discussion	44
2.4 Biological Results	49
2.5 Conclusion	53
2.6 Experimental	53
2.7 References	66
3. Synthesis of HDAC inhibitors containing a ferrocene unit	70
3.1 Overview	70
3.2 Introduction	70
3.2.1 Mechanism of HATs and HDACs	72
3.3 Results and Discussion	79
3.3.1 Modelling	83
3.4 Biological Results	84
3.5 Conclusion	91
3.6 Experimental	94
3.7 References	105
4. Synthesis of ferrocene-based kinase inhibitors containing a pentafluorosulfanyl moiety	109
4.1 Overview	109
4.2 Introduction	109
4.3 Results and Discussion	122
4.4 Biological Results	127
4.4.1 Biochemical assays	127
4.4.2 Cell-based assays	131
4.4.3 Modelling	139
4.5 Conclusion	141
4.6 Experimental	141
4.7 References	149

5. Conclusion, future direction and thesis outcome	151
<i>5.1 Conclusion.....</i>	<i>151</i>
<i>5.2 Future directions</i>	<i>154</i>
<i>5.3 Thesis outcomes.....</i>	<i>155</i>

Chapter 1

Introduction

1.1 Uses of iron complexes in medicinal chemistry

Cisplatin is no doubt the best known and most used metal complex in chemotherapy.¹ Many cisplatin analogues have since been developed and used for cancer chemotherapy, for example, carboplatin, oxaliplatin, heptaplatin, nedaplatin and lobaplatin, to address issues such as toxicity, resistance, selectivity and limited cancer scope of cisplatin.²

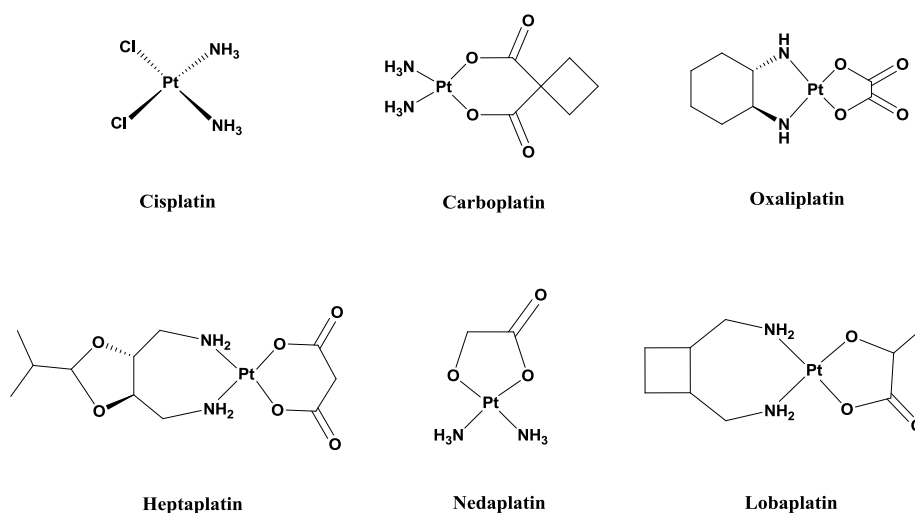


Figure 1.1. Cisplatin and its analogues.

These results have induced researchers to design other novel metal complexes for chemotherapy. Iron is also one of the essential transition metals that can be found in the body and is involved in many biological systems such as haemoglobin, transferrin and cytochromes.³⁻⁴ In many publications iron complexes have displayed potent anticancer activities.⁵⁻⁶ Usually iron has two common oxidation states in ferrous, Fe(II) and ferric forms, Fe(III). The first reported anticancer iron compounds were ferrocenium picrate and ferrocenium trichloroacetate salts.⁷⁻⁸

Ferrocene and its derivatives are popular iron complexes that researchers have synthesised and studied for their biological effects given its stability in aqueous and aerobic media and its electrochemical properties.⁹⁻¹⁰

1.2 Background on ferrocene

Ferrocene or dicyclopentadienyliron or bis(η^5 - cyclopentadienyl)iron is a compound containing iron (II) and two cyclopentadienyl rings. It was accidentally discovered by 2 groups; Peter L. Pauson and Thomas J. Kealy¹¹ in 1951, when they attempted to make fulvalene, and by Samuel A. Miller when they had tried to prepare amines from saturated or unsaturated hydrocarbons and nitrogen, they reacted cyclopentadiene and N_2 at 300 °C, but they obtained the unexpected product.¹²⁻¹³ They obtained a yellow solid compound, however the chemical formula did not fit with $C_{10}H_8$ but was formulated as $FeC_{10}H_{10}$.¹⁴ The compound structure is contributed by resonance and intermediate forms (Figure 1.2).

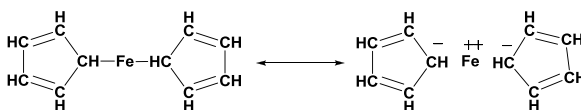


Figure 1.2. The compound structure proposed by Pauson and Kealy.

Later, three chemists; Ernst Otto Fisher, Robert B. Woodward and Geoffrey Wilkinson¹⁵ were persuaded that the structure proposed by Pauson and Kealy was wrong and they contributed the new structures which have the same electronic configuration as krypton (Kr, noble gas) (Figure 1.3). Woodward¹⁶ suggested the name of ferrocene for $[Fe(C_5H_5)_2]$ and later applied to the chemicals in general form $[M(C_5H_5)_2]$ called metallocenes (or sandwich compounds).

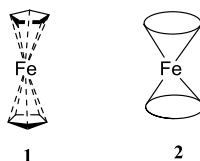


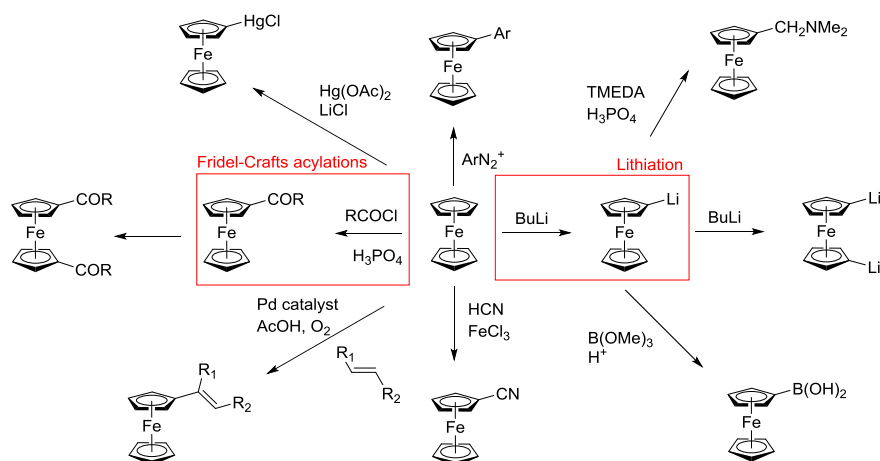
Figure 1.3. The compound structure proposed by Woodward and Wilkinson **1** and by Fischer **2**.

Ferrocene is a π -complex in which interactions between the d-orbitals of the Fe^{2+} metal centre with the π -orbitals of the two planar cyclopentadienyl ligands (C_5H_5^-) form the metal-ligand bonds. Ferrocene is an air stable orange solid and it can be oxidized to the ferrocenium cation, $[(\text{C}_5\text{H}_5)_2\text{Fe}]^+$. Ferrocene at room temperature crystallizes in a monoclinic form and shows the staggered conformation (D_{5d}), while in the gas phase it has an eclipsed conformation (D_{5h}).¹⁷ The discovery of ferrocene was a starting point of organometallic chemistry¹⁸ and then has been merged with biochemistry to herald a new area of chemistry called bioorganometallic chemistry¹⁹⁻²⁰ and the use of ferrocene in this area has increased rapidly.

Ferrocene and its derivatives have been used in many areas such as bio-analysis, bioconjugation, material sciences, organic synthesis (chiral catalysis), homogeneous catalysis (olefin polymerization), fuel additives, medicinal chemistry, and so on. In our research, we have focused on using ferrocene in medicinal chemistry.

1.2.1 Chemistry of ferrocene

The cyclopentadienyl rings in ferrocene are aromatic and undergo many reactions similar to benzene. Ferrocene is more reactive than benzene, since it is more electron rich, in electrophilic substitutions. Some important reactions of ferrocene include Friedel-Crafts acylations and lithiation reactions (Scheme 1.1).²¹ Friedel-Crafts reaction are a group of reactions enabling the substitution of an aromatic ring developed by Charles Friedel and James Crafts in 1877.²² In the case of ferrocene acylations or alkylations proceed by adding keto or alkyl groups to the cyclopentadienyl ring using an acetic anhydride/acetyl chloride or alkyl halide under Lewis acid catalysed conditions.²³ Here, formally the electrophile replaces the hydrogen atom and a new carbon-carbon bond is formed (Scheme 1.1).



Scheme 1.1. Some reactions of ferrocene.

1.3 Bioisosteres in medicinal chemistry

Bioisosteres are atoms or chemical groups with similar physical or chemical properties, which are usually used in drug design. The use of bioisosteres introduces structural changes. Bioisosteres are useful to address a number of aspects connected with the design and development of drug candidates, for example, improving potency, increasing selectivity, modifying some physical properties, reducing toxicity and so on. Bioisosteres can be classified in 2 different groups, which are classical and nonclassical bioisosteres.²⁴⁻²⁵

1.3.1 Classical bioisosteres

Classical bioisosteres show the results of an early evaluation of the concept and include structurally simple atoms or groups. Examples of classical bioisosteres and isosteres are shown below:

1.3.1.1 monovalent atoms or groups. such as:

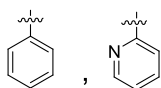
D and H, F and H.

NH₂ and OH, RSH and ROH.

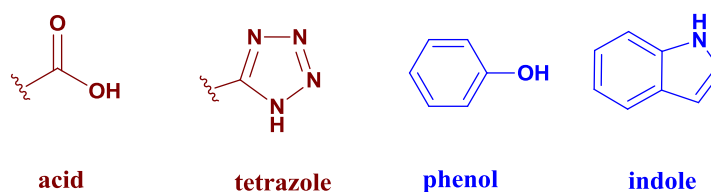
F and CH₃, Cl and OH, etc.

1.3.1.2 divalent atoms or groups. such as:C=C, C=N, C=O, C=S, -CH₂-, -NH-, -O-, -S-**1.3.1.3 trivalent atoms or groups.** such as:

-CH=, -N=

1.3.1.4 tetrasubstituted atoms. such as:R₄C, R₄Si, R₄N⁺**1.3.1.5 ring equivalents.** such as:**1.3.2 Non-classical bioisosteres**

Non-classical bioisosteres are structurally distinct, normally containing different number of atoms and display different steric and electronic properties. Non-classical bioisosteres can be divided into 2 different groups, which are 1) cyclic and acyclic bioisosteres and 2) exchangeable group isosterism in which the properties of separate functional elements are imitated. Example of non-classical bioisosteres; include a tetrazole, which is a more lipophilic bioisostere of a carboxylic acid and indole is a bioisostere of a phenol (Scheme 1.2).

**Figure 1.4.** Some non-classical bioisosteres.

1.4 Applications of ferrocene in medicinal chemistry

Ferrocene has attracted special attention as it offers attractive properties such as neutrality, lipophilicity, good redox properties, chemical stability and low toxicity.²⁶⁻²⁷ A lot of ferrocenyl compounds display fascinating antifungal,²⁸⁻²⁹ antimalarial,³⁰⁻³¹ DNA-cleaving,³² cytotoxic³³ and antitumour activity.³⁴⁻³⁵ The use of ferrocene in medicinal chemistry is a vigorous research area, some ferrocene derivatives are highly active in *in vitro* and *in vivo* assays.

In 1978, the anticancer potential of ferrocenyl compounds bearing amine or amide groups against lymphocytic leukemia P-388 cell lines, was disclosed.³⁶ Their concept was to design a ferrocene compound that can bind to a tumour cell surface nucleic acid bringing about an immune response. Polyamines, for example, putrescine, spermidine and spermine have been generally found in nature and interact strongly with nucleic acids.³⁷ These compounds were tested along with a ferrocene derivative in mice, and showed that the presence of a ferrocenyl group could increase antitumour activity (Figure 1.5).³⁶

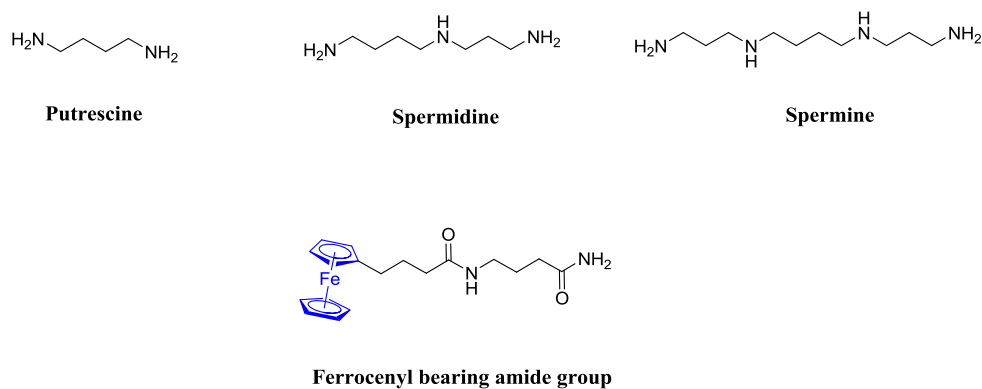


Figure 1.5. The compound structures of putrescine, spermidine, spermine and ferrocenyl bearing amide group.

A ferrocenyl group was linked to the acridine group of **3** (Figure 1.6) and the resulting compound **4** was compared with a benzylamine compound **5**. *In vitro* studies showed the compound **4** was highly toxic to cancer cell line tested, but the benzylamine analogue **5** was inactive. From these results they concluded that combining the cytotoxic effects of a ferrocenyl group with the DNA intercalation ability of an acridine led to enhanced target binding and increased cytotoxicity.³⁸

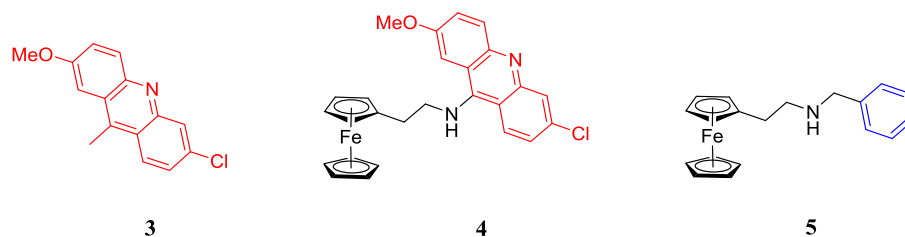


Figure 1.6. Structures of an acridine **3**, a ferrocenyl acridine **4** and a benzylamine containing ferrocene **5**.

In 2005, ferrocenyl compounds were studied for their biological activity against topoisomerase II α and β . Topoisomerases are enzymes that are involved with the winding and unwinding of DNA. In normal cells the activity of topoisomerase II is highly regulated but in cancer cells it is overexpressed. The results showed that **6** and **7** (Figure 1.7) interacted with topoisomerase II and inhibited its activity thus causing cell death.³⁹

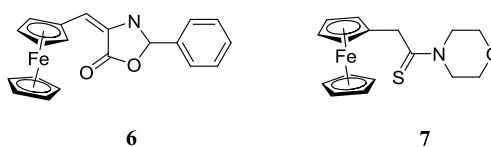


Figure 1.7. Azalactone ferrocene **6** and a thiourea ferrocene **7**.

A series of ferrocenyl compounds was tested *in vitro* against the human lung carcinoma cell line H1299. Most of them showed IC₅₀ values lower than 10 μ M.⁴⁰⁻⁴¹ Especially, the γ -aminobutyric acid ethyl ester, **8** (Figure 1.8)⁴² had an IC₅₀ value of 0.62 μ M, which is more active *in vitro* than cisplatin.⁴³

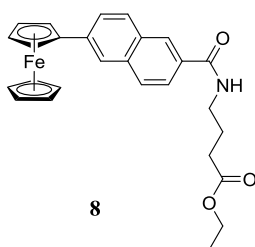


Figure 1.8. An anticancer ferrocene derivative.

Azole compounds including adenine, imidazole and pyrazole are used as privileged structures in many drugs and have attracted many researchers (Figure 1.9). For example, a series of ferrocenylalkyl azoles were studied for tumour growth inhibition and toxicity *in vivo*. The results are comparable with cisplatin. The results showed compound **9** was the best with up to 100% tumour growth inhibition.⁴⁴

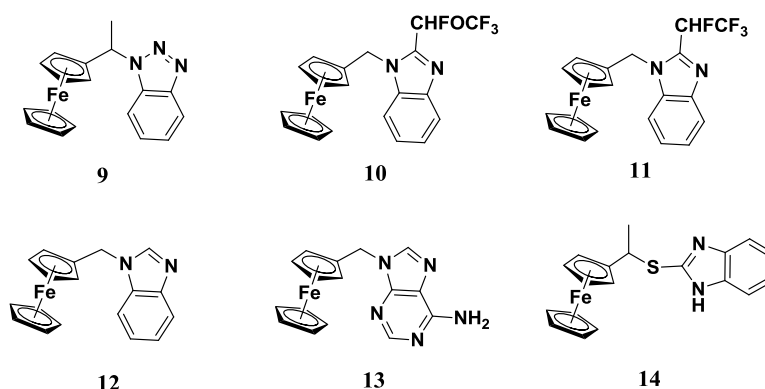


Figure 1.9. Some examples of ferrocenylalkylazole compounds.

They suggested that compound **9** was successful because; (1) the lipophilicity of the ferrocenyl group which enabled membrane permeability, (2) the hydrophilicity of the benzotriazolyl group enabled transport in aqueous media, (3) the ferrocenium form can be generated, (4) the azolyl group can form hydrogen bonds with the phosphate groups of DNA, (5) the planar heterocyclic ring in the molecule can intercalate between the planes of DNA nucleic bases, (6) the flexible, swinging, alkyl bridge can aid formation of ligand-receptor complexes.⁴⁴

Retinoids are a class of chemical compounds related to vitamin A and play an important role in vertebrate growth and development, embryonic development, immune response, supporting cell differentiation and reproduction.⁴⁵ Some trans-retinoid acids are currently used for treatment of dermatological diseases and used as chemotherapeutic agents against various cancer cells. Their actions involve binding and activation of the retinoic acid receptors (RARs) or retinoid X receptors (RXRs).⁴⁶ A novel retinoyl derivative of ferrocene, **15** (Figure 1.8) was synthesized and studied their antiproliferative activity toward a human lung cancer cell line (A549), human liver cancer cell line (BEL7404), and human tongue cancer cell line (Tca), although the results showed ferrocenyl analogues had higher antiproliferative activities when compared to the parent 13-*cis*-retinoic acid ($IC_{50} = 0.46 - >1 \mu M$), the IC_{50} values of novel compounds are being 19-40 μM .⁴⁷

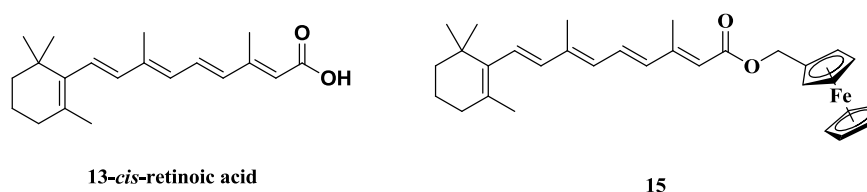


Figure 1.10. 13-*cis*-retinoic acid and retinoyl derivative of ferrocene.

Ferrocifens are the most widely studied of ferrocene derivatives for cancer therapeutics, which have promising results for breast cancer.⁴⁸⁻⁴⁹ Jaouen and co-workers have synthesized e.g. **16**, **17** and **18** (Figure 1.11). **18** was differentiated by the length of the alkyl chain connected to the dimethyl amino group, $n = 2-5$, and 8.⁴⁸⁻⁴⁹ The antiproliferative effects of **18** were assessed on MCF-7 cells (hormone-dependent breast cancer cells), **18** being slightly more potent than hydroxytamoxifen at 0.1 μM concentration and higher at 1 μM . While **17** was inactive on hormone-independent cells and **18** showed a remarkable low IC_{50} value.⁴⁸⁻⁴⁹

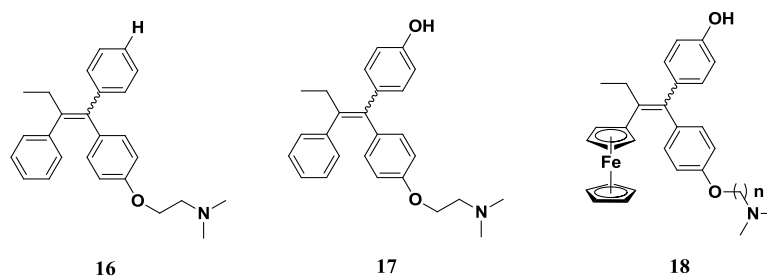


Figure 1.11. Structures of tamoxifen **16**, hydroxytamoxifen **17** and hydroxyferrocifens **18**.

A comparison of compounds **19** and **20** (Figure 1.12) differing by the linkage in the cyclopentadienyl rings, showed the conjugated compound **19** is more cytotoxic than the non-conjugated compound **20** with the antiproliferative effect on hormone-independent PC-3 cells and MDA-MB-231 with IC_{50} value of $0.09 \mu M$.⁵⁰⁻⁵¹

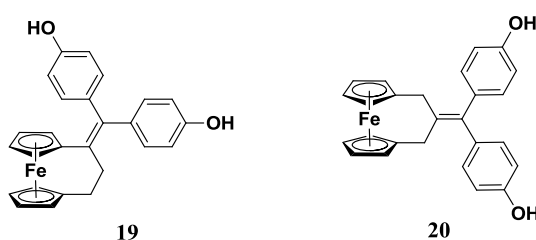


Figure 1.12. Ferrocenophane compounds structurally related to tamoxifen.

The same group also synthesized and characterized a new family of ferrocenophanic suberamides (Figure 1.13) with potent antiproliferative activities against triple-negative MDA-MB-231 breast cancer cell lines and hormone dependent MCF-7 breast cancer cells. The results showed redox activation could occur in the ferrocenophane. Hence, they can be converted into ferrocenium intermediates, which are able to show a strong antiproliferative activity of ferrocene and ferrocenophanic compounds.⁵²

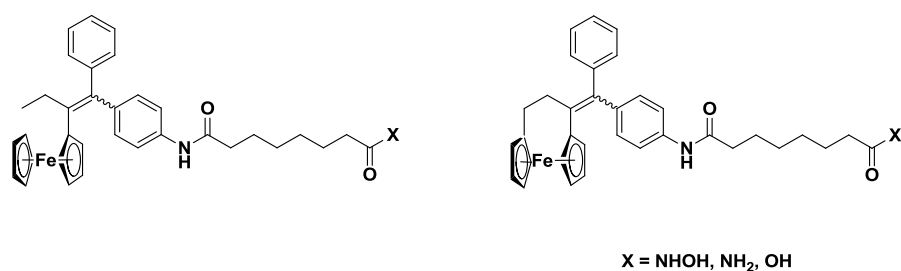


Figure 1.13. Ferrocenophanic suberamides.

Replacement of a phenyl ring by a ferrocenyl moiety, on raloxifene (**21**, Figure 1.14), maintained cytotoxic activity against ovarian, cervical, lung, colon and breast cancer cell lines. Among all the compounds, [3-ferrocenyl-6-methoxybenzo[b]thiophen-2-yl][4-(piperazin-1-yl)methylphenyl]methanone (**22**, Figure 1.14) showed IC₅₀ values in the low-micromolar range, lower than those of cisplatin.⁵³

This represents a general strategy in this body of work, whereby a phenyl or bulky alkyl group is replaced by a ferrocenyl group, thereby modifying the molecules' physical properties without adversely affecting its biological activity as in the "bioisostere" (bio-equivalent) replacement approach (Section 1.3)

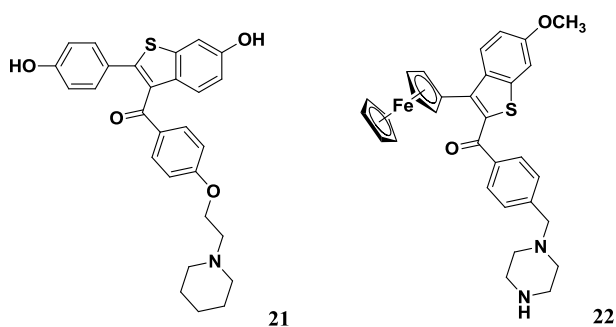


Figure 1.14. raloxifene **21** and "FeCp"- raloxifene **22**

Jaouen and co-workers attempted to improve the therapeutic activity of nilutamide (**23**, Figure 1.15) by replacing positions in the molecule by a ferrocenyl group (nilutamide is a non-steroidal anti-androgen therapeutic used in prostate cancer). The novel compound (**24**, Figure 1.15) showed cytotoxic activity against PC-3 hormone-independent prostate cancer cells with an IC_{50} value of 5.4 μ M. The idea of attaching ferrocene to androgens and anti-androgens seems to be a promising way to create efficient drugs for hormone-dependent prostate cancers.⁵⁴

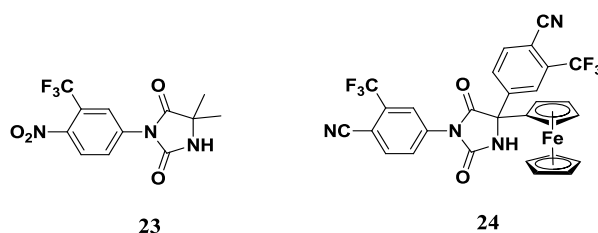


Figure 1.15. Nilutamide **23** and a ferrocenyl-nilutamide analogue **24**.

Novel hydroxyl-substituted Schiff-bases were synthesized containing ferrocenyl moieties and were evaluated for their antioxidant and anticancer activities. The results showed dual antioxidant and anticancer activities for compound **25** (Figure 1.16), which contains both ferrocenyl and *o*-dihydroxyl groups. The ferrocenyl moiety has dual functions; increasing the lipophilicity and lowering the redox potentials of the *o*-dihydroxyl groups.⁵⁵

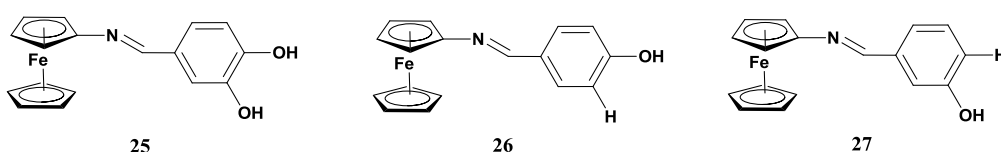


Figure 1.16. Hydroxyl-substituted Schiff-bases containing ferrocenyl moieties.

A series of novel iminosugar–ferrocene hybrids displayed potent inhibition of fucosidase (bovine kidney) and inactivation of MDA-MB-231 breast cancer cell proliferation at the low μM range. A number of compounds were prepared by varying the length of the linker connecting ferrocene to the iminosugar for establishing structure–activity relationships (Figure 1.17).⁵⁶

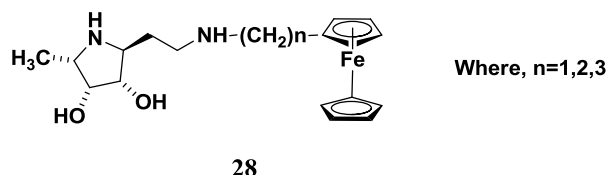


Figure 1.17. Iminosugar–ferrocene hybrids.

The antimalarial, chloroquine **29** has been used extensively since its original synthesis.⁵⁷ Recently researchers have improved this by replacing the alkyl linker by a ferrocenyl group and called the resulting molecule “ferroquine” **30**. Ferroquine is a novel antimalarial drug candidate and was designed by Christophe Biot.⁵⁸ Malaria is caused by single cell protozoan parasites of the *Plasmodium* species, of which *P. falciparum* is the most dangerous. **30** proved to be the best antimalarial candidate (Figure 1.18).⁵⁹

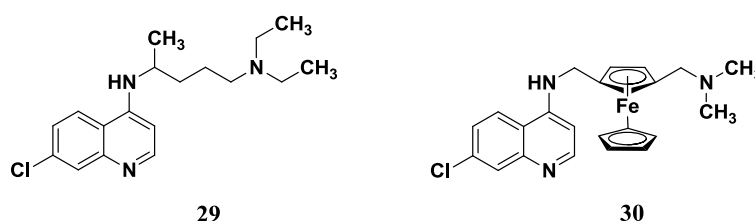


Figure 1.18. Antimalarials chloroquine **29** and **30** ferroquine.

Spencer and co-workers have designed ferrocene analogues and shown them to have anticancer activity and act as metallodrugs in many examples such as erlotinib and gefitinib. Some ferrocene analogues based on a 6,7-dimethoxy-N-phenylquinazolin-4-amine template have been synthesized (compounds **31**, **32** and **33**) and tested for *in vitro* anticancer activities against epidermal growth receptor (EGFR) with IC_{50} value in the sub- μM range (Figure 1.19).⁶⁰

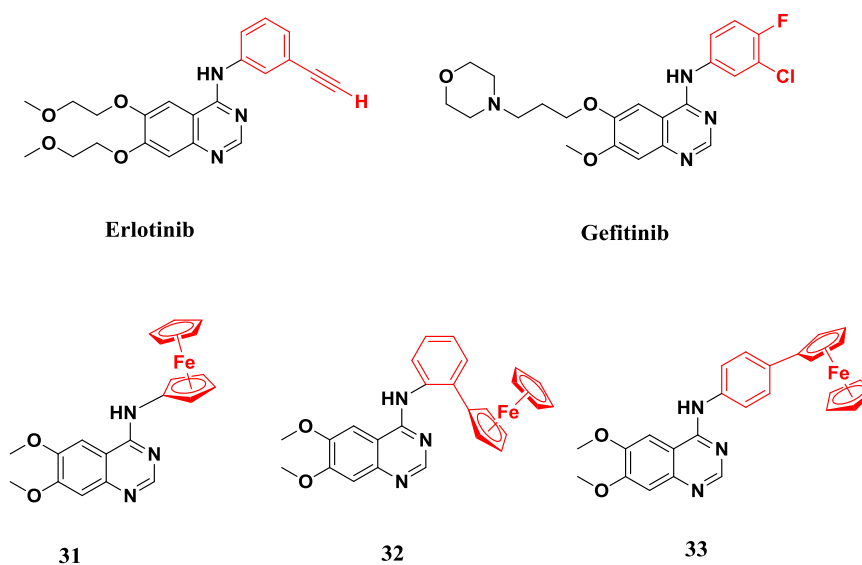


Figure 1.19. Ferrocene-based EGFR inhibitors.

Suberoyl anilide hydroxamic acid (SAHA) is a compound that shows promise for the treatment of cancer and has been clinically approved against CTCL (cutaneous T-cell lymphoma). SAHA **34** has activity against HDACs (histone deacetylases) and is effective in cancer cell lines.⁶¹ Other work from Spencer and co-workers described *N*⁸-ferrocenyl-*N*¹-hydroxy-octanediamine (JAHA), an analogue of SAHA, containing a ferrocenyl group as a phenyl bioisostere. JAHA analogues **35** displayed anticancer activity and inhibition of some classes of HDACs.⁶² “Click JAHA” **36** also have been synthesized and displayed excellent HDAC inhibition, Figure 1.20.⁶³

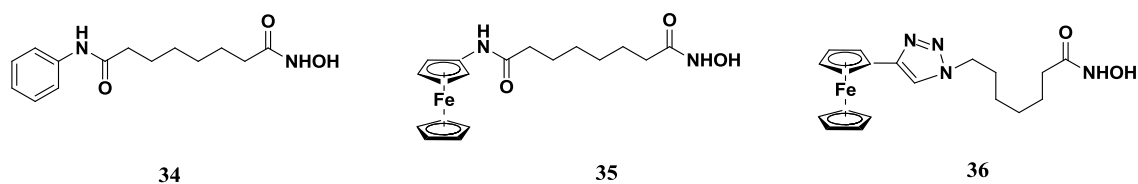


Figure 1.20. SAHA **34**, JAHA **35** and click JAHA **36**.

Tucker's group have studied functional supramolecular systems and ferrocene chemistry, and some of their work focused on designing the molecules containing ferrocene e.g. by using ferrocene to mimic the DNA structure (artificial nucleic acids) called ferrocene nucleic acids (FcNA), **37**. The phosphate-sugar-phosphate fragment in an oligomer is replaced by ferrocene molecule, the eight units of ferrocene and sixteen thymine (T) nucleobases gave the molecule called (Fc-TT)₈, **38** and they then studied their electrochemical behaviour.⁶⁴ Later, in 2014 they reported nucleoside analogues containing ferrocene as a replacement of the five-membered sugar ring and in the cell lines studied they found these novel ferrocenyl nucleoside analogues display anticancer activity, e.g. **39**.⁶⁵

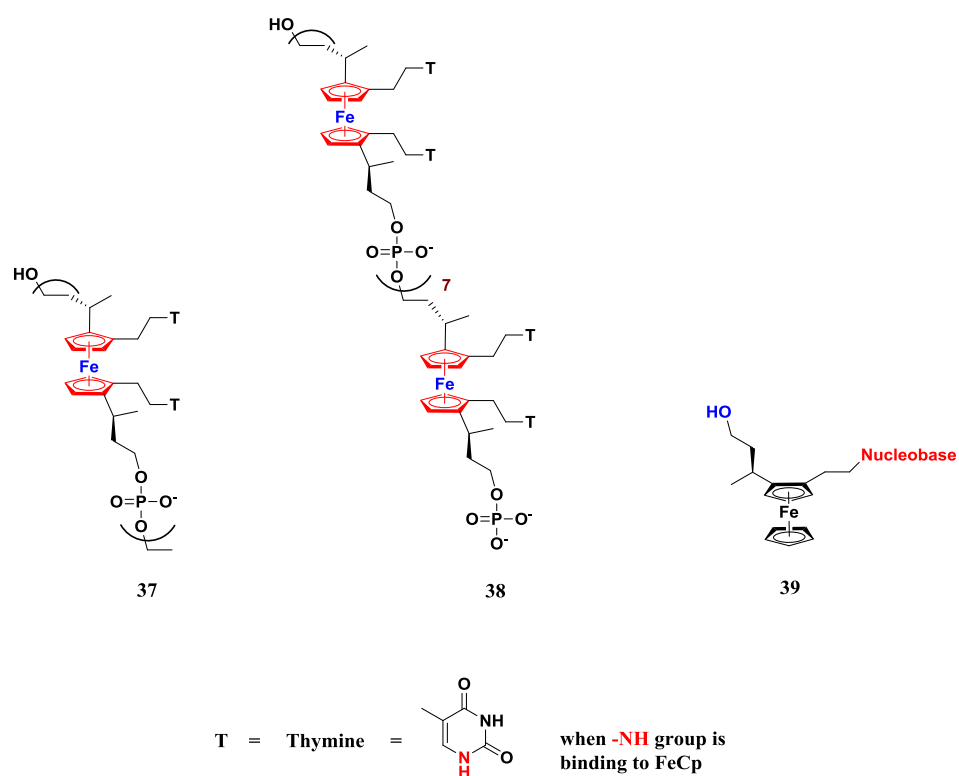


Figure 1.21. FcNA **37**, (Fc-TT)₈ **38** and nucleoside-Fc **39**.

Gasser and co-workers are also interested in the synthesis and study of the biological activity of organometallic compounds and recently reported the synthesis and biological study of sandwich and half-sandwich derivatives of platensimycin, a natural antibiotic. The results failed to show any antibacterial activity and they reasoned that this could be because of cell permeability problems of bioorganometallics.⁶⁶ Gasser also synthesized ferrocenyl derivatives of praziquantel (Fc-PZQ) against schistosomiasis, where praziquantel (PZQ), **40** is a drug for treat some types of parasitic worm infections. The results *in vitro* showed that some compounds have the IC₅₀ values in the μM range. Even the most active compound was not good enough to go through *in vivo* testing but this study will be open new mode in the search for novel drug candidates against schistosomiasis.⁶⁷

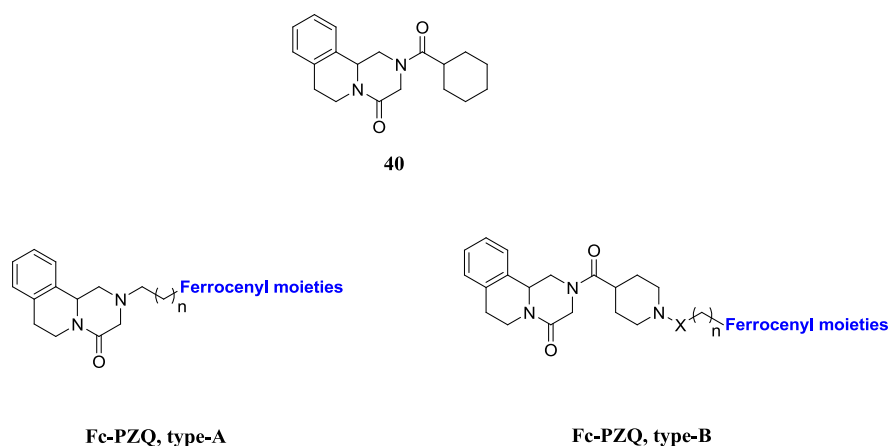


Figure 1.22. Praziquantel (PZQ) **40**, Fc-PZQ (type-A) and Fc-PZQ (type-B).

Other work from Gasser has shown the synthesis of light activated organometallic HDAC inhibitors, p-Fc-SAHA (**41**, Figure 1.22), that release a JAHA-type HDAC inhibitor,⁶⁸ as shown in the cleavable linker.

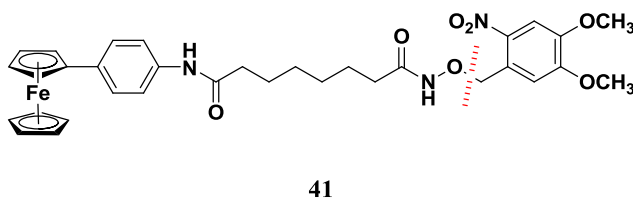


Figure 1.23. Light activatable organometallic HDAC inhibitor, p-Fc-SAHA.

Orvig and co-workers have synthesized and studied the anticancer activity of ferrocenyl-aminoquinoline-carboxamide conjugates, **42** and **43** (Figure 1.24), *in vitro* and these showed good activity against human breast cancer cells. The ferrocenyl derivatives were highly potent against colon and breast cancer cells but not very selective versus normal cell line.⁶⁹

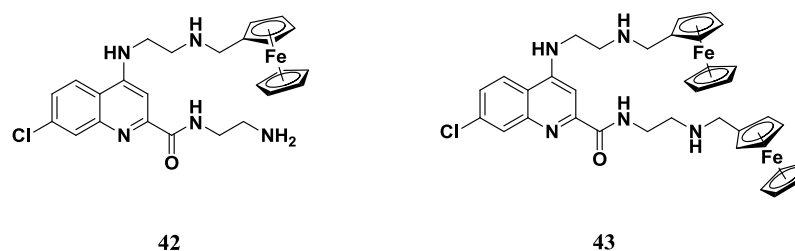


Figure 1.24. ferrocenyl-aminoquinoline-carboxamide conjugates compounds.

Carbonic anhydrase (CA) inhibitors have uses in the treatment of glaucoma, seizure disorder and so on. CA is an enzyme that catalyzes the decomposition of carbonic acid into carbon dioxide and water and CA exists in several isoforms including CA II, IX and XII. Metallocene-based compounds have been synthesized and evaluated as carbonic anhydrase inhibitors (Figure 1.25) by Poulsen and colleagues. They used either ferrocene or ruthenocene in the molecules. *In vitro* studies found these compounds were moderate to good CA inhibitors, and compounds containing a metallocene fragment showed similar SAR to the phenyl rings but in CA II, IX and XII the metallocene compounds have better potency to CA inhibition compared to phenyl-compounds.⁷⁰

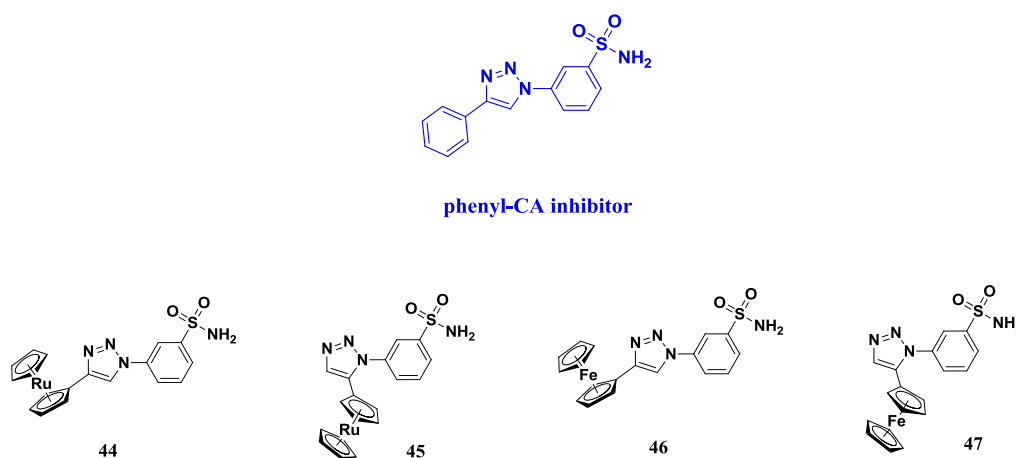


Figure 1.25. Some novel ruthenocene and ferrocene-based CA inhibitors.

The synthesis and biological evaluation, in two murine cell lines (mouse embryonic fibroblasts, NIH-3T3 and pheochromocytoma of the rat adrenal medulla, PC-12) and two human cell lines (adenocarcinomic human alveolar basal epithelial cells, A-549 and hepatocellular carcinoma, Hep-G2) of gold complexes incorporating different ferrocenyl-amide phosphine ligands (Figure 1.26) was carried out. These were compared with silver analogues. The results showed the gold complexes to be more active than the silver derivatives.⁷¹

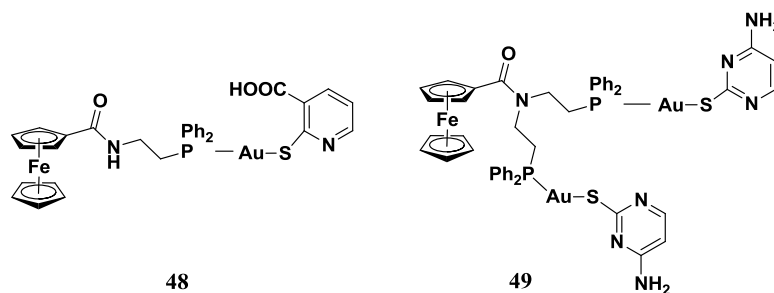


Figure 1.26. Some gold complexes with ferrocenyl-amide phosphine ligands.

A series of ferrocene-appended terpyridine copper(II) complexes combined with phenanthroline bases (Figure 1.27) was synthesized and their DNA binding, photoinduced DNA cleavage activity in visible light, and cytotoxicity in HeLa cells were studied. The results showed efficient DNA photocleavage activity in visible light at different wavelengths. These results are of importance toward developing the chemistry of bioorganometallic complexes as metal-based photoactivated anticancer agents showing DNA cleavage activity.⁷²

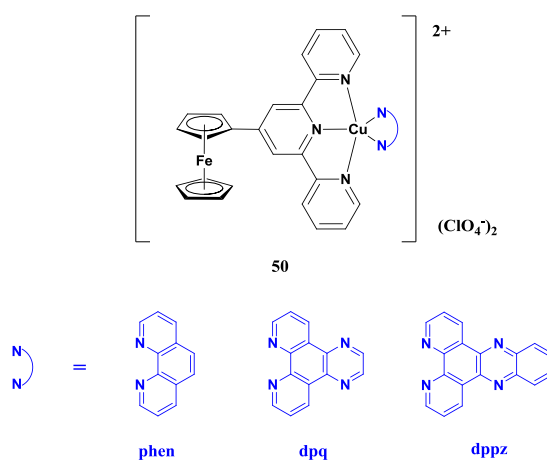


Figure 1.27. Some ferrocene-appended terpyridine copper(II) complexes with phenanthroline bases.

Ruthenocenyl-6-aminopenicillanic acid and ferrocenyl compounds have been synthesized and their antibacterial activity studied against CTX-M- β -lactamase. The researchers obtained the crystal structure of these organometallic complexes and protein residues. In this conclusion they found compound **53** to be an inhibitor of β -lactamase, and the potential use of this product as a novel scaffold for drug discovery against β -lactamases, while compound **52** was inactive due to the steric clashes and electrostatic in the protein.⁷³

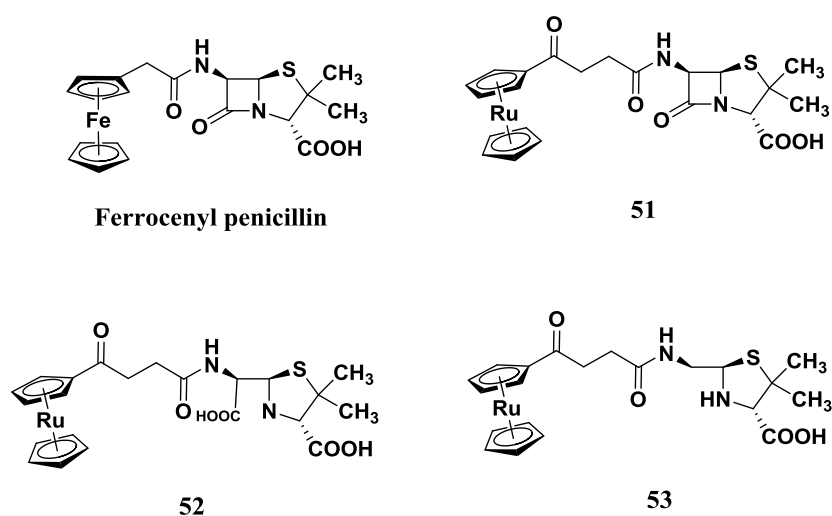


Figure 1.28. Structures of **51** and hydrolyzed products **52** and **53**.

Ferrocenyl paclitaxel and docetaxel analogues have been synthesized and their antiproliferative and cytotoxic effects studied. They used ferrocene as a bioisostere of a phenyl ring and the results showed the most active compound to be **54**, which has better antiproliferative activity than that of the parent (paclitaxel or taxol) compound with an IC₅₀ of 0.11 versus 1.11 μ M. (Figure 1.29).⁷⁴

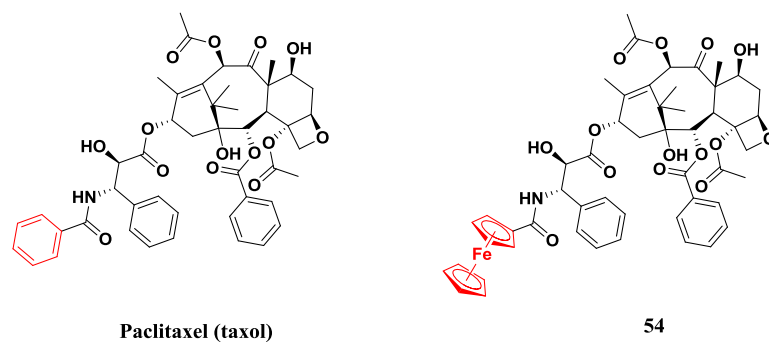


Figure 1.29. Ferrocenyl paclitaxel analogue.

Two isomers of clotrimazole (**55** and **56**) have been synthesized by replacing the phenyl ring with ferrocene and their cell growth inhibitory activity on two types of human cancer cell lines was tested. It was found that the cytotoxicity of the ferrocene analogues showed almost twice increase activity against HT29 colorectal cancer cells, whilst the activity against MCF-7 breast cancer cell lines was close to the parent compound.⁷⁵

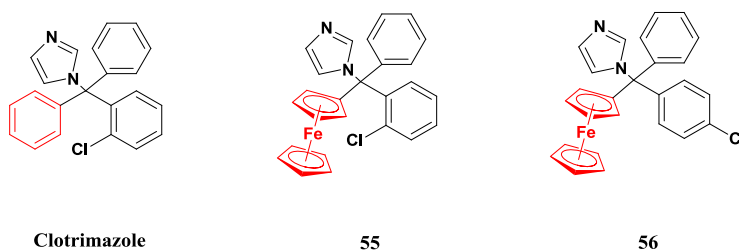


Figure 1.30. Ferrocene-clotrimazole compounds **55** and **56**.

1.5 Other metal complexes in medicinal chemistry

As stated earlier, cisplatin is a widely used anticancer agent and this success has inspired researchers to develop other metal-based drugs and apply these to other applications in medicinal areas such as using the organometallic complexes in fluorescence cell imaging,⁷⁶ contrast agents in MRI⁷⁷ and so on.

Fluorescence cell imaging relates to the use of chemicals for monitoring organ, tissues, some diseases or even tracking systems inside the body, as in a selection of imaging agents **57**, **58** and **59** based on a variety of metal atoms i.e. Rh, Re and Tc, respectively.

The bioconjugation of a rhodium (Rh) complex with biotin has used as a fluorescent stain in cell imaging, (Figure 1.31) also known as called “biotinylation”. Biotin is a vitamin B₇, it is a coenzyme for carboxylate enzymes related with the synthesis of isoleucine, valine, fatty acids and metabolic pathway of the generation of glucose (gluconeogenesis). The results showed **57** had luminescence properties inside cells.⁷⁸

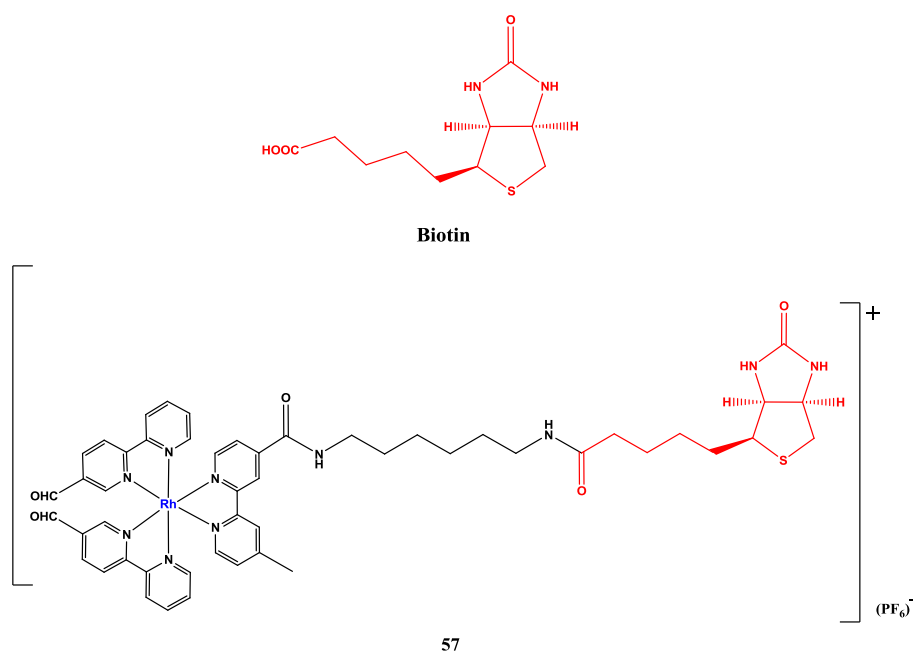


Figure 1.31. Rh complex imaging agent.

The design of $\text{Re}(\text{CO})_3$ -based complexes has been developed over the last 15 years.⁷⁹ Many luminescent rhenium complexes which target different organs have been studied and published, (Figure 1.32) e.g. **58**.⁷⁶⁻⁸⁰

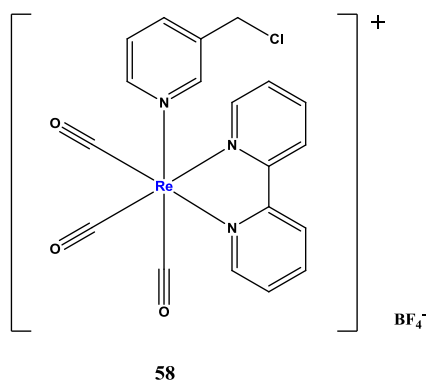


Figure 1.32. Re complex imaging agent.

Technetium (Tc) complexes have been synthesized and used as cell imaging agents.⁸¹ Tc is the most widely used in diagnostic medicine, a number of Tc-based radiopharmaceuticals have been developed and approved by the FDA.⁸² Figure 1.33 shows an example of a Tc cell imaging agent **59**.

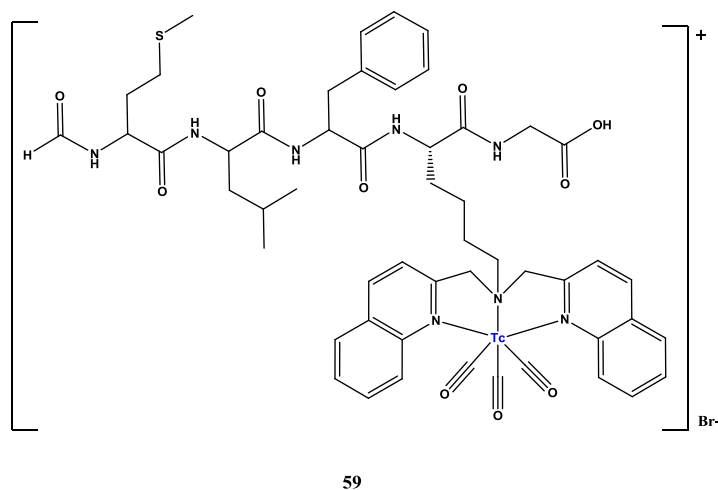


Figure 1.33. Tc complex imaging agent.

Nuclear magnetic resonance (NMR) is used for determining compound structure. The related magnetic resonance imaging (MRI) uses a similar principle but with a larger magnetic field size. It is used for medical diagnosis by detecting the difference between water molecules according to their environment, either in fluids or soft tissue in the body. Patients will take the paramagnetic metal complex before running the MRI, in this case the image will be enhanced due to the complex acting as a small magnet and will induce NMR changes in water molecules and then will be detected by MRI. Some MRI contrast agents include dotarem **60** and teslascan **61** based on Gd and Mn respectively (Figure 1.34).⁷⁷

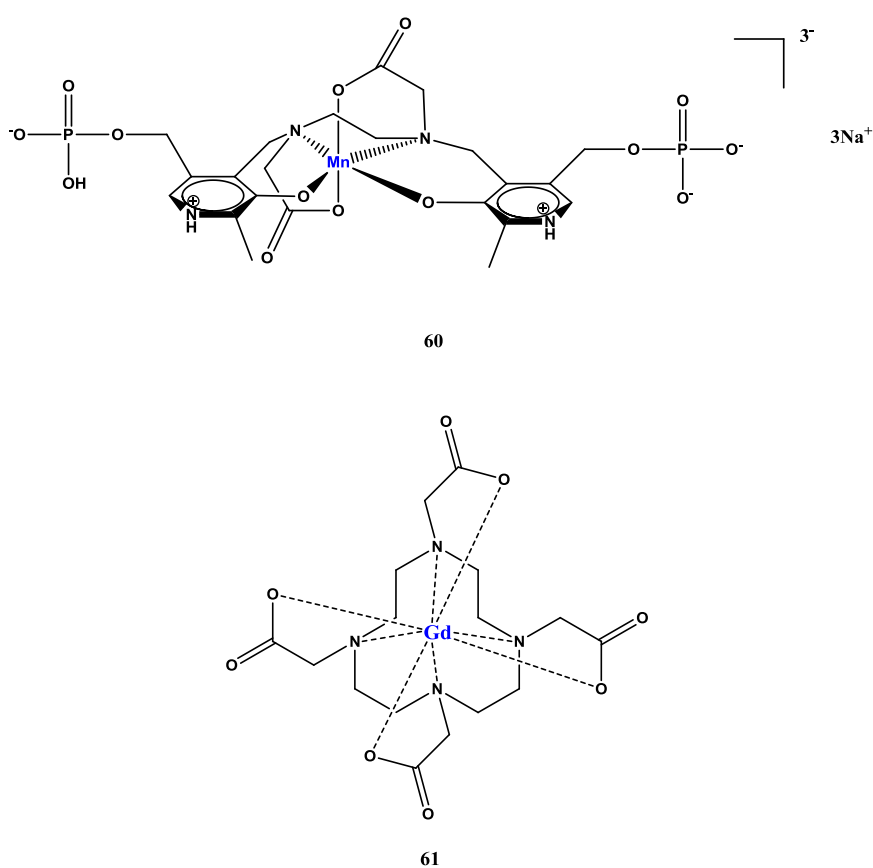


Figure 1.34. MRI contrast agents, dotarem **60** and teslascan **61**.

A number of compounds from the Meggers group show promise as selective kinase inhibitors. They propose the role of metals as “hypervalent carbon”, enabling octahedral coordination for example and enabling interactions with the kinase pocket that are not possible with tetrahedral carbon.⁸³

The pyridocarbazole platinum complex has been synthesized to mimic the structure of staurosporine, which is a natural product that is isolated from bacterium and it also had the anti-fungal, anti-hypertensive activities, inhibitor protein kinase and so on.⁸⁴ Staurosporine acts as a kinase inhibitor, by binding to the ATP-binding site on the kinase instead of ATP, stopping phosphorylation. However, staurosporine is unselective and could not be used as a drug as it needs to be more specific since it binds to a number of the 500+ kinases present in the body. Figure 1.35 shows a Pt-staurosporine complex **62**, which shows high affinity binding to glycogen synthase kinase 3 (GSK-3 α).⁸⁵

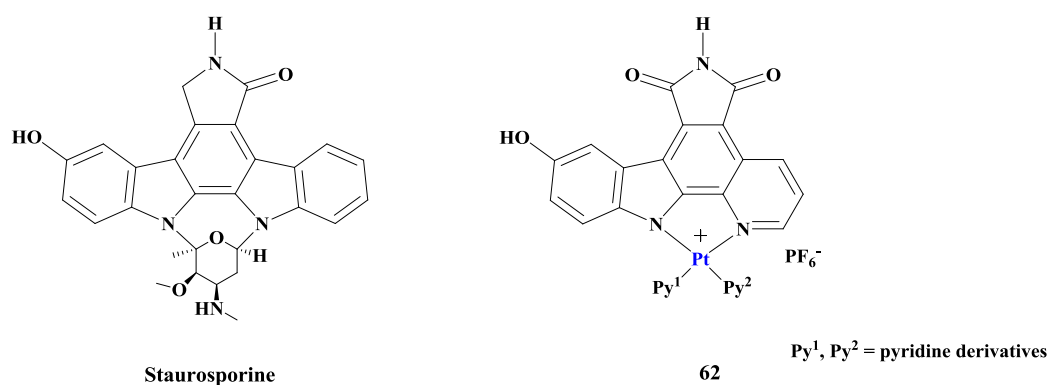


Figure 1.35. Pt-staurosporine complex **62**.

Ruthenium complex (SPM1) **63** (Figure 1.36) has been synthesized and its study shown against acetylcholinesterase (AChE) with an IC_{50} of 200 nM compared to the parent compound $[Ru(phen)_3]Cl_2$ (IC_{50} of 10 μ M). AChE is an enzyme which catalyzes the breakdown of acetylcholine and some other choline esters and is related to neurotransmitters.⁸⁶⁻⁸⁷

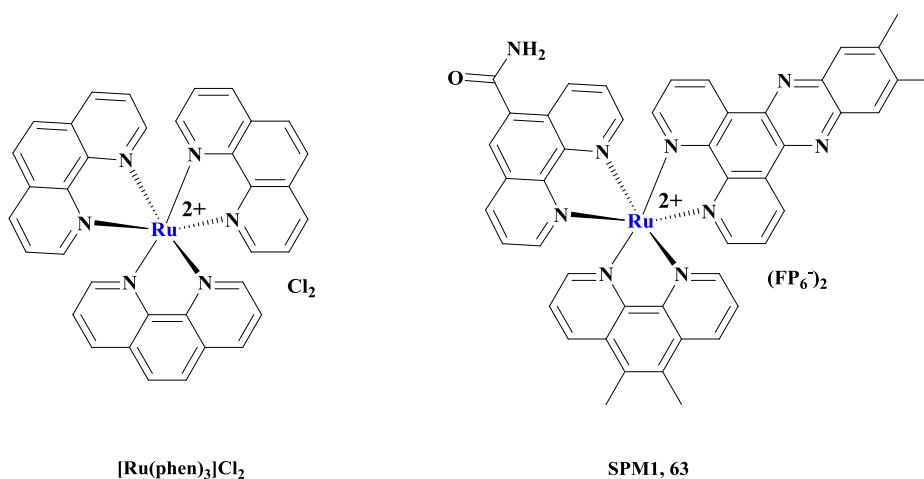


Figure 1.36. Structure of SPM1, **63**.

Another protein kinase inhibitor based on octahedral iridium (Ir) complex **64** (Figure 1.37) has been synthesized and studied for its angiogenesis properties, which is related with the growth of new blood vessels. It showed a remarkable selectivity for VEGFR3 (vascular endothelial growth factor receptor 3) over other protein kinases.⁸⁸

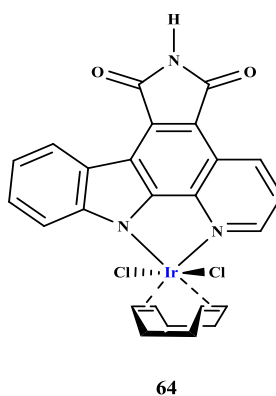
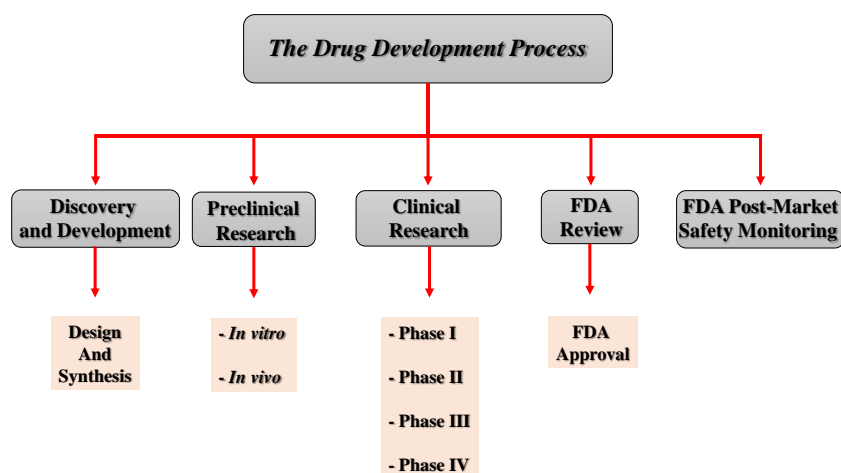


Figure 1.37. Octahedral Ir complex **64**.

The applications of metals in medical uses are increasing either via the design of new ligands or of metal-based complexes. Normally, therapeutic agents and drugs will be tested in *in vitro* to provide initial information about cytotoxicity (preliminary data) then *in vivo* assays will provide the pharmacokinetics data, these 2 steps are called “preclinical step”. The next step will be “clinical trials” which consist of phase I, II, III and IV, these steps are concerned with dosage, safety and efficacy. The two-last steps will be FDA review and FDA post-market safety monitoring (U.S. Food & Drug Administration). Typically, a drug costs over \$1 billion to develop and it takes 10-15 years.



Scheme 1.2. The drug development process.

There are now many metal compounds that have been used as therapies or reached clinical trials such as carboplatin,¹ arsenic trioxide,⁸⁹ gallium nitrate,⁹⁰ NAMI-A, KP1019,⁹¹ BEOV,⁷⁷ ferroquine⁹² and so on. The structure of those compounds is shown in Figure 1.38.⁷⁷

Carboplatin¹ is a chemotherapy drug containing platinum metal used to treat some cancers including lung, brain, breast, ovarian, testicular, bladder, head and neck. It is used by intravenous injection. Side effects of carboplatin include nausea, low blood cell levels and allergic reactions to the body.

Arsenic trioxide or Trisenox^{®89} is anticancer drug for acute promyelocytic leukemia (APL), it is administered via an intravenous injection.

Gallium nitrate⁹⁰ is a drug which used for treating symptomatic hypercalcemia (hypercalcemia associated with cancer).

NAMI-A (New Anti-Tumor Metastasis Inhibitor)⁹¹ is a compound based on ruthenium metal and now has entered to the clinical trials phase II. It used for treatment of metastatic cancer. Side effects are nausea, vomiting, diarrhea, fatigue, inflammation in mouth and lips, fever, etc. It is thought to act as a prodrug to Ru(II) in hypoxic (low oxygen) solid tumours.

KP1019 or *trans*-[tetrachlorobis(1 H-indazole)ruthenate(III)]⁹¹ is also based on ruthenium metal and has been to clinical trials phase I. It is used for metastatic cancer and shown potent cytotoxicity against colorectal cancer.

BEOV or bis(ethylmaltolato)oxovanadium(IV)⁷⁷ is based on vanadium metal and has entered clinical trials phase II. It is used to treat diabetes. In clinical trials phase I, it has been given orally to non-diabetic volunteers and the results showed no side effects.

Ferroquine (FQ)⁹² is a compound containing with ferrocene and has entered clinical trials phase II. It is used as an antimalarial agent.

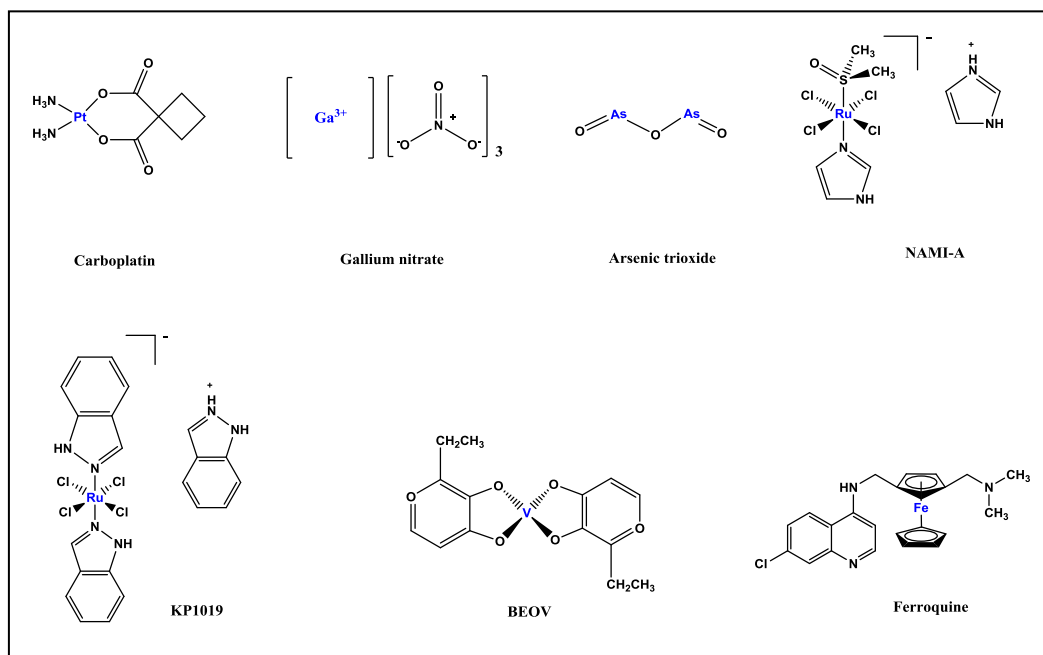


Figure 1.38. Structures of some metal complexes in medicine.

1.6 Conclusions

Above, an overview of some uses of metals in medicinal chemistry has been provided, focussing mainly on ferrocene-based chemistry. This is certainly an area of vibrant research activity but, unfortunately, due to space restraints, only a small amount of this chemistry has been mentioned. Hereafter, the study of ferrocene as a bioisostere of aryl and bulky alkyl groups is presented, supported by solid state (x-ray) studies and biological assays. In many cases nM or submicromolar ferrocene-based metallo-drugs or bioorganometallic complexes are described.

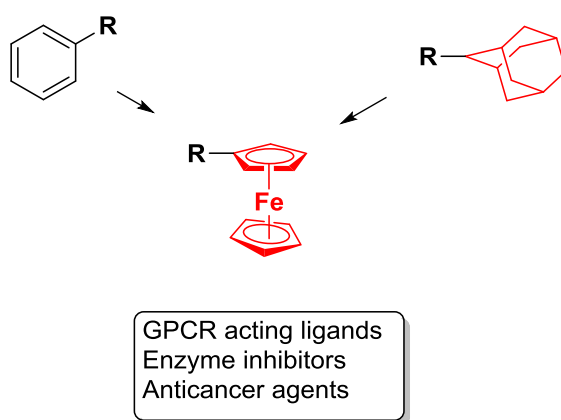


Figure 1.39. Ferrocene bioisostere principle used in this thesis.

1.7 References

- 1 I. Ott and R. Gust, *Arch.Pharm.Chem.LifeSci.*, 2007, **340**, 117–126.
- 2 I. Ali, W. A. Wani, K. Saleem and A. Haque, *Anticancer. Agents Med. Chem.*, 2013, **13**, 296–306.
- 3 M. Franchini and D. Veneri, *Hematol. J.*, 2004, **5**, 381–3.
- 4 M. Arredondo and M. T. Núñez, *Mol. Aspects Med.*, 2005, **26**, 313–327.
- 5 D. R. Richardson, P. C. Sharpe, D. B. Lovejoy, D. Senaratne, D. S. Kalinowski, M. Islam and P. V. Bernhardt, *J. Med. Chem.*, 2006, **49**, 6510–6521.
- 6 D. S. Kalinowski, P. C. Sharpe, P. V. Bernhardt and D. R. Richardson, *J. Med. Chem.*, 2007, **50**, 6212–6225.
- 7 P. Kopf-Maier, H. Kopf and E. W. Neuse, *Cancer Res. Clin. Oncol.*, 1984, **108**, 336–340.
- 8 S. Saha, R. Majumdar, M. Roy, R. R. Dighe and A. R. Chakravarty, *Inorg. Chem.*, 2009, **48**, 2652–2663.
- 9 C. S. Allardyce, A. Dorcier, C. Scolaro and P. J. Dyson, *Appl. Organomet. Chem.*, 2005, **19**, 1–10.
- 10 Ayfer, M. E. Hanhan and B. H. Menten, *Appl. Organomet. Chem.*, 2007, **21**, 369–411.
- 11 T. J. Kealy and P. L. Pauson, *Nature*, 1951, **168**, 1039–1040.
- 12 H. Werner, *Angew. Chemie - Int. Ed.*, 2012, **51**, 6052–6058.
- 13 A. Miller, J. A. Tebboth and F. Tremaine, *J. Chem. Soc.*, 1952, 632–635.
- 14 P. Laszlo and R. Hoffmann, *Angew. Chemie - Int. Ed.*, 2000, **39**, 123–124.
- 15 G. Wilkinson, M. Rosenblum, M. C. Whiting and R. B. Woodward, *J. Am. Chem. Soc.*, 1952, **74**, 2125–2126.
- 16 R. B. Woodward, M. Rosenblum and M. C. Whiting, *J. Am. Chem. Soc.*, 1952, **74**, 3458–3459.
- 17 N. Mohammadi, A. Ganesan, C. T. Chantler and F. Wang, *J. Organomet. Chem.*, 2012, **713**, 51–59.

- 18 K. Heinze and H. Lang, *Organometallics*, 2013, **32**, 5623–5625.
- 19 R. H. Fish and G. Jaouen, *Organometallics*, 2003, **22**, 2166–2177.
- 20 G. Jaouen, A. Vessieres and I. S. Butler, *Acc. Chem. Res.*, 1993, **26**, 361–369.
- 21 M. Bochmann, *Organometallics and Catalysis*, Oxford University Press, 2014.
- 22 C. Friedel and J. M. Crafts, *J. Chem. Soc.*, 1877, **32**, 725.
- 23 L. Kürti and B. Czakó, in *Strategic applications of named reactions in organic synthesis*, ed. J. Hayhurst, Elsevier Academic Press, 2005, p. 176.
- 24 G. L. Patrick, in *An Introduction to Medicinal Chemistry*, 2009, vol. 40, p. 230.
- 25 G. Patani and E. J. LaVoie, *Chem. Rev.*, 1996, **96**, 3147–3176.
- 26 K. E. Dombrowski, W. Baldwin and J. E. Sheats, *J. Organomet. Chem.*, 1986, **302**, 281–306.
- 27 R. A. Yeary, *Toxicol. Appl. Pharmacol.*, 1969, **15**, 666–676.
- 28 T. Itoh, S. Shirakami, N. Ishida, Y. Yamashita, T. Yoshida, H. S. Kim and Y. Wataya, *Bioorganic Med. Chem. Lett.*, 2000, **10**, 1657–1659.
- 29 C. Biot, N. Francois, L. MacIejewski, J. Brocard and D. Poulain, *Bioorganic Med. Chem. Lett.*, 2000, **10**, 839–841.
- 30 X. Wu, P. Wilairat and M. L. Go, *Bioorganic Med. Chem. Lett.*, 2002, **12**, 2299–2302.
- 31 D. Dive and C. Biot, *ChemMedChem*, 2008, **3**, 383–391.
- 32 M. Nakayama, T. Ihara, K. Nakano and M. Maeda, *Talanta*, 2002, **56**, 857–866.
- 33 T. Siden, T. Jie, A. Vessieres, C. Daniele, P. Christian and G. Jaouen, *J. Chem. Inf. Model.*, 1996, 955–956.
- 34 P. Kopf-Maier, H. Kopf and E. W. Neuse, *Angew. Chemie - Int. Ed.*, 1984, **6**, 456–457.
- 35 J. Quirante, F. Dubar, A. Gonzalez, C. Lopez, M. Cascante, R. Cortes, I. Forfar, B. Pradines and C. Biot, *J. Organomet. Chem.*, 2011, **696**, 1011–1017.
- 36 V. J. Fiorina, R. J. Dubois and S. Brynes, *J. Med. Chem.*, 1978, **172**, 393–395.
- 37 L. Frydman, P. C. Rossomando, V. Frydman, C. Fernandez, B. Frydman and K. Samejimat, *Proc. Natl. Acad. Sci.*, 1992, **89**, 9186–9190.

- 38 C. Ong, C.; Jeng, J.; Juang, S.; Chen, *Bioorg. Med. Chem. Lett.*, 1992, **2**, 929–932.
- 39 A. D. S. Krishna, G. Panda and A. K. Kondapi, *Arch. Biochem. Biophys.*, 2005, **438**, 206–216.
- 40 A. Goel, D. Savage, S. R. Alley, P. N. Kelly, D. O’Sullivan, H. Mueller-Bunz and P. T. M. Kenny, *J. Organomet. Chem.*, 2007, **692**, 1292–1299.
- 41 A. J. Corry, A. Goel, S. R. Alley, P. N. Kelly, D. O’Sullivan, D. Savage and P. T. M. Kenny, *J. Organomet. Chem.*, 2007, **692**, 1405–1410.
- 42 A. Mooney, A. J. Corry, N. C. Ruairc, T. Mahgoub, D. O’Sullivan, N. O’Donovan, J. Crown, S. Varughese, S. M. Draper, D. K. Rai and P. T. M. Kenny, *Dalton Trans.*, 2010, **39**, 8228–8239.
- 43 Á. Mooney, A. J. Corry, D. O’Sullivan, D. K. Rai and P. T. M. Kenny, *J. Organomet. Chem.*, 2009, **694**, 886–894.
- 44 L. V. Snegur, Y. S. Nekrasov, N. S. Sergeeva, Z. V. Zhilina, V. V. Gumenyuk, Z. A. Starikova, A. A. Simenel, N. B. Morozova, I. K. Sviridova and V. N. Babin, *Appl. Organomet. Chem.*, 2008, **22**, 139–147.
- 45 J. Paik, S. Vogel, R. Piantedosi, A. Sykes, W. S. Blaner and K. Swisshelm, *Biochemistry*, 2000, **39**, 8073–8084.
- 46 A. Nudelman and A. Rephaeli, *J. Med. Chem.*, 2000, **43**, 2962–2966.
- 47 B. Long, S. Liang, D. Xin, Y. Yang and J. Xiang, *Eur. J. Med. Chem.*, 2009, **44**, 2572–2576.
- 48 A. Nguyen, A. Vessières, E. a. Hillard, S. Top, P. Pigeon and G. Jaouen, *Chim. Int. J. Chem.*, 2007, **61**, 716–724.
- 49 S. Top, A. Vessières, G. Leclercq, J. Quivy, J. Tang, J. Vaissermann, M. Huché and G. Jaouen, *Chem. - A Eur. J.*, 2003, **9**, 5223–5236.
- 50 D. Plazuk, A. Vessières, E. A. Hillard, O. Buriez, E. Labbé, P. Pigeon, M. A. Plamont, C. Amatore, J. Zakrzewski and G. Jaouen, *J. Med. Chem.*, 2009, **52**, 4964–4967.
- 51 M. Görmén, P. Pigeon, S. Top, E. A. Hillard, M. Huché, C. G. Hartinger, F. de Montigny, M. A. Plamont, A. Vessières and G. Jaouen, *ChemMedChem*, 2010, **5**, 2039–2050.

- 52 O. Buriez, E. Labbe, S. Top and C. Amatore, *Organometallics*, 2013, **2**.
- 53 A. P. Ferreira, J. L. F. da Silva, M. T. Duarte, M. F. M. da Piedade, M. P. Robalo, S. G. Harjivan, C. Marzano, V. Gandin and M. M. Marques, *Organometallics*, 2009, **28**, 5412–5423.
- 54 O. Payen, S. Top, A. Vessières, E. Brulé, M.-A. Plamont, M. J. McGlinchey, H. Müller-Bunz and G. Jaouen, *J. Med. Chem.*, 2008, 1791–1799.
- 55 W. Chen, W. Ou, L. Wang, Y. Hao, J. Cheng, J. Li and Y. Liu, *Dalton Trans.*, 2013, **42**, 15678–86.
- 56 A. Hottin, F. Dubar, A. Steenackers, P. Delannoy, C. Biot and J.-B. Behr, *Org. Biomol. Chem.*, 2012, **10**, 5592.
- 57 W. S. Johnson and B. G. Buell, *J. Am. Chem. Soc.*, 1952, **74**, 4513–4516.
- 58 C. Biot, *Curr. Med. Chem. - Anti-Infective Agents*, 2004, **3**, 135–147.
- 59 F. Dubar, J. Khalife, J. Brocard, D. Dive and C. Biot, *Molecules*, 2008, **13**, 2900–2907.
- 60 J. Amin, I. Chuckowree, G. J. Tizzard, S. J. Coles, M. Wang, J. P. Bingham, J. A. Hartley and J. Spencer, *Organometallics*, 2013, **32**, 509–513.
- 61 L. M. Butler, X. Zhou, W.-S. Xu, H. I. Scher, R. A. Rifkind, P. A. Marks and V. M. Richon, *Proc. Natl. Acad. Sci. U. S. A.*, 2002, **99**, 11700–5.
- 62 J. Spencer, J. Amin, M. Wang, G. Packham, S. S. S. Alwi, G. J. Tizzard, S. J. Coles, R. M. Paranal, J. E. Bradner and T. D. Heightman, *ACS Med. Chem. Lett.*, 2011, 358–362.
- 63 J. Spencer, J. Amin, R. Boddiboyena, G. Packham, B. E. Cavell, S. S. S. Alwi, R. M. Paranal, T. D. Heightman, M. Wang, B. Marsden, P. Coxhead, M. Guille, G. J. Tizzard, S. J. Coles and J. E. Bradner, *Medchemcomm*, 2012, **3**, 1–5.
- 64 H. V. Nguyen, Z. Zhao, A. Sallustrau, S. L. Horswell, L. Male, A. Mulas and J. H. R. Tucker, *Chem. Comm.*, 2012, **48**, 11184–11186.
- 65 H. V. Nguyen, A. Sallustrau, J. Balzarini, M. R. Bedford, J. C. Eden, N. Georgousi, N. J. Hodges, J. Kedge, Y. Mehellou, C. Tselepis and J. H. R. Tucker, *J. Med. Chem.*, 2014, **57**, 5817–5822.

- 66 M. Patra, G. Gasser, M. Wenzel, K. Merz, J. E. Bandow and N. Metzler-Nolte, *Organometallics*, 2012, **31**, 5760–5771.
- 67 M. Patra, K. Ingram, V. Pierroz, S. Ferrari, B. Spingler, J. Keiser and G. Gasser, *J. Med. Chem.*, 2012, **55**, 8790–8798.
- 68 A. Leonidova, C. Mari, C. Aebersold and G. Gasser, *Organometallics*, 2016, **35**, 851–854.
- 69 A. Esparza-Ruiz, C. Herrmann, J. Chen, B. O. Patrick, E. Polishchuk and C. Orvig, *Inorganica Chim. Acta*, 2012, **393**, 276–283.
- 70 A. J. Salmon, M. L. Williams, Q. K. Wu, J. Morizzi, D. Gregg, S. A. Charman, D. Vullo, C. T. Supuran and S.-A. Poulsen, *J. Med. Chem.*, 2012, **55**, 5506–5517.
- 71 H. Goitia, Y. Nieto, M. D. Villacampa, C. Kasper, A. Laguna and M. C. Gimeno, *Organometallics*, 2013, **32**, 6069–6078.
- 72 B. Maity, M. Roy, B. Banik, R. Majumdar, R. R. Dighe and A. R. Chakravarty, *Organometallics*, 2010, **29**, 3632–3641.
- 73 E. M. Lewandowski, J. Skiba, N. J. Torelli, A. Rajnisz, J. Solecka, K. Kowalski and Y. Chen, *Chem. Commun.*, 2015, **51**, 6186–6189.
- 74 A. Wieczorek, A. Błaż, A. Żal, H. J. Arabshahi, J. Reynisson, C. G. Hartinger, B. Rychlik and D. Plažuk, *Chem. - A Eur. J.*, 2016, **22**, 11413–11421.
- 75 S. Pedotti, M. Ussia, A. Patti, N. Musso, V. Barresi and D. F. Condorelli, *J. Organomet. Chem.*, 2017, **830**, 56–61.
- 76 F. L. Thorp-Greenwood, *Organometallics*, 2012, **31**, 5686–5692.
- 77 J. C. Dabrowiak, *Metals in Medicine*, John Wiley & Sons, Ltd, 2009.
- 78 S. K. Leung, K. Y. Kwok, K. Y. Zhang and K. K. W. Lo, *Inorg. Chem.*, 2010, **49**, 4984–4995.
- 79 R. G. Balasingham, M. P. Coogan and F. L. Thorp-Greenwood, *Dalt. Trans.*, 2011, **40**, 11663–74.
- 80 V. Fernández-Moreira, F. L. Thorp-Greenwood, A. J. Amoroso, J. Cable, J. B. Court, V. Gray, A. J. Hayes, R. L. Jenkins, B. M. Kariuki, D. Lloyd, C. O. Millet, C. F. Williams and M. P. Coogan, *Org. Biomol. Chem.*, 2010, **8**, 3888.

- 81 K. A. Stephenson, S. R. Banerjee, T. Besanger, O. O. Sogbein, M. K. Levadala, N. McFarlane, J. A. Lemon, D. R. Boreham, K. P. Maresca, J. D. Brennan, J. W. Babich, J. Zubieta and J. F. Valliant, *J. Am. Chem. Soc.*, 2004, **126**, 8598–8599.
- 82 S. S. Jurisson and J. D. Lydon, *Chem. Rev.*, 1999, **99**, 2205–2218.
- 83 S. Blanck, J. Maksimoska, J. Baumeister, K. Harms, R. Marmorstein and E. Meggers, *Angew. Chemie - Int. Ed.*, 2012, **51**, 5244–5246.
- 84 N. Funato, H. Takayanagi, Y. Konda, Y. Toda, Y. Harigaya, Y. Iwai and S. Omura, *Tetrahedron Lett.*, 1994, **35**, 1251–1254.
- 85 D. S. Williams, P. J. Carroll and E. Meggers, *Inorg. Chem.*, 2007, **46**, 2944–2946.
- 86 E. Meggers, *Chem. Commun.*, 2009, 1001–1010.
- 87 S. P. Mulcahy, S. Li, R. Korn, X. Xie and E. Meggers, *Inorg. Chem.*, 2008, **47**, 5030–5032.
- 88 A. Wilbuer, D. H. Vlecken, D. J. Schmitz, K. Kräling, K. Harms, C. P. Bagowski and E. Meggers, *Angew. Chemie - Int. Ed.*, 2010, **49**, 3839–3842.
- 89 E. Lengfelder, W.-K. Hofmann and D. Nowak, *Leukemia*, 2012, **26**, 433–442.
- 90 P. Collery, B. Keppler, C. Madoulet and B. Desoize, *Crit. Rev. Oncol. Hematol.*, 2002, **42**, 283–296.
- 91 P. C. Bruijninx and P. J. Sadler, *Curr. Opin. Chem. Biol.*, 2008, **12**, 197–206.
- 92 C. Biot, *Curr. Med. Chem. Anti-Infective Agents*, 2004, **3**.

Chapter 2

Synthesis of CB₂ agonists and FAAH inhibitors containing a ferrocene unit.

2.1 Overview

Ferrocenylamine has been explored as a bioisostere¹ of bulky amines in a series of potential CB₁ and CB₂ (cannabinoid) receptor agonists. A series of ferrocene analogues has been synthesized by the amide coupling reaction of aminoferrocene with carboxylic acid-functionalised isoxazole, quinolinone and pyridinone rings as CB₂ agonists and their application as potent FAAH (fatty acid amide hydrolase) inhibitors has been studied. The products were characterized by elemental analyses, NMR spectroscopy, mass spectrometry, LC-MS and, many were further analysed by X-ray crystallographic studies. Ferrocene analogues of known bioactive adamantylamides were found to be effective cannabinoid receptor (CB₁ and CB₂) agonists, with low nanomolar potency. X-ray crystallography showed intramolecular hydrogen bonding to be important for activity as N-methylation of the amide resulted in the loss of hydrogen bonding and biological activity. Biological studies were undertaken through a collaboration with a medicinal chemistry group in Lille, France, who recently published work on FAAH inhibitors and CB₂ agonists,²⁻³ where they found that bulky amine substituents were beneficial for biological activity.⁴

2.2 Introduction

G protein-coupled receptors (GCRs) are an important and large group of therapeutic targets. They play a central role in many biological processes and are linked to a wide range of disease areas. The GPCR-G-protein activation/deactivation cycle⁵ is shown in Scheme 2.1.

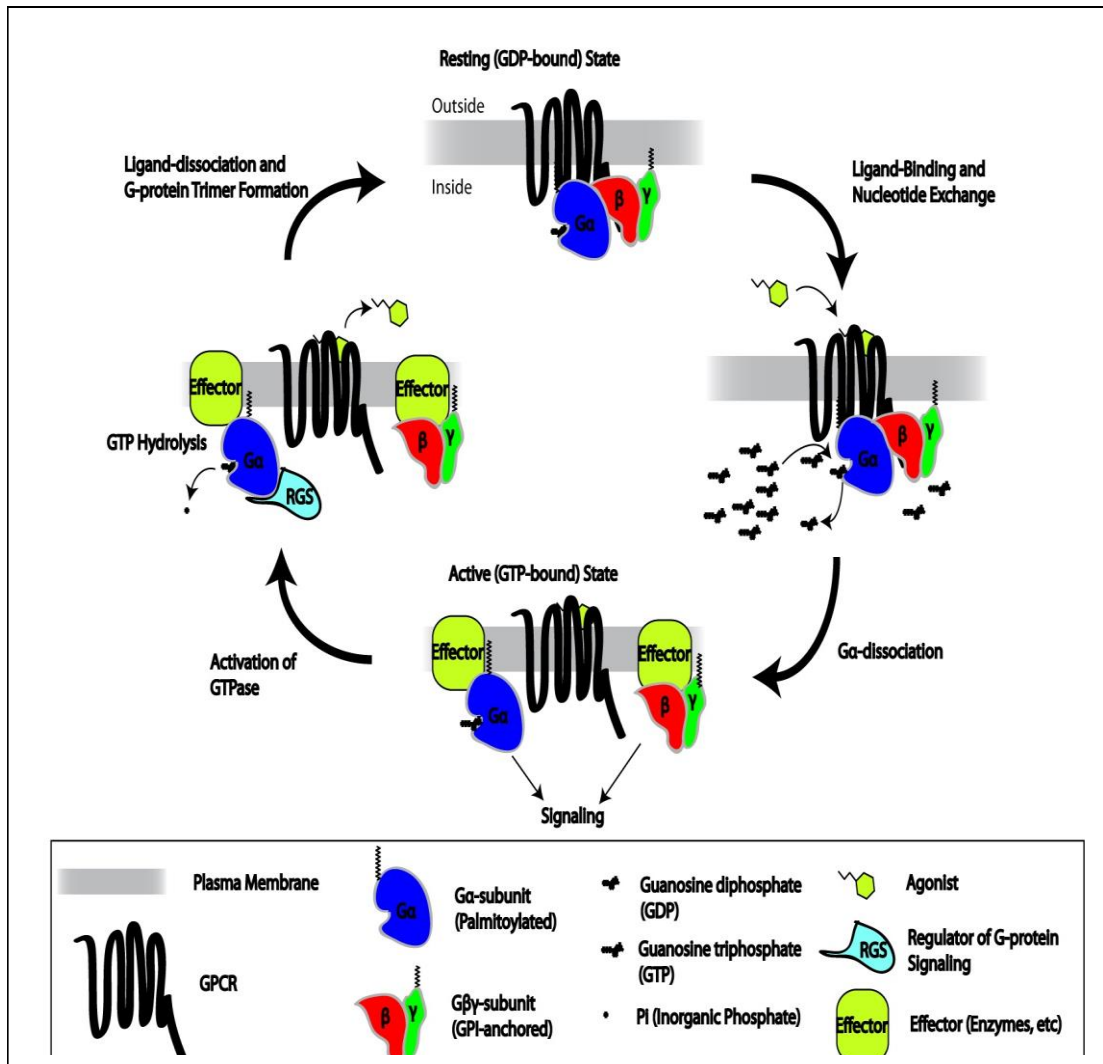


Figure 2.1. GPCR-G-protein activation/deactivation cycle
(Licensed under a Creative Commons Distribution by Repapetito).

About 20-30% of drugs in the market act on GPCRs⁶⁻⁷ such as ranitidine, salbutamol, chlorpromazine, doxepin, cinnarizine and so on.

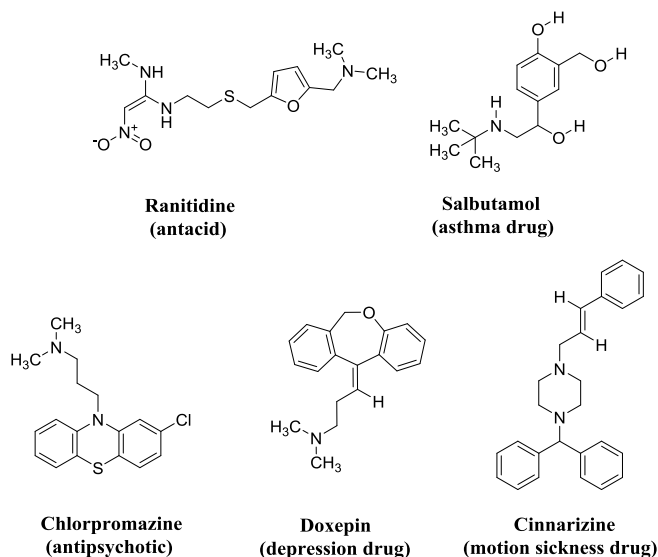


Figure 2.2. Some medications acting on GPCRs.

Cannabinoid receptors are also receptors that belong to the GPCR family, and contain two different subtypes CB_1 and CB_2 (both are in the endocannabinoid system), CB_1 is found mainly in central nervous system while CB_2 is found in the immune system.⁸ Known endocannabinoids that are involved in a variety of physiological processes such as pain sensation, mood and memory include *N*-arachidonoyl ethanolamine (anandamide, AEA)⁹ which acts as a ligand of central CB_1 cannabinoid receptors and has also been shown to be a potent and selective inhibitor of the proliferation of human breast cancer cells that can activate the cannabinoid receptor.¹⁰ Arachidonoylglycerol (2-AG)¹¹⁻¹² also acts as a ligand for the cannabinoid CB_1 receptor.¹³

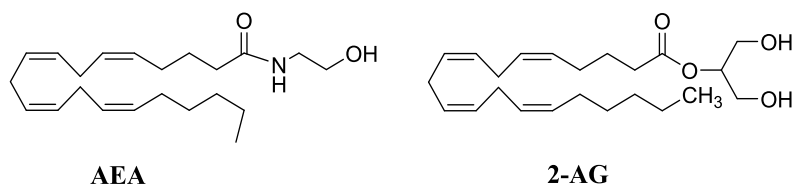


Figure 2.3. The molecular structures of AEA and 2-AG.

CB₂ receptors have been proposed to have a significant role in inflammation.¹⁴ Overexpression of CB₂ receptors was found after an inflammation stimulus.¹⁵ Activation of CB₂ receptors occurred with the suppression of macrophage activation, the blockage of calcium signals in nociceptors (these are sensory nerve cells which relay signals to the spinal cord and brain upon possible damage or stimuli), and the modulation of nociceptor excitability, related to anti-inflammation, neuroprotection, gastroprotection, or other protective effects.¹⁶ The CB₂ receptor is coupled to a G $\alpha_{i/0}$ signalling target which inhibits adenylyl cyclase (AC is an enzyme and there are ten known isoforms of adenylyl cyclases in mammals) and cyclic adenosine monophosphate **65** (cAMP is a derivative of ATP and important for the intracellular signal transduction) production.¹⁷ Ligands for CB₂ receptors can be classified as agonists, antagonists and inverse agonists when agonists activate CB₂ receptors and then repress adenylyl cyclase resulting in a decrease in cAMP concentration, antagonists prevent the activation of receptors by endocannabinoids, and inverse agonists reduce CB₂ receptor activity and induce an accumulation of cAMP through upregulation of adenylyl cyclase activity.¹⁸

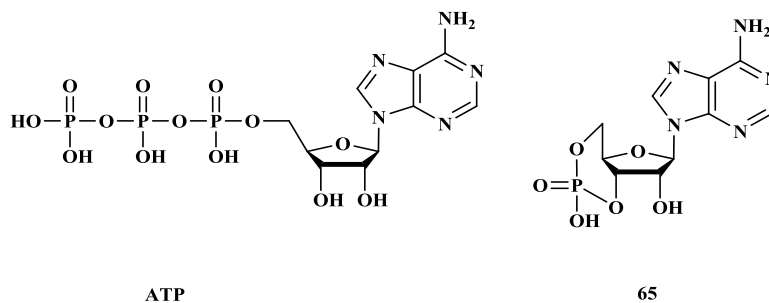


Figure 2.4. The molecular structures of ATP and cAMP **65**.

CB₂ agonists have been described to produce anti-inflammatory, analgesic, and other protective efficacies by the modulation of calcium signal and nociceptor excitability.^{16,19} CB₂ antagonists/inverse agonists showed potential in the treatment of bone-dependent disorders (such as osteoporosis) through regulation of bone proliferation.²⁰⁻²¹ In addition, inverse agonists have been identified to exert immunomodulatory (capable of modifying or regulating one or more immune functions) ability and therapeutic potential for inflammation through regulating the migration of inflammatory cells and immune cells, including leukocytes (white blood cells).²²⁻²³

CB₂ ligands have been observed as an interesting approach for the treatment of a range of nervous or immune system disorders. Over the last decades, research on CB₂ ligands has significantly progressed. Several CB₂ agonists, antagonists, and inverse agonists have been described. WIN 55,212-2 or (*R*)-(+)-[2,3-Dihydro-5-methyl-3-(4-morpholinylmethyl)pyrrolo[1,2,3-de]-1,4-benzoxazin-6-yl]-1-naphthalenylmethanone, **66**, one of the most potent dual CB₁/CB₂ agonists, has been widely used for the investigation of cannabinoid-receptor-dependent biological responses.²⁴ It exerts antinociceptive efficacy in a model of spinal cord injury and inhibits the proliferation of cancer cells.²⁵⁻²⁶ (2-Iodo-5-nitrophenyl)-[1-[(1-methylpiperidin-2-yl)methyl]indol-3-yl]methanone, **67** (AM-1241), an aminoalkylindole derivative, has been shown to act as a potent selective CB₂ agonist and shows efficacy in a variety of *in vivo* pain and inflammation models, including spinal nerve ligation (SNL)-induced nociception and 2,4,6-trinitrobenzenesulfonic acid (TNBS)-induced colitis.²⁷ Molecule **68** (SR144528) was the first selective CB₂ antagonist, discovered by Sanofi Research, and was later identified to possess temperature-dependent inverse agonist properties.²⁸ It was further identified to upregulate the expression of CB₂ receptors.²⁹⁻³⁰ 6-Iodopravadoline, **69** (AM630), a potent selective CB₂ inverse agonist, showed potential to attenuate titanium-particle-induced osteoporosis.³¹⁻³² Two other well-known CB₂ inverse agonists, **70** (Sch225336) and **71** (Sch414319), can relieve inflammation by modulating the migration of immune cells.²⁰⁻²³

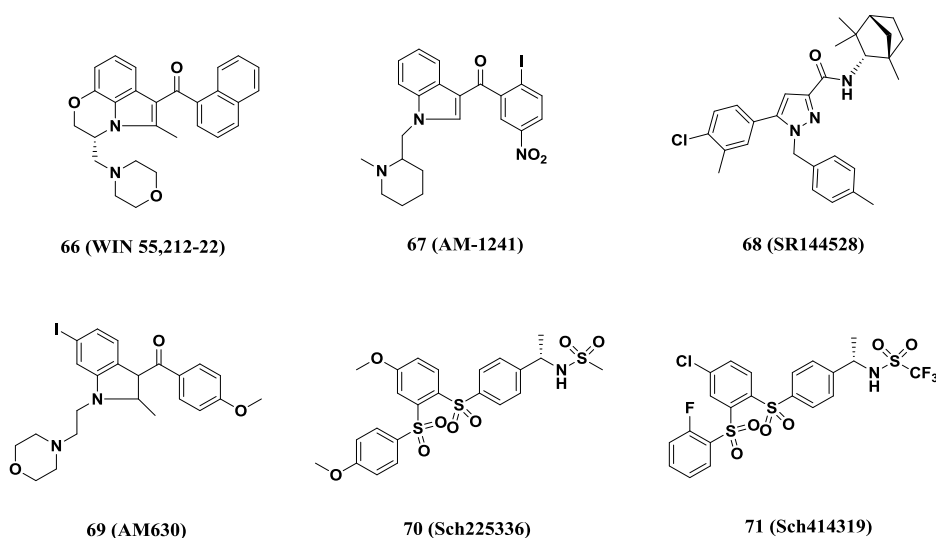


Figure 2.5. Structures of some well-known CB₂ ligands.

4-Oxo-1,4-dihydropyridine and 4-oxo-1,4-dihydroquinolinone have been synthesized as potent CB₂ agonists or inverse agonists.³³⁻³⁴ Actually, derivatives with a 1-adamantylamine group were noted to be potent and functionally selective CB₂ ligands. For instance, the 4-oxo-1,4-dihydroquinolinone derivative **72** was identified as a CB₂ agonist ($K_i = 16.4$ nM, $E_{\max}(\text{GTP}\gamma\text{S}) = 125.6\%$). In the 4-oxo-1,4-dihydropyridines series, derivative **73** showed partial agonist properties, while compound **74** was identified as a full agonist for CB₂ receptors ($K_i = 20$ and 29 nM, $E_{\max}(\text{GTP}\gamma\text{S}) = 148\%$ and 212% , $EC_{50}(\text{GTP}\gamma\text{S}) = 5.5$ and 12.2 nM, respectively). These compounds showed good selectivity over CB₁ receptors (selectivity index (SI) > 100).³⁵⁻³⁶ Another 4-oxo-1,4-dihydropyridine derivative, **75** ($K_i = 4$ nM, $E_{\max}(\text{GTP}\gamma\text{S}) = 39\%$, $EC_{50}(\text{GTP}\gamma\text{S}) = 3.2$ nM, SI = 148), containing a phenyl ring rather than an alkyl group at the C6 position, acts as a CB₂ inverse agonist.³⁵ Depending on the substituent at position-6 (methyl, tert-butyl, or phenyl group), the biological response changed from CB₂ agonist to CB₂ inverse agonist.³⁵

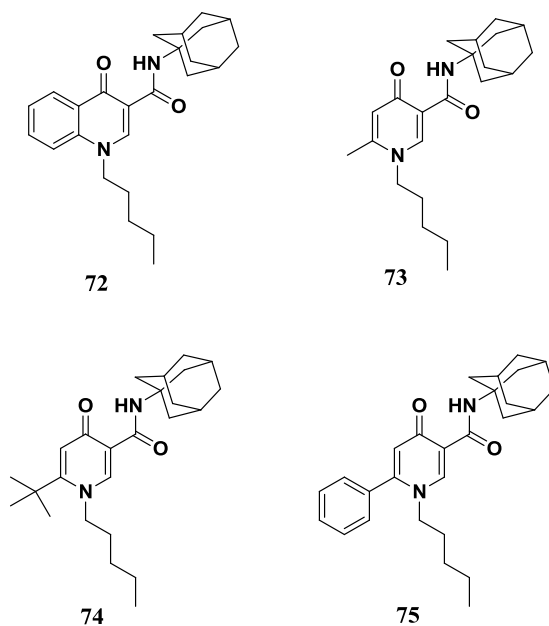
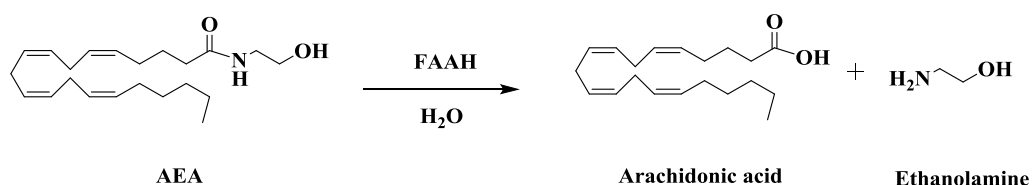


Figure 2.6. 4-Oxo-1,4-dihydropyridine/4-oxo-1,4-dihydroquinolinone derived CB₂ ligands containing an adamantylamine group.

Fatty acid amide hydrolase (FAAH) is an enzyme that hydrolyses fatty acid derivatives such as anandamide (AEA), palmitoylethanolamide (PEA) or oleoylethanolamide (OEA).³⁷ Enzymatic activity was described in the 1960s showing it to produce ethanolamine³⁸ but the role of FAAH in hydrolyzing anandamide was first reported in 1993.³⁹



Scheme 2.1. The hydrolysis of AEA by FAAH.

Elevated levels of AEA are known to offer protection in inflammation. Hence, preventing its removal, by inhibiting FAAH, could be a useful approach in treating diseases including IBS (Irritable Bowel Syndrome) and other disorders such as colitis. Figure 2.7 shows the structure of FAAH inhibitors reported by others. URB597 is particularly active against acute, inflammatory disorders and protects against experimental colitis⁴⁰ and OL-135 is described as a potent FAAH inhibitor.⁴¹

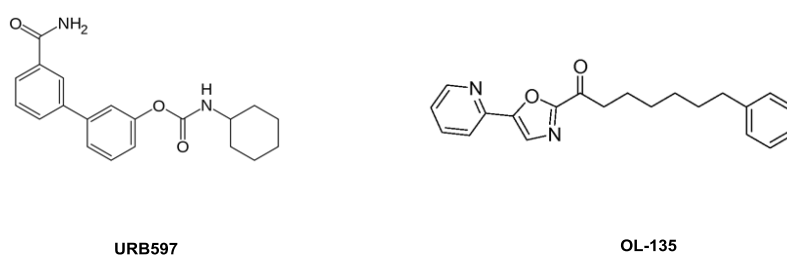


Figure 2.7. Literature FAAH inhibitors.

New FAAH inhibitors based on a 3-carboxamido-5-aryl-isoxazole scaffold have been synthesized by our collaborator (Millet group). Results showed that compounds **76** and **77** inhibit the development of dextran sulfate sodium (DSS)-induced acute colitis in mice.²

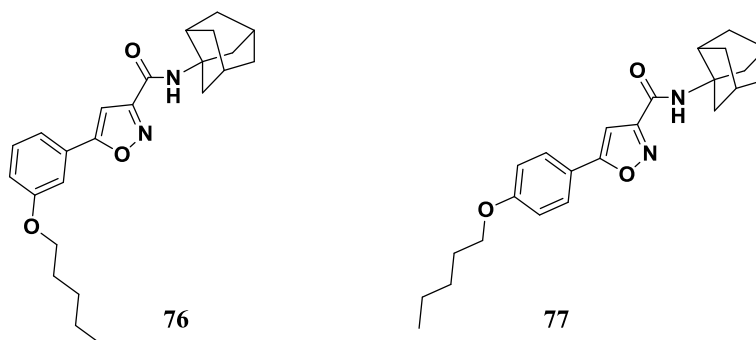


Figure 2.8. FAAH inhibitors **76** and **77**.

Ferrocene, an organometallic complex, shows advantageous properties for the design of potential pharmaceutical agents. For instance, its lipophilicity ($\log P = 2.66$ for ferrocene vs 2.69 for adamantane)⁴² endows its derivatives with suitable bioavailability and membrane penetration.⁴³⁻⁴⁴ The rotation of the aromatic cyclopentadienyl ring confers conformational diversity on ferrocene (staggered or overlapped conformation), which is favourable for orientating ferrocene-derived ligands into their receptor pockets.⁴⁵ Additionally, ferrocene derivatives have been identified to produce a variety of biological responses, including anticancer,⁴⁶⁻⁴⁷ antimalarial,⁴⁸ antioxidant,⁴⁹ antibacterial,⁵⁰ and glucose-sensing properties.⁵¹ Thus, development of ferrocene derivatives could be regarded as an interesting approach to discover potential novel pharmaceutical agents and tool compounds.

2.3 Results and Discussion

On the basis of these interesting literature results, we decided to observe the influence of the replacement of the 1-adamantyl group by a bulky, lipophilic, potentially ferrocene unit bioisostere (Figure 2.9) in terms of synthetic and biological potential.

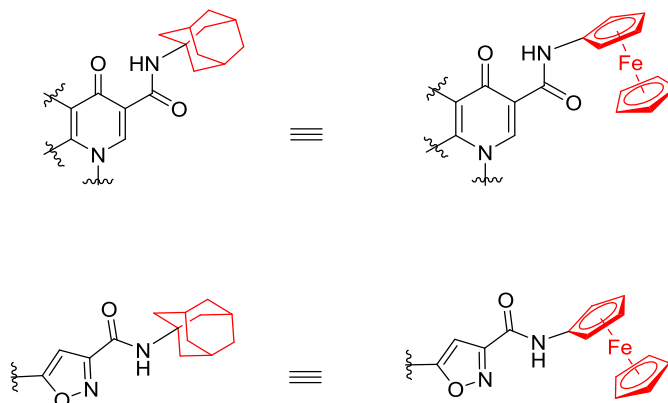
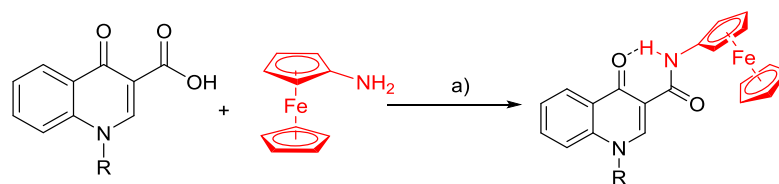
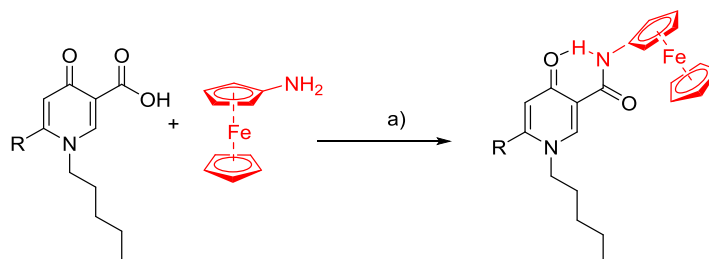


Figure 2.9. A ferrocenylamine replacement of a 1-adamantylamine group.

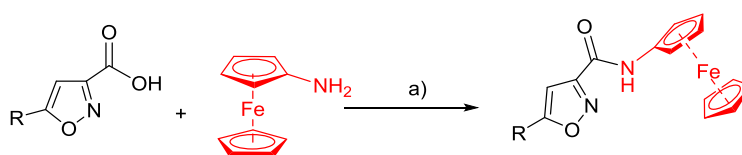
Herein, we report the synthesis and biological evaluation of a novel series of ferrocenyl 4-oxo-1,4-dihydropyridine and dihydroquinoline derivatives and 3-carboxamido-isoxazole derivatives (Scheme 2.2). All series of compounds were easily synthesized by standard amide coupling protocols and were characterized by ^1H and ^{13}C NMR spectroscopy, mass spectrometry, and combustion analysis, for solids, or by percentage purity by LCMS for oils. In the case of solids, six of these air-stable derivatives were further characterized in the solid state by X-ray crystallography, some of them confirming the presence of an intramolecular hydrogen bond between the ketone and amide functionalities (Figure 2.10), which is also observed in solution-based studies ($\delta = \text{ca. } 11.5 \text{ ppm}$ in their ^1H NMR spectra) and the ^1H NMR spectrum of isoxazole compounds showed the most downfield signal was assigned to the $-\text{NH}$ amide ($\delta 7.50\text{--}8.00 \text{ ppm}$) located next to the heterocyclic ring. The results from elemental analysis and mass spectrometry corresponded to the calculated values and the solid state molecular structures of compounds were determined by X-Ray crystallography (Figure 2.11).



78: R = Cy, 75%
79: R = n-Pent, 43%
80: R = CH₂CH₂-N-morphinyl, 47%



81: R = CH₃, 52%
82: R = t-Bu, 49%
83: R = Ph, 62%



84: R = CH₃, 45%
85: R = 2-O-n-Pent-C₆H₄, 70%
86: R = 4-O-n-Pent-C₆H₄, 72%

a) HOBt, HBTU, DIEPA, CHCl₃, RT 24 h.

Scheme 2.2. Synthesis of ferrocenylamides.

Often, an intramolecular hydrogen bond acts as a conformational lock, stabilizing an active conformation of a molecule and improving its binding to a receptor or enzyme.⁵²

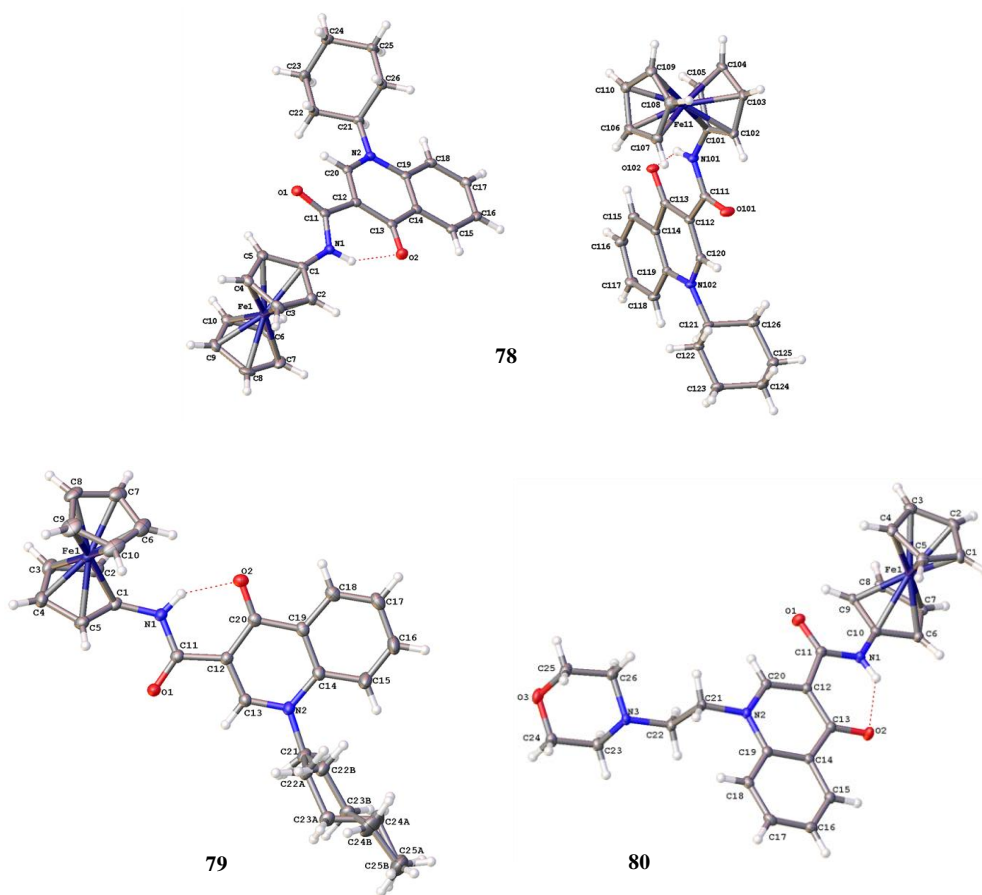


Figure 2.10. X-ray structures of **78**, **79** and **80**.

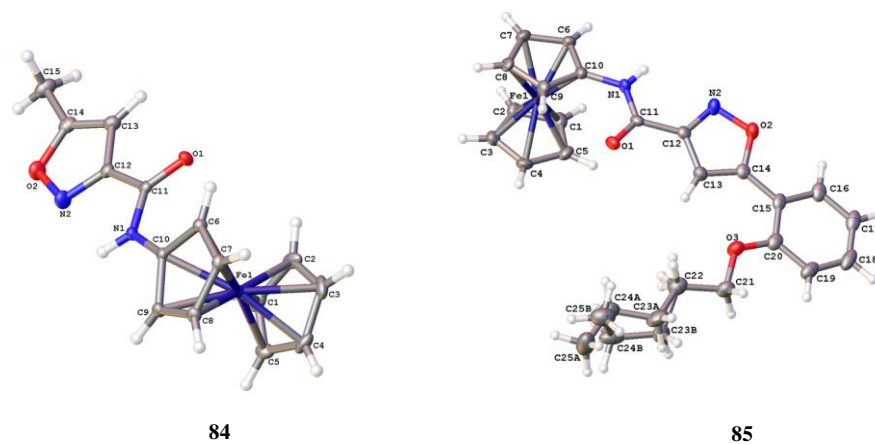
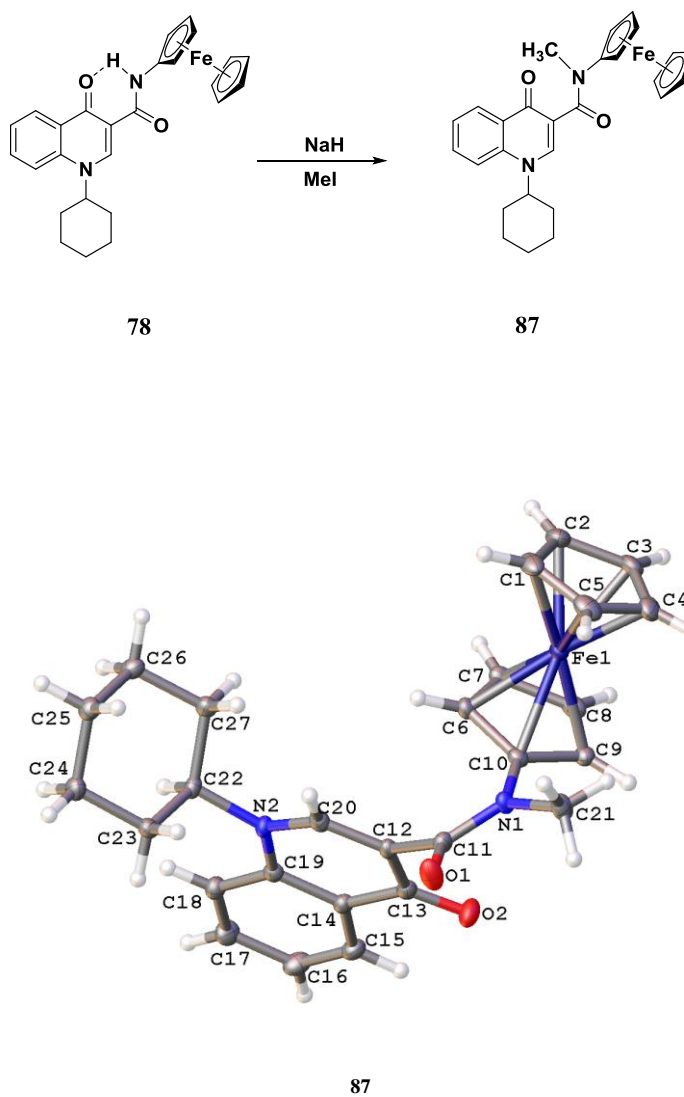


Figure 2.11. X-ray structures of **84** and **85**.

We then decided to synthesize a N-Me amide derivative **87** to compare its receptor binding to its NH-amide precursor **78**, and hence the role of intramolecular hydrogen bonding on receptor binding. We confirmed its structure by X-ray crystallography, which clearly shows a change of molecular structure by the loss of the intramolecular H-bond (Scheme 2.3).



Scheme 2.3. N-Methylation reaction of **78** and X-ray structure of **87**.

The ^1H NMR spectrum of **87**, even at variable temperature, showed a broad signal and was indicative of a fluxional molecule, but could also be due to the increased solubility of compound when the temperature is raised (Figure 2.12).

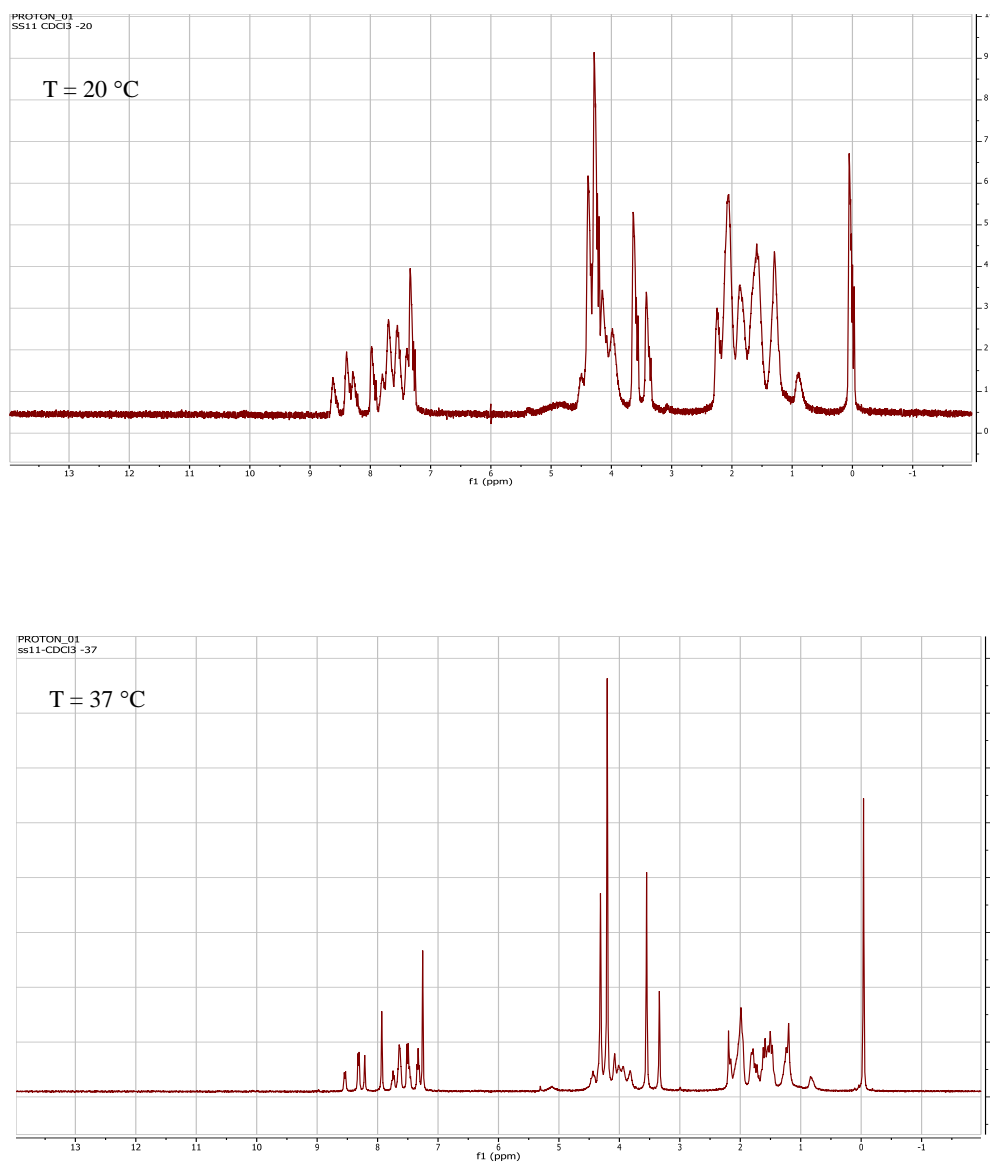


Figure 2.12. ^1H NMR spectrum of **87** in CDCl_3 at $20\text{ }^\circ\text{C}$ and $37\text{ }^\circ\text{C}$.

2.4 Biological Results

The affinities of each synthesized compound for both CB₁ and CB₂ receptors were determined by a competitive radioligand displacement assay using the dual CB₁/CB₂ ligand [3H]-CP55,940.^{53,3} Compounds **78**, **79**, **80**, **81**, **82**, and **83** (Scheme 2.2) showed good CB₂ affinity (5 nM < K_i < 220 nM). Specifically, for the 4-oxo-1,4-dihydroquinoline derivatives, a lipophilic alkyl chain on the endocyclic nitrogen (**78**, K_i = 36.7 nM; **77**, K_i = 10.9 nM) gives a superior affinity to the compound compared with a hydrophilic morpholinoethyl group (**80**, K_i = 133.6 nM). As expected, the methylation of the amide group of compound **78** brought about a sharp decrease in affinity for CB₂ (**87**, K_i > 1 μM). In the 4-oxo-1,4-dihydropyridine series, a bulky group (such as a tert-butyl or a phenyl group, **82**, K_i = 59.5 nM, and **83**, K_i = 5.2 nM, respectively) is preferred for CB₂ affinity rather than a small alkyl group (such as a methyl, **81**, K_i = 218.8 nM) at the C6 position. Compared to previously developed CB₂ ligands (such as **72**, **73**, **74**, and **75**, SI > 100), the replacement of the 1-adamantyl group by a ferrocene seems to maintain the CB₂ affinity of the molecules, with only a weak decrease in affinity for **81** compared to **73**. However, it brings about an obvious increase in affinity for CB₁ receptors (**81**, **82**, and **83**, SI < 15).

Compounds displaying potent CB₂ affinity were further studied for their functionality by cAMP assays in Chinese hamster ovary cells (CHO) expressing CB₂ receptors (CHO-CB₂).⁵⁴⁻⁵⁵ Cells were treated with forskolin, **88** in order to activate adenylyl cyclase and cAMP production. In Table 2.1, the maximum efficacy (E_{max}) of a compound represents the maximum response at 10⁻⁶ M and is expressed as the percentage of forskolin-induced cAMP production. Compound potency was also evaluated in the presence of increasing concentrations of each compound and was expressed as the concentration that exhibits the half-maximal response (EC₅₀). Although 4-oxo-1,4-dihydroquinolines **78** and **79** were determined to show potent affinity for CB₂ receptors, their binding to the receptors did not significantly affect CB₂-mediated regulation of cAMP production (E_{max} cAMP = 74% and 78%, respectively). The replacement of the N-substituted alkyl group of 4-oxo-1,4-dihydroquinoline-3-carboxamide derivatives by an N-ethyl morpholine gave rise to an obvious increase in CB₂ agonist functionality of the molecule (**80**, E_{max} cAMP = 52%), which might be attributed to probable hydrogen-binding interactions between morpholine and CB₂ receptors. The 4-oxo-1,4-

dihydropyridine-3-carboxamide derivatives bearing an alkyl substituent at the C6 position (**81** and **82**) show CB₂ agonist properties (E_{\max} cAMP = 50% and 55%, respectively). In the 4-oxo-1,4-dihydropyridine-3-carboxamide series, compound **83** (E_{\max} cAMP = 500%), bearing a 6-substituted phenyl group instead of an alkyl substituent, appears to behave as a CB₂ inverse agonist. These observations are consistent with the previous published results.¹⁴ **83**-induced accumulation of cAMP (EC_{50} cAMP = 12 nM) is approximately 65-fold greater than for compound **69** (EC_{50} cAMP = 785 nM), one of the most potent CB₂ inverse agonists reported to date. Interestingly, as illustrated in Table 2.1, replacement of the 1-adamantyl group (**73**, **74**, and **75**) by a ferrocene (**81**, **82**, and **83**) does not alter the functionality of these compounds and their ability to regulate cAMP formation. Of the isoxazole series only compound **85** displayed activity, in the ca. 30 nM range.

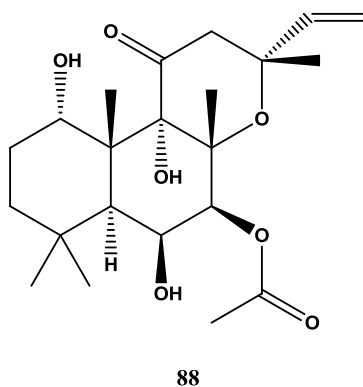


Figure 2.13. Structure of forskolin, **88**.

The cytotoxicity of these compounds was determined at 10 μ M using a cell proliferation assay on Chinese hamster ovary cells wild type (CHO-WT), CHO-CB₂, and human colorectal adenocarcinoma cells HT29. No significant cytotoxicity was observed for these new compounds except for derivative **80**, which slightly inhibited the proliferation of HT29 cells (48% at 10 μ M).⁵⁶

The affinities (K_i Values), Maximum Efficacy (E_{max}), and/or Half-Maximal Response (EC_{50}) of compounds **73–75**, **78–80**, **81–83**, **87**, and reference compounds (WIN-55,212-2, AM630) toward *hCB*₂ and *hCB*₁ Cannabinoid Receptors, Selectivity Ratios *hCB*₂ versus *hCB*₁, and Cytotoxicity on CHO-WT, CHO-CB₂, and HT29 Cells are shown in Table 2.1.

We are awaiting FAAH biological studies of **84**, **85** and **86** from our Lille-2 University partners to establish: i) if the bioisostere changes lead to retention or loss of biological activities and ii) if other analogues need to be made, once SAR (structure activity relationship) has been established.

Table.2.1. Biological activity results of 4-oxo-1,4-dihydropyridine/
4-oxo-1,4 dihydroquinolinone – ferrocene derivatives.

compounds	<i>h</i> CB ₂ and <i>h</i> CB ₁ binding assays ^a			CB ₂ cAMP assays ^a			Cytotoxicity assays % inhibition at 10 μ M		
	CB ₂ K _i (nM)	CB ₁ K _i (nM)	ratio CB ₁ /CB ₂	E _{max} (%) ^b	EC ₅₀ (nM)	CHO-WT	CHO-CB ₂	HT29	
73	20 \pm 3 ^c	> 3000 ^c	> 150 ^c	63 \pm 8	8.0 \pm 3.3	N.D. ^d	N.D. ^d	N.D. ^d	
74	29 \pm 3 ^c	> 3000 ^c	> 103 ^c	51 \pm 14	21 \pm 10	N.D. ^d	N.D. ^d	N.D. ^d	
75	4.0 \pm 0.4 ^c	592 \pm 97 ^c	148 ^c	458 \pm 106	36 \pm 6	N.D. ^d	N.D. ^d	N.D. ^d	
78	36.7 \pm 20.4	372.2 \pm 27.6	10.1	74 \pm 13	N.D. ^d	0	0	0	
79	10.9 \pm 2.2	5.5 \pm 2.0	0.5	78 \pm 14	N.D. ^d	0	0	0	
80	133.6 \pm 25.6	475.4 \pm 51.7	3.6	52 \pm 9	9.9 \pm 1.5	0	5	48	
81	218.8 \pm 15.8	204.9 \pm 33.7	0.9	50 \pm 14	11.0 \pm 4.9	0	0	1	
82	59.5 \pm 13.8	747.2 \pm 106.1	12.6	55 \pm 13	21 \pm 14	0	0	0	
83	5.2 \pm 0.4	23.4 \pm 1.9	4.5	500 \pm 32	12.0 \pm 1.5	0	0	0	
84	N.D. ^d	N.D. ^d	N.D. ^d	N.D. ^d	N.D. ^d	N.D. ^d	N.D. ^d	N.D. ^d	
85	32.54 \pm 11.37	25133.33 \pm 731.56	77.24	N.D. ^d	N.D. ^d	N.D. ^d	N.D. ^d	N.D. ^d	
86	N.D. ^d	N.D. ^d	N.D. ^d	N.D. ^d	N.D. ^d	N.D. ^d	N.D. ^d	N.D. ^d	
87	> 1000	N.D. ^d	N.D. ^d	N.D. ^d	N.D. ^d	0	0	0	
forskolin				100					
WIN55,212-2	6.9 \pm 2.0	13.9 \pm 4.0	2.0	45 \pm 7	4.3 \pm 1.1				
AM630	31.2 \pm 12.4 ^d	5152 \pm 567 ^c	165 ^c	232 \pm 79	785 \pm 7				

^aData represent the mean \pm SEM (SEM is Standard Error of Mean) of three or four experiments performed in duplicate or triplicate. ^bE_{max} values are expressed as a percentage of forskolin-induced cAMP production. ^cData from ref 34.

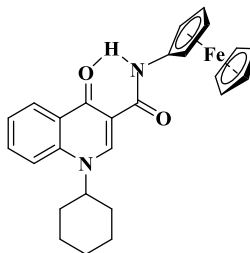
^dN.D. means not determined. ^eData from ref 30.

2.5 Conclusion

A series of ferrocenylamine-based 4-oxo-1,4-dihydropyridine and dihydroquinoline derivatives has been synthesized. Many display potency even at low (nM) concentrations vs CB₁ and CB₂ receptors. A crucial intramolecular (NH---O=C) hydrogen bond, evidenced in both solution and the solid state, appears to be important for receptor binding since N-methylation, and loss of this hydrogen bond, leads to a loss of affinity. This study demonstrates that aminoferrocene-based compounds can replace adamantanyl amines in GPCR-targeting bioorganometallic agents.⁵⁷ Whether or not this effect is simply a size/shape similarity of a ferrocene moiety compared to an adamantanyl group or if there is the induction of reactive oxygen species (ROS), as is often the case with ferrocenyl groups in bioorganometallic chemistry, is beyond the scope of this study, but the latter cannot be ruled out.^{58,59,60}

2.6 Experimental

The acids precursors for making compound **76-84** were provided by our Lille-2 University partners, solvents and reagents were purchased from commercial suppliers and were used without purification. Ferrocenylamine was purchased from TCI, UK and used as such. All reactions were performed in a fume hood. ¹H, ¹³C-NMR spectra were recorded on Varian 500 MHz or 400 MHz spectrometers and chemical shifts are reported in ppm, usually referenced to TMS as an internal standard. LCMS were performed on a 5 μm C18 110 Å column and percentage purities were ran over 30 minutes in water/acetonitrile with 0.1% formic acid (5 min at 5%, 5%-95% over 20 min, 5 min at 95%) with the UV detector at 254 nm. High resolution mass spectrometry (HRMS) were performed by the EPSRC National Mass Spectrometry Facility, University of Swansea. Elemental analyses were conducted by Stephen Boyer (London Metropolitan University).



1-Cyclohexyl-*N*-ferrocenyl-4-oxo-1,4-dihydroquinoline-3-carboxamide, 78.

The title compound was prepared by a coupling reaction; 1-cyclohexyl-4-oxo-1,4-dihydroquinoline-3-carboxylic acid (271 mg, 1 mmol) was reacted with 1-Hydroxybenzotriazole (HOBT) (68 mg, 0.5 mmol), O-(benzotriazol-1-yl)-*N,N,N',N'*-tetramethyluronium hexafluorophosphate (HBTU) (570 mg, 1.5 mmol), and *N,N*-Diisopropylethylamine (DIPEA) (0.35 mL) in CHCl₃ solution (20 mL). The reaction mixture was stirred at RT for 45 min, and then aminoferrocene (241 mg, 1.2 mmol) was added and the mixture was stirred for 24 h. Afterward, the reaction mixture was washed with NaOH (0.5 N, 20 mL), HCl (1 N, 20 mL), and H₂O (20 mL). The organic layer was dried with MgSO₄ and evaporated to a 3 mL volume and purified by column chromatography. The orange band was eluted with a hexane/ethyl acetate (7:3) mixture and was collected and evaporated to dryness. The yield was 340 mg, 75% (orange solid). Crystallization by diffusion between CH₂Cl₂ and hexane provided orange crystals.

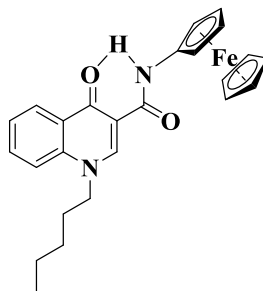
¹H NMR (CDCl₃, 500 MHz): δ = 11.56 (1H, s, NH), 9.04 (1H, s, CH), 8.62 (1H, dd, J = 8.1, 1.6, CH), 7.78–7.76 (1H, m, CH), 7.68 (1H, d, J = 8.7, CH), 7.55–7.53 (1H, m, CH), 4.82 (2H, d, J = 1.8, 2CH), 4.53–4.51 (1H, m, CH), 4.19 (5H, s, Cp), 4.05 (2H, d, J = 1.8, 2CH), 2.22–2.19 (2H, m, CH₂), 2.08–2.05 (2H, m, CH₂), 1.89–1.86 (3H, m, CH₂+ CH), 1.60–1.57 (2H, m, CH₂), 1.36–1.34 (1H, m, CH).

¹³C NMR (CDCl₃, 126 MHz): δ = 176.2, 163.2, 143.1, 139.4, 132.8, 128.1, 127.6, 125.0, 115.2, 111.8, 94.5, 69.2, 64.5, 61.8, 59.8, 32.8, 25.9, 25.2.

HRMS-ESI (m/z): found 455.1396, calcd for [C₂₆H₂₆FeN₂O₂ + H]⁺ 455.1416.

Anal. Calcd (%) for C₂₆H₂₆FeN₂O₂: C, 68.73; H, 5.77; N, 6.17.

Found (%): C, 68.50; H, 5.89; N, 6.06.



***N*-Ferrocenyl-4-oxo-1-pentyl-1,4-dihydroquinoline-3-carboxamide, 79.**

4-Oxo-1-pentyl-1,4-dihydroquinoline-3-carboxylic acid (25.9 mg, 0.1 mmol) was reacted with HOBt (6.8 mg, 0.05 mmol), HBTU (57 mg, 0.15 mmol), and DIPEA (0.035 mL) in CHCl₃ solution (2 mL). The reaction mixture was stirred at RT for 45 min, and then aminoferrocene (24.1 mg, 0.12 mmol) was added and the mixture was stirred for 24 h. Workup was as above. The orange band was eluted with a hexane/ethyl acetate (1:1) mixture and was collected and evaporated to dryness. The yield was 19 mg, 43% (orange solid). Crystallization by diffusion between CH₂Cl₂ and hexane provided yellow crystals.

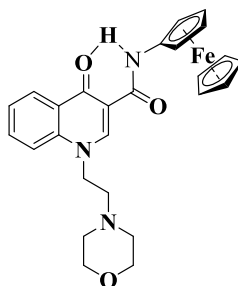
¹H NMR (CDCl₃, 500 MHz): δ = 11.51 (1H, s, NH), 8.84 (1H, s, CH), 8.61–8.58 (1H, m, CH), 7.79–7.77 (1H, m, CH), 7.54–7.52 (2H, m, Ar), 4.81 (2H, d, J = 1.9, 2CH), 4.30–4.27 (2H, m, CH₂), 4.20 (5H, s, Cp), 4.05 (2H, d, J = 1.9, 2CH), 1.42–1.38 (6H, m, 3CH₂), 0.94–0.90 (3H, m, CH₃).

¹³C NMR (CDCl₃, 126 MHz): δ = 176.6, 163.1, 147.4, 139.0, 132.9, 128.0, 127.5, 125.2, 115.9, 111.9, 94.4, 69.2, 64.6, 62.0, 54.4, 28.7, 28.8, 22.2, 13.8.

HRMS-ESI (m/z): found 443.1412, calcd for [C₂₅H₂₆FeN₂O₂ +H]⁺ 443.1416.

Anal. Calcd (%) for C₂₅H₂₆FeN₂O₂: C, 67.88; H, 5.92; N, 6.33.

Found (%): C, 67.87; H, 6.05; N, 6.45.



***N*-Ferrocenyl-1-(2-morpholinoethyl)-4-oxo-1,4-dihydroquinoline-3-carboxamide,
80.**

1-(2-Morpholinoethyl)-4-oxo-1,4-dihydroquinoline-3-carboxylic acid (30.2 mg, 0.1 mmol) was reacted with HOBt (6.8 mg, 0.05 mmol), HBTU (57 mg, 0.15 mmol), and DIPEA (0.035 mL) in CHCl_3 solution (2 mL). The reaction mixture was stirred at RT for 45 min, and then aminoferrocene (24.1 mg, 0.12 mmol) was added and the mixture was stirred for 24 h. Workup was as above. The orange band was eluted with a hexane/ethyl acetate (3:7) mixture and was collected and evaporated to dryness. The yield was 23 mg, 47% (yellow solid). Crystallization by diffusion between acetone and hexane provided orange crystals.

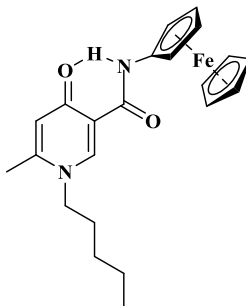
^1H NMR (CDCl_3 , 500 MHz): δ = 11.46 (1H, s, NH), 8.84 (1H, s, CH), 8.60 (1H, dd, J = 8.1, 1.5, CH), 7.79–7.76 (1H, m, CH), 7.58–7.54 (2H, m, Ar), 4.82–4.79 (1H, m, CH), 4.39 (2H, d, J = 1.9, 2CH), 4.20 (5H, s, Cp), 4.13–4.11 (1H, m, CH), 4.08–4.05 (1H, m, CH), 3.70–3.68 (2H, m, CH_2), 2.85–2.83 (1H, m, CH), 2.53 (2H, m, CH_2), 2.05 (1H, s, CH), 1.29–1.26 (3H, m).

^{13}C NMR (CDCl_3 , 126 MHz): δ = 176.6, 162.9, 148.2, 139.0, 133.0, 128.0, 127.6, 125.2, 115.6, 111.8, 94.3, 69.2, 66.8, 64.6, 62.0, 56.5, 53.8, 51.4.

HRMS-ESI (m/z): found 486.1471, calcd for $[\text{C}_{26}\text{H}_{27}\text{FeN}_3\text{O}_3 + \text{H}]^+$ 486.1475.

Anal. Calcd (%) for $\text{C}_{26}\text{H}_{27}\text{FeN}_3\text{O}_3$: C, 64.34; H, 5.61; N, 8.66.

Found (%): C, 64.27; H, 5.54; N, 8.63.



***N*-Ferrocenyl-6-methyl-4-oxo-1-pentyl-1,4-dihydropyridine-3-carboxamide, 81.**

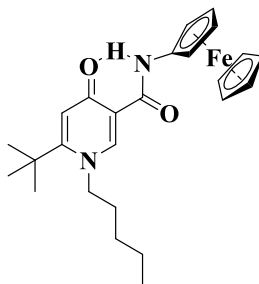
6-Methyl-4-oxo-1-pentyl-1,4-dihydropyridine-3-carboxylic acid (22.3 mg, 0.1 mmol) was combined with HOBt (6.8 mg, 0.05 mmol), HBTU (57 mg, 0.15 mmol), and DIPEA (0.035 mL) in CHCl₃ (2 mL). The reaction mixture was stirred at RT for 45 min, and then aminoferrocene (24.1 mg, 0.12 mmol) was added. Workup was as above. The orange band was eluted with a hexane/ethyl acetate (2:3) mixture and was collected and evaporated to dryness. The yield was 21 mg, 52% (orange oil).

¹H NMR (CDCl₃, 500 MHz): δ = 11.72 (1H, s, NH), 8.45 (1H, s, CH), 6.46 (1H, s, CH), 4.88–4.84 (2H, m, CH₂), 4.24 (5H, s, Cp), 4.15–4.12 (2H, m, 2CH), 3.91 (2H, d, J = 1.9, 2CH), 2.39 (3H, s, CH₃), 1.80–1.76 (2H, m, CH₂), 1.38–1.32 (4H, m, 2CH₂), 0.94–0.90 (3H, m, CH₃).

¹³C NMR (CDCl₃, 126 MHz): δ = 177.4, 162.4, 147.8, 144.9, 121.4, 118.9, 69.6, 65.0, 62.0, 53.9, 30.6, 29.7, 28.5, 22.2, 19.0, 13.8.

HRMS-ESI(m/z): found 407.1414, calcd for [C₂₂H₂₆FeN₂O₂ + H]⁺ 407.1416.

LCMS purity (UV) = 100%, t_R 19.13 min. LCMS purity (positive ion, TIC) = 93.5%, t_R 19.20 min.



6-tert-Butyl-N-ferrocenyl-4-oxo-1-pentyl-1,4-dihydropyridine-3-carboxamide, 82.

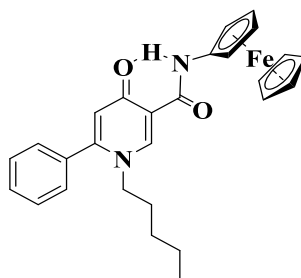
6-(tert-Butyl)-4-oxo-1-pentyl-1,4-dihydropyridine-3-carboxylic acid (26.5 mg, 0.1 mmol) was combined with HOBt (6.8 mg, 0.05 mmol), HBTU (57 mg, 0.15 mmol), and DIPEA (0.035 mL) in CHCl_3 (2 mL). The reaction mixture was stirred at RT for 45 min, and then aminoferrocene (24.1 mg, 0.12 mmol) was added and the mixture was stirred for 24 h. Workup was as above. The orange band was eluted with a hexane/ethyl acetate (1:1) mixture, which was collected and evaporated to dryness. The yield was 22 mg, 49% (orange oil).

^1H NMR (CDCl_3 , 500 MHz): δ = 11.70 (1H, s, NH), 8.48 (1H, s, CH), 6.66 (1H, s, CH), 4.78–4.76 (2H, m, 2CH), 4.16 (5H, s, Cp), 4.13–4.10 (2H, m, 2CH) 4.04–4.02 (2H, m, CH_2), 2.19–2.15 (2H, m, CH_2), 1.46 (9H, s, t-Bu), 1.42–1.38 (4H, m, 2 CH_2), 0.98–0.92 (3H, m, CH_3).

^{13}C NMR (CDCl_3 , 126 MHz): 177.7, 162.4, 158.5, 147.0, 119.0, 118.2, 110.0, 94.0, 69.2, 64.6, 62.1, 59.5, 54.9, 35.8, 32.0, 30.4, 28.7, 22.2, 13.9.

HRMS-ESI(m/z) found 449.1886, calcd for $[\text{C}_{25}\text{H}_{32}\text{FeN}_2\text{O}_2 + \text{H}]^+$ 449.1886.

LCMS purity (UV) = 100%, t_R 23.68 min. LCMS purity (positive ion, TIC) = 96.8%, t_R 23.76 min.



***N*-Ferrocenyl-4-oxo-1-pentyl-6-phenyl-1,4-dihydropyridine-3-carboxamide, 83.**

4-Oxo-1-pentyl-6-phenyl-1,4-dihydropyridine-3-carboxylic acid (28.5 mg, 0.1 mmol) was reacted with HOBt (6.8 mg, 0.05 mmol), HBTU (57 mg, 0.15 mmol), and DIPEA (0.035 mL) in CHCl₃ (2 mL). The reaction mixture was stirred at RT for 45 min, and then aminoferrocene (24.1 mg, 0.12 mmol) was added and the mixture stirred for 24 h. Workup was as above. The orange band was eluted with a hexane/ethyl acetate (1:1) mixture, which was collected and evaporated to dryness. The yield was 29 mg, 62% (orange solid).

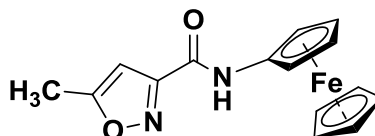
¹H NMR (CDCl₃, 500 MHz): δ = 11.80 (1H, s, NH), 8.61 (1H, s, CH), 7.56–7.52 (3H, m, Ar), 7.39–7.35 (2H, m, Ar), 6.54 (1H, s, CH), 4.80 (2H, d, J = 1.9, 2CH), 4.20 (5H, s, Cp), 4.05 (2H, d, J = 1.9, 2CH), 3.85–3.83 (2H, m, CH₂), 1.65–1.61 (2H, m, CH₂), 1.18–1.16 (4H, m, 2 CH₂), 0.81 (3H, t, J = 7.1, CH₃).

¹³C NMR (CDCl₃, 126 MHz): δ = 177.1, 162.4, 151.8, 144.8, 133.2, 130.1, 129.0, 128.5, 122.4, 119.4, 93.9, 69.2, 64.7, 62.1, 54.4, 30.6, 28.2, 21.9, 13.7.

HRMS-ESI(*m/z*): found 469.1576, calcd for [C₂₇H₂₈FeN₂O₂ + H]⁺ 469.1573.

Anal. Calcd (%) for C₂₇H₂₈FeN₂O₂: C, 69.24; H, 6.03; N, 5.98.

Found (%): C, 68.89; H, 6.13; N, 5.81.

**5-Methyl-N-ferrocenylisoxazole-3-carboxamide, 84.**

The title compound was prepared by a coupling reaction. 5-Methylisoxazole-3-carboxylic acid (127 mg, 1 mmol) was reacted with HOBT (68 mg, 0.5 mmol), HBTU (570 mg, 1.5 mmol) and DIPEA (0.35 mL) in CHCl_3 (20 mL). The reaction mixture was stirred at RT for 45 min. and then aminoferrocene (241 mg, 1.2 mmol) was added and the mixture was stirred for 24 hr. Workup was as above. During flash chromatography, the orange band was eluted with a hexane: ethyl acetate (6:4) mixture, which was collected and evaporated to dryness. The yield was 160 mg, 45% (orange solid). Crystallization by diffusion between CH_2Cl_2 and hexane provided the orange crystals.

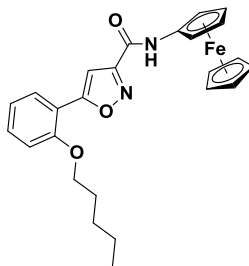
^1H NMR (CDCl_3 , 500 MHz): δ = 7.90 (1H, s, NH), 6.50 (1H, s, Ar), 4.72-4.69 (2H, m, 2CH), 4.20 (5H, s, Cp), 4.07-3.97 (2H, m, 2CH), 2.52 (3H, s, CH_3).

^{13}C NMR (CDCl_3 , 126 MHz): δ = 171.5, 158.8, 156.9, 101.4, 93.3, 76.7, 69.3, 64.9, 61.6, 12.4.

HRMS-ESI(m/z): found 311.0471, calcd. for $[\text{C}_{15}\text{H}_{14}\text{FeN}_2\text{O}_2 + \text{H}]^+$ 311.0477.

Anal. Calcd (%) for $\text{C}_{15}\text{H}_{14}\text{FeN}_2\text{O}_2$: C, 58.09; H, 4.55; N, 9.03.

Found (%): C, 58.20; H, 4.63; N, 9.13.



5-(2-(Pentyloxy)phenyl)-N-ferrocenylisoxazole-3-carboxamide, 85.

The title compound was prepared by a coupling reaction. 5-(2-(Pentyloxy)phenyl)isoxazole-3-carboxylic acid (27.5 mg, 0.1 mmol) was reacted with HOBt (6.8 mg, 0.05 mmol), HBTU (57 mg, 0.15 mmol) and DIPEA (0.035 mL) in CHCl_3 (2 mL). The reaction mixture was stirred at RT for 45 min. and then added aminoferrocene (24.1 mg, 0.12 mmol) stirred for 24 hr. Workup was as above. The orange band was eluted with a hexane: ethyl acetate (1:1) mixture, which was collected and evaporated to dryness. The yield was 34 mg, 70% (orange solid). Crystallization by diffusion between CH_2Cl_2 and hexane provided the orange crystals.

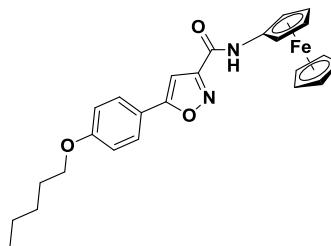
^1H NMR (CDCl_3 , 500 MHz): δ = 8.00-7.80 (2H, m, Ar), 7.44-7.39 (1H, m, Ar), 7.27 (1H, s, Ar), 7.07-6.93 (2H, m, Ar), 4.76 (2H, d, J = 1.9, 2CH), 4.23 (5H, s, Cp), 4.15 (2H, d, J = 1.9, 2CH), 4.09-3.92 (2H, m, CH_2), 1.96-1.91 (2H, m, CH_2), 1.48-1.42 (4H, m, 2 CH_2), 0.97 (3H, t, J = 7.1, CH_3).

^{13}C NMR (CDCl_3 , 126 MHz): δ = 169.5, 165.2, 159.1, 156.0, 139.8, 131.8, 127.7, 120.6, 112.2, 110.0, 102.8, 69.4, 68.7, 64.9, 61.7, 28.8, 28.2, 22.4, 14.0.

HRMS-ESI(m/z): found 481.1184, calcd. for $[\text{C}_{25}\text{H}_{26}\text{FeN}_2\text{O}_3 + \text{Na}]^+$ 481.1185.

Anal. Calcd (%) for $\text{C}_{25}\text{H}_{26}\text{FeN}_2\text{O}_3$: C, 65.51; H, 5.72; N, 6.11.

Found (%): C, 65.41; H, 5.80; N, 6.12.



5-(4-(Pentyloxy)phenyl)-*N*-ferrocenylisoxazole-3-carboxamide, 86.

The title compound was prepared by a coupling reaction. 5-(4-(Pentyloxy)phenyl)isoxazole-3-carboxylic acid (27.5 mg, 0.1 mmol) was reacted with HOBt (6.8 mg, 0.05 mmol), HBTU (57 mg, 0.15 mmol) and DIPEA (0.035 mL) in CH₂Cl₂ (2 mL). The reaction mixture was stirred at RT for 45 min. and then added aminoferrocene (24.1 mg, 0.12 mmol) stirred for 24 hr. Workup was as above. The orange band was eluted with a hexane: ethyl acetate (1:1) mixture, which was collected and evaporated to dryness. The yield was 35 mg, 72% (orange solid).

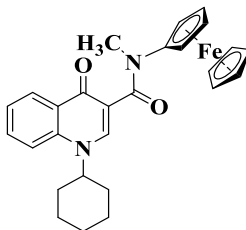
¹H NMR (CDCl₃, 500 MHz): δ = 7.94 (1H, s, Ar), 7.75-7.70 (2H, m, Ar), 7.27 (2H, s, Ar), 7.00-6.93 (2H, m, 2CH₂), 6.89 (1H, s, Ar), 4.75-4.71 (2H, m, 2CH), 4.22 (5H, s, Cp), 4.06-4.01 (2H, m, 2CH) 1.83-1.76 (2H, m, CH₂), 1.45-1.42 (4H, m, 2CH₂), 0.96 (3H, s, CH₃).

¹³C NMR (CDCl₃, 126 MHz): δ = 172.0, 161.2, 159.1, 156.9, 127.6, 119.2, 115.1, 97.5, 93.2, 69.3, 68.3, 64.9, 61.7, 28.8, 28.1, 22.4, 14.0.

HRMS-ESI(*m/z*): found 459.1333, calc. for [C₂₅H₂₆FeN₂O₃ + H]⁺ 459.1366.

Anal. Calcd (%) for C₂₅H₂₆FeN₂O₃: C, 65.51; H, 5.72; N, 6.11.

Found (%): C, 65.51; H, 5.82; N, 6.18.



1-Cyclohexyl-*N*-ferrocenyl-*N*-methyl-4-oxo-1,4-dihydroquinoline-3-carboxamide, 87.

The title compound was prepared by reacting 1-cyclohexyl-*N*-ferrocenyl-4-oxo-1,4-dihydroquinoline-3-carboxamide (110 mg, 0.2 mmol) with NaH (10 mg, 0.4 mmol) in dry DMF (5 mL). The reaction mixture was stirred at RT for 20 min, and then iodomethane (45 μ L, 0.7 mmol) was added. After stirring at RT overnight the mixture was extracted with EtOAc, then washed with brine and H₂O, dried over MgSO₄, and evaporated. A yellow band was eluted, using chromatography, with a hexane/ethyl acetate (2:3) mixture, collected, and evaporated to dryness. The yield was 38 mg, 41% (yellow solid). Crystallization by diffusion between CH₂Cl₂ and hexane provided yellow crystals.

HRMS-ESI(*m/z*): found 469.1576, calcd for [C₂₇H₂₈FeN₂O₂ + H]⁺ 469.1573.

Anal. Calcd (%) for C₂₇H₂₈FeN₂O₂: C, 69.24; H, 6.03; N, 5.98.

Found (%): C, 69.19; H, 6.10; N, 6.03.

LCMS purity (UV) = 100%, *t_R* 18.20 min. LCMS purity (positive ion, TIC) = 91.6%, *t_R* 18.27 min.

Competition Binding Assay.

Stock solutions of the compounds were prepared in DMSO and further diluted with the binding buffer to the desired concentration. Briefly, [3H]-CP-55,940 (0.5 nM), nonselective human CB₁ and CB₂ cannabinoid receptor, were added to 6 µg of membranes from CB₁- or CB₂-overexpressing CHO cells in binding buffer (50 mM Tris-HCl, 5 mM MgCl₂, 2.5 mM EDTA, 0.5 mg/mL BSA, pH 7.4). After 90 min at 30 °C, the incubation was stopped and the solutions were rapidly filtered over a UniFilter-96 GF/C glass fiber plate, presoaked in PEI (0.05%) on a Filtermate UniFilter 96-Harvester (PerkinElmer), and washed 10 times with ice-cold 50 mM Tris-HCl pH 7.4. The radioactivity on the filters was measured using a TopCount NXT microplate scintillation counter (PerkinElmer) using 30 µL of MicroScint 40 (PerkinElmer). Assays were performed at least in triplicate in three independent experiments. The nonspecific binding was determined in the presence of 5 µM (R)-(+)-WIN 55,212-2 (Sigma).

Cell-Based HTRF cAMP Assay.

Cellular cAMP levels were measured using reagents supplied by Cisbio International (HTRF dynamic 2 cAMP kit). Briefly, CHO-CB₂ cells were harvested and were collected by centrifugation for 5 min at 1200 rpm. The cells were then resuspended in an appropriate final volume of culture medium and incubated with the phosphodiesterase inhibitor IBMX (0.5 mM). Cells were incubated for 15 min with the compounds at room temperature in a 384-well plate (2000 cells per well) before the addition of forskolin (3 µM) for 30 min at room temperature. The dye d2-conjugated cAMP and Europium cryptate-conjugated anti-cAMP antibodies were added to the assay plate, according to the manufacturer's instructions. After 1 h incubation at room temperature, the plate was read on a Spectramax microplate reader (Molecular Devices) with excitation wavelength at 340 nm and emission wavelengths at 665 and 620 nm.

Cell Culture and Proliferation Assay.

CHO-WT, CHO-CB₂, and HT29 cells were grown at 37 °C in a humidified atmosphere containing 5% CO₂, in DMEM-GlutaMAX medium (Life Technologies) supplemented with 10% fetal bovine serum, penicillin (100 IU/mL), and streptomycin (100 µg/mL). In the cell proliferation assay, cells were plated in triplicate on 96-well plates (3 × 10³ cells per well) and incubated for 24 h. Cells were then incubated in culture medium that contained 10 µM test compounds. After 72 h, cell growth was estimated by the colorimetric MTS test.

X-ray Crystallography.

Single-crystal X-ray diffraction analyses were performed using a Rigaku FRE+ equipped with either VHF (**78,80**) or HF Varimax confocal mirrors (**79, 87**), an AFC10 goniometer, and an HG Saturn 724+ detector equipped with an Oxford Cryosystems low-temperature apparatus operating at T = 100(2) K.⁶¹ CrystalClear-SM Expert 3.1 b27 was used to record images, process data, and apply empirical absorption corrections, and unit cell parameters were refined against all data. The structures were solved by charge flipping using SUPERFLIP and refined on F_o² by full-matrix least-squares refinements using SHELXL-2012⁶² as implemented within OLEX2. All non-hydrogen atoms were refined with anisotropic displacement parameters. Hydrogen atoms were added at calculated positions except those attached to heteroatoms, which were located from the difference map and restrained to a reasonable geometry. All hydrogen atoms were refined using a riding model with isotropic displacement parameters based on the equivalent isotropic displacement parameter (U_{eq}) of the parent atom. Figures were produced using OLEX2^{iv}. The CIF files for the crystal structures of **78-80** and **87** have been deposited with the CCDC and have been given the deposition numbers 1479553–1479556, respectively.⁴ Those for **84, 85** will be deposited once we publish this work.

2.7 References

- 1 K. Schlotter, F. Boeckler, H. Hübner and P. Gmeiner, *J. Med. Chem.*, 2005, **48**, 3696–3699.
- 2 A. Tourteau, N. Leleu-Chavain, M. Body-Malapel, V. Andrzejak, A. Barczyk, M. Djouina, B. Rigo, P. Desreumaux, P. Chavatte and R. Millet, *Bioorganic Med. Chem. Lett.*, 2014, **24**, 1322–1326.
- 3 A. Tourteau, V. Andrzejak, M. Body-Malapel, L. Lemaire, A. Lemoine, R. Mansouri, M. Djouina, N. Renault, J. El Bakali, P. Desreumaux, G. G. Muccioli, D. M. Lambert, P. Chavatte, B. Rigo, N. Leleu-Chavain and R. Millet, *Bioorganic Med. Chem.*, 2013, **21**, 5383–5394.
- 4 W. Tuo, N. Leleu-Chavain, J. Spencer, S. Sansook, R. Millet and P. Chavatte, *J. Med. Chem.*, 2017, **60**, 4–46.
- 5 Repapetitto, Heterotrimeric G-protein activation/deactivation cycle in the context of GPCR signaling,
https://upload.wikimedia.org/wikipedia/commons/c/c9/GPCR_cycle.jpg,
(accessed 21 December 2016).
- 6 A. L. Hopkins and C. R. Groom, *Nat. Rev. Drug Discov.*, 2002, **1**, 727–30.
- 7 E. Jacoby, R. Bouhelal, M. Gerspacher and K. Seuwen, *ChemMedChem*, 2006, **1**, 760–782.
- 8 S. Galiegue, S. Mary, J. Marchand, D. Dussossoy, D. Carriere, P. Carayon, M. Bouaboula, D. Shire, G. Fur and P. Casellas, *Eur. J. Biochem.*, 1995, **232**, 54–61.
- 9 W. A. Devane, L. Hanus, A. Breuer, R. G. Pertwee, L. A. Stevenson, G. Griffin, D. Gibson, A. Mandelbaum and A. Etinger, *Science (80-.)*, 1992, **258**, 1946–1949.
- 10 L. De Petrocellis, D. Melck, a Palmisano, T. Bisogno, C. Laezza, M. Bifulco and V. Di Marzo, *Proc. Natl. Acad. Sci. U. S. A.*, 1998, **95**, 8375–8380.
- 11 T. Sugiura, S. Kondo, A. Sukagawa, S. Nakane, A. Shinoda, K. Itoh, A. Yamashita and K. Waku, *Biochem Biophys Res Commun*, 1995, 215, 89–97.
- 12 T. P. Dinh, T. F. Freund and D. Piomelli, *Chem. Phys. Lipids*, 2002, **121**, 149–158.
- 13 T. Sugiura, T. Kodaka, S. Nakane, T. Miyashita, S. Kondo, Y. Suhara, H. Takayama, K. Waku, C. Seki, N. Baba and Y. Ishima, *J. Biol. Chem.*, 1999, **274**, 2794–2801.
- 14 N. Leleu-Chavain, M. Body-Malapel, J. Spencer, P. Chavatte, P. Desreumaux and

- R. Millet, *Curr. Med. Chem.*, 2012, **19**, 3457–3474.
- 15 K. Wright, N. Rooney, M. Feeney, J. Tate, D. Robertson, M. Welham and S. Ward, *Gastroenterology*, 2005, **129**, 437–453.
- 16 J. Guindon and a G. Hohmann, *Br. J. Pharmacol.*, 2008, **153**, 319–334.
- 17 J. L. Shoemaker, M. B. Ruckle, P. R. Mayeux and P. L. Prather, *J. Pharmacol. Exp. Ther.*, 2005, **315**, 828–838.
- 18 D. G. Demuth and A. Molleman, *Life Sci.*, 2006, **78**, 549–563.
- 19 W. Yang, Q. Li, S.-Y. Wang, F. Gao, W.-J. Qian, F. Li, M. Ji, X.-H. Sun, Y. Miao and Z. Wang, *Neuroscience*, 2016, **313**, 213–24.
- 20 C. A. Lunn, E.-P. Reich, J. S. Fine, B. Lavey, J. A. Kozlowski, R. W. Hipkin, D. J. Lundell and L. Bober, *Br. J. Pharmacol.*, 2008, **153**, 226–239.
- 21 G. Ragusa, M. Gómez-Cañas, P. Morales, D. P. Hurst, F. Deligia, R. Pazos, G. A. Pinna, J. Fernández-Ruiz, P. Goya, P. H. Reggio, N. Jagerovic, M. García-Arencibia and G. Murineddu, *Eur. J. Med. Chem.*, 2015, **101**, 651–667.
- 22 P. Yang, K.-Z. Myint, Q. Tong, R. Feng, H. Cao, A. A. Almhizia, M. H. Alqarni, L. Wang, P. Bartlow, Y. Gao, J. Gertsch, J. Teramachi, N. Kurihara, G. D. Roodman, T. Cheng and X.-Q. Xie, *J. Med. Chem.*, 2012, **55**, 9973–9987.
- 23 C. A. Lunn, J. S. Fine, A. Rojas-Triana, J. V Jackson, X. Fan, T. T. Kung, W. Gonsiorek, M. A. Schwarz, B. Lavey, J. A. Kozlowski, S. K. Narula, D. J. Lundell, R. W. Hipkin and L. A. Bober, *J. Pharmacol. Exp. Ther.*, 2006, **316**, 780–788.
- 24 C. C. Felder, K. E. Joyce, E. M. Briley, J. Mansouri, K. Mackie, O. Blond, Y. Lai, A. L. Ma and R. L. Mitchell, *Mol Pharmacol*, 1995, **48**, 443–450.
- 25 M. M. Ahmed, S. Rajpal, C. Sweeney, T. A. Gerovac, B. Allcock, S. McChesney, A. U. Patel, J. I. Tilghman, G. S. Miranpuri and D. K. Resnick, *Spine J.*, 2010, **10**, 1049–1054.
- 26 S. Sreevalsan and S. Safe, *Mol Cancer Ther*, 2013, **12**, 2483–2493.
- 27 M. M. Ibrahim, H. Deng, A. Zvonok, D. A. Cockayne, J. Kwan, H. P. Mata, T. W. Vanderah, J. Lai, F. Porreca, A. Makriyannis and T. P. Malan, *Proc. Natl. Acad. Sci. U. S. A.*, 2003, **100**, 10529–33.
- 28 M. Rinaldi-Carmona, F. Barth, J. Millan, J. M. Derocq, P. Casellas, C. Congy, D. Oustric, M. Sarran, M. Bouaboula, B. Calandra, M. Portier, D. Shire, J. C. Breliere and G. L. Le Fur, *J. Pharmacol. Exp. Ther.*, 1998, **284**, 644–650.
- 29 M. Portier, M. Rinaldi-Carmona, F. Pecceu, T. Combes, C. Poinot-Chazel, B. Calandra, F. Barth, G. le Fur and P. Casellas, *J. Pharmacol. Exp. Ther.*, 1999, **288**,

- 582–589.
- 30 M. Bouaboula, D. Dussosoy and P. Casellas, *Biochemistry*, 1999, **274**, 20397–20405.
- 31 R. A. Ross, H. C. Brockie, L. A. Stevenson, V. L. Murphy, F. Templeton, A. Makriyannis and R. G. Pertwee, *Br. J. Pharmacol.*, 1999, **126**, 665–72.
- 32 D. C. Geng, Y. Z. Xu, H. L. Yang, X. S. Zhu, G. M. Zhu and X. B. Wang, *J. Biomed. Mater. Res. - Part A*, 2010, **95**, 321–326.
- 33 E. Stern, G. G. Muccioli, R. Millet, J.-F. Goossens, A. Farce, P. Chavatte, J. H. Poupaert, D. M. Lambert, P. Depreux and J.-P. Hénichart, *J. Med. Chem.*, 2006, **49**, 70–79.
- 34 E. Stern, E. Stern, G. G. Muccioli, G. G. Muccioli, B. Bosier, B. Bosier, L. Hamtiaux, L. Hamtiaux, R. Millet, R. Millet, J. H. Poupaert, J. H. Poupaert, J.-P. Hénichart, J.-P. Hénichart, P. Depreux, P. Depreux, J.-F. Goossens, J.-F. Goossens, D. M. Lambert and D. M. Lambert, *J. Med. Chem.*, 2007, **50**, 5471–5484.
- 35 J. El Bakali, G. G. Muccioli, N. Renault, D. Pradal, M. Body-Malapel, M. Djouina, L. Hamtiaux, V. Andrzejak, P. Desreumaux, P. Chavatte, D. M. Lambert and R. Millet, *J. Med. Chem.*, 2010, **53**, 7918–7931.
- 36 J. El Bakali, P. Gilleron, M. Body-Malapel, R. Mansouri, G. G. Muccioli, M. Djouina, A. Barczyk, F. Klupsch, V. Andrzejak, E. Lipka, C. Furman, D. M. Lambert, P. Chavatte, P. Desreumaux and R. Millet, *J. Med. Chem.*, 2012, **55**, 8948–8952.
- 37 D. G. Deutsch, N. Ueda and S. Yamamoto, *Prostaglandins Leukot. Essent. Fat. Acids*, 2002, **66**, 201–210.
- 38 N. R. Bachur and S. Udenfriend, *J. Biol. Chem.*, 1966, **241**, 219–222.
- 39 D. G. Deutsch and S. A. Chin, *Biochem. Pharmacol.*, 1993, **46**, 791–796.
- 40 M. Mor, A. Lodola, S. Rivara, F. Vacondio, A. Duranti, A. Tontini, S. Sanchini, G. Piersanti, J. R. Clapper, A. R. King, G. Tarzia and D. Piomelli, *J. Med. Chem.*, 2008, **51**, 3487–3498.
- 41 J. Garfinkle, C. Ezzili, T. J. Rayl, D. G. Hochstatter, I. Hwang and D. L. Boger, *J. Med. Chem.*, 2008, **51**, 4392–4403.
- 42 R. Ahmedi and T. Lanez, *Asian J Chem*, 2010, **22**, 299–306.
- 43 M. Zanozi and Z. Bayat, *Der Chem. Sin.*, 2011, **2**, 288–293.
- 44 J. Skiba, C. Schmidt, P. Lippmann, P. Ensslen, H.-A. Wagenknecht, R. Czerwieńec, F. Brandl, I. Ott, T. Bernaś, B. Krawczyk, D. Szczukocki and K.

- Kowalski, *Eur. J. Inorg. Chem.*, 2017, **2017**, 297–305.
- 45 N. Chavain and C. Biot, *Curr. Med. Chem.*, 2010, **17**, 2729–2745.
- 46 J. Spencer, A. P. Mendham, A. K. Kotha, S. C. W. Richardson, E. A. Hillard, G. Jaouen, L. Male and M. B. Hursthouse, *Dalt. Trans.*, 2009, **9226**, 918–921.
- 47 J. Spencer, J. Amin, M. Wang, G. Packham, S. S. S. Alwi, G. J. Tizzard, S. J. Coles, R. M. Paranal, J. E. Bradner and T. D. Heightman, *Med. Chem. Lett.*, 2011, 358–362.
- 48 C. Biot, *Curr. Med. Chem. - Anti-Infective Agents*, 2004, **3**, 135–147.
- 49 R. A. Hussain, A. Badshah, M. Sohail, B. Lal and K. Akbar, *J. Mol. Struct.*, 2013, **1048**, 367–374.
- 50 E. M. Lewandowski, J. Skiba, N. J. Torelli, A. Rajnisz, J. Solecka, K. Kowalski and Y. Chen, *Chem. Commun.*, 2015, **51**, 6186–6189.
- 51 M. Saleem, H. Yu, L. Wang, Zain-ul-Abdin, H. Khalid, M. Akram, N. M. Abbasi and J. Huang, *Anal. Chim. Acta*, 2015, **876**, 9–25.
- 52 B. Kuhn, P. Mohr and M. Stahl, *J. Med. Chem.*, 2010, **53**, 2601–2611.
- 53 S. J. Govaerts, E. Hermans and D. M. Lambert, *Eur. J. Pharm. Sci.*, 2004, **23**, 233–243.
- 54 B. Horváth, L. Magid, P. Mukhopadhyay, S. Bátkai, M. Rajesh, O. Park, G. Tanchian, R. Y. Gao, C. E. Goodfellow, M. Glass, R. Mechoulam and P. Pacher, *Br. J. Pharmacol.*, 2012, **165**, 2462–2478.
- 55 P. Marini, M. G. Cascio, A. King, R. G. Pertwee and R. A. Ross, *Br. J. Pharmacol.*, 2013, **169**, 887–899.
- 56 R. N. Bose, L. Maurmann, R. J. Mishur, L. Yasui, S. Gupta, W. S. Grayburn, H. Hofstetter, T. Salley and T. Milton, *Proc. Natl. Acad. Sci. U. S. A.*, 2008, **105**, 18314–9.
- 57 S. Sansook, W. Tuo, L. Lemaire, A. Tourteau, A. Barczyk, X. Dezitter, F. Klupsch, N. Leleu-Chavain, G. J. Tizzard, S. J. Coles, R. Millet and J. Spencer, *Organometallics*, 2016, **35**, 3361–3368.
- 58 M. Librizzi, A. Longo, R. Chiarelli, J. Amin, J. Spencer and C. Luparello, .
- 59 G. Jaouen, A. Vessières and S. Top, *Chem. Soc. Rev.*, 2015, **44**, 8802–17.
- 60 A. Leonidova, P. Anstaett, V. Pierroz, C. Mari, B. Spingler, S. Ferrari and G. Gasser, *Inorg. Chem.*, 2015, **54**, 9740–9748.
- 61 S. J. Coles and P. A. Gale, *Chem. Sci.*, 2012, **3**, 683–689.
- 62 G. M. Sheldrick, *Acta Crystallogr. Sect. A Found. Crystallogr.*, 2015, **71**, 3–8.

Chapter 3

Synthesis of HDAC inhibitors containing a ferrocene unit.

3.1 Overview

Benzamide compounds containing ferrocene have been synthesized and their application as HDAC inhibitors has been studied. The products were characterized by elemental analyses, NMR spectroscopy, mass spectrometry, LC-MS, IR spectroscopy and some were further analysed by X-ray crystallographic studies. One of them, *N*¹-(2-aminophenyl)-*N*⁸-ferrocenyloctanediamide, (*Pojamide*) **111** displayed nanomolar potency vs. HDAC3 compared to **RGFP966**, a potent and selective HDAC3 inhibitor. *Pojamide* had better activity in HCT116 colorectal cancer cell invasion assays; however, **TCH106** and **Romidepsin**, potent HDAC1 inhibitors, are more effective than *Pojamide* in cellular proliferation and colony formation assays. These latter's data propose that HDAC 1 & 3 *polypharmacology* (acting on multiple targets) is amenable to achieving maximum anti-cancer advantages. *Pojamide* has also been investigated in redox-pharmacology and its activity rationalised by molecular modelling. Indeed, treating HCT116 cells (Human colon carcinoma) with *Pojamide* and SNP (sodium nitroprusside) led to greatly enhanced cytotoxicity and DNA damage attributed to activation to an Fe(III) species.

3.2 Introduction

Histone deacetylases (HDACs) are a class of enzymes which remove acetyl groups (H₃C-C=O) from histones, which are proteins that DNA wraps around in the nucleus. HDACs have been classified into three classical HDAC classes which contain 11 HDACs according to their subcellular location, homology to yeast proteins, and enzymatic activities, there are Class I (HDAC 1, 2, 3, 8), Class IIa (HDAC 4, 5, 7, 9), Class IIb (HDAC6, 10) and Class IV (HDAC11) as well as sirtuins.¹ HDACs are promising therapeutic targets for cancer treatment. HDAC inhibitors (HDACis) are a class of therapeutics with potential as anticancer drugs and can be classified into several groups

by their functional groups that can bind to the zinc ion of the HDAC such as hydroxamic acids (or hydroxamates), thiols, benzamides, electrophilic ketones and aliphatic acid compounds.² Their pharmacophore contains a cap-linker-ZBG (zinc binding group) (Figure 3.2). Well known HDACis include suberoylanilide hydroxamic acid (**SAHA** or Vorinostat) and Romidepsin³ which are clinically useful anticancer agents that have received Food and Drug Administration approval for treating patients with cutaneous T-cell lymphoma.⁴⁻⁵ Selective inhibitors of HDAC3 such as **TCH106** and **RGFP966**⁶ usually contain a benzamide (or ortho-anilide) ZBG and are found in CNS applications² and cancer.⁷ Recent studies using HDAC3-overexpressing HCT116 cells showed that silencing individual HDACs (1-3) through RNA interference (RNAi) is insufficient to achieve similar levels of growth arrest and apoptosis induced by unselective HDACis e.g. **Trichostatin A**⁸ (Figure 3.2).

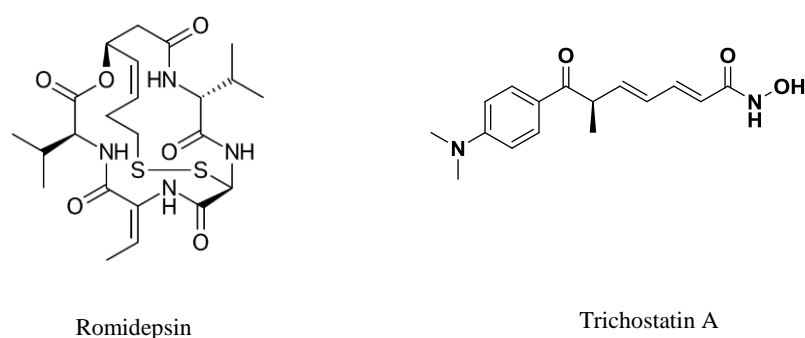


Figure 3.1. Romidepsin and Trichostatin A.

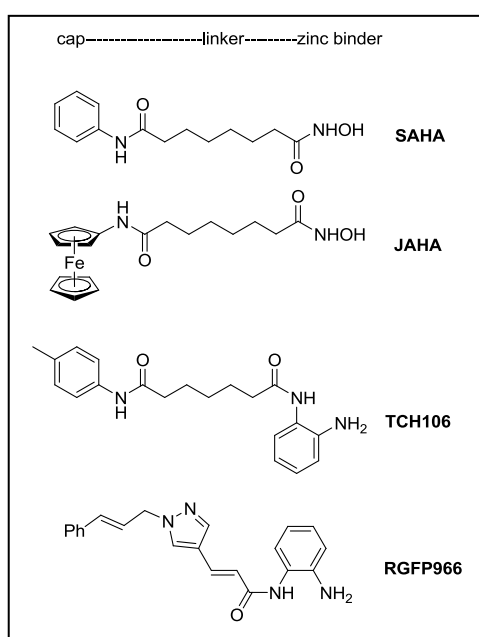


Figure 3.2. Hydroxamic acid based SAHA, JAHA and known selective benzamide HDAC3is.

The binding mode of **SAHA** in HDAC3 (PDB code: 1T69) is shown in Figure 3.4.¹¹

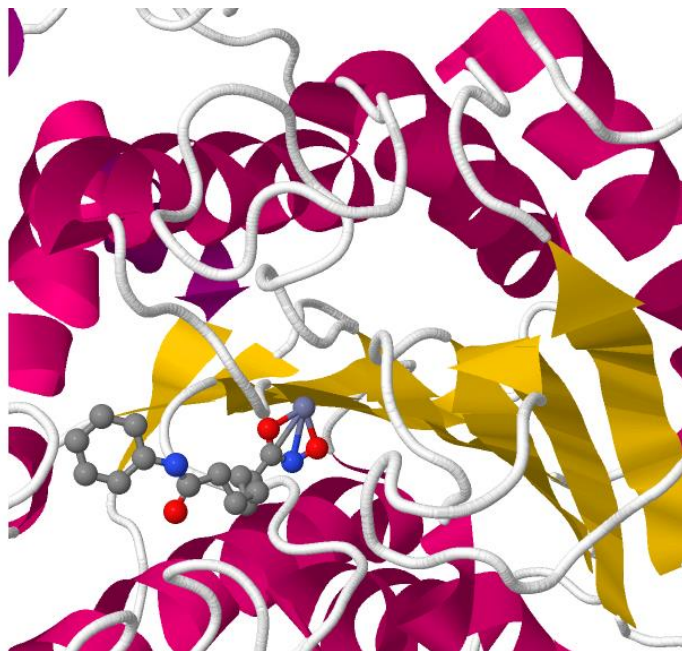
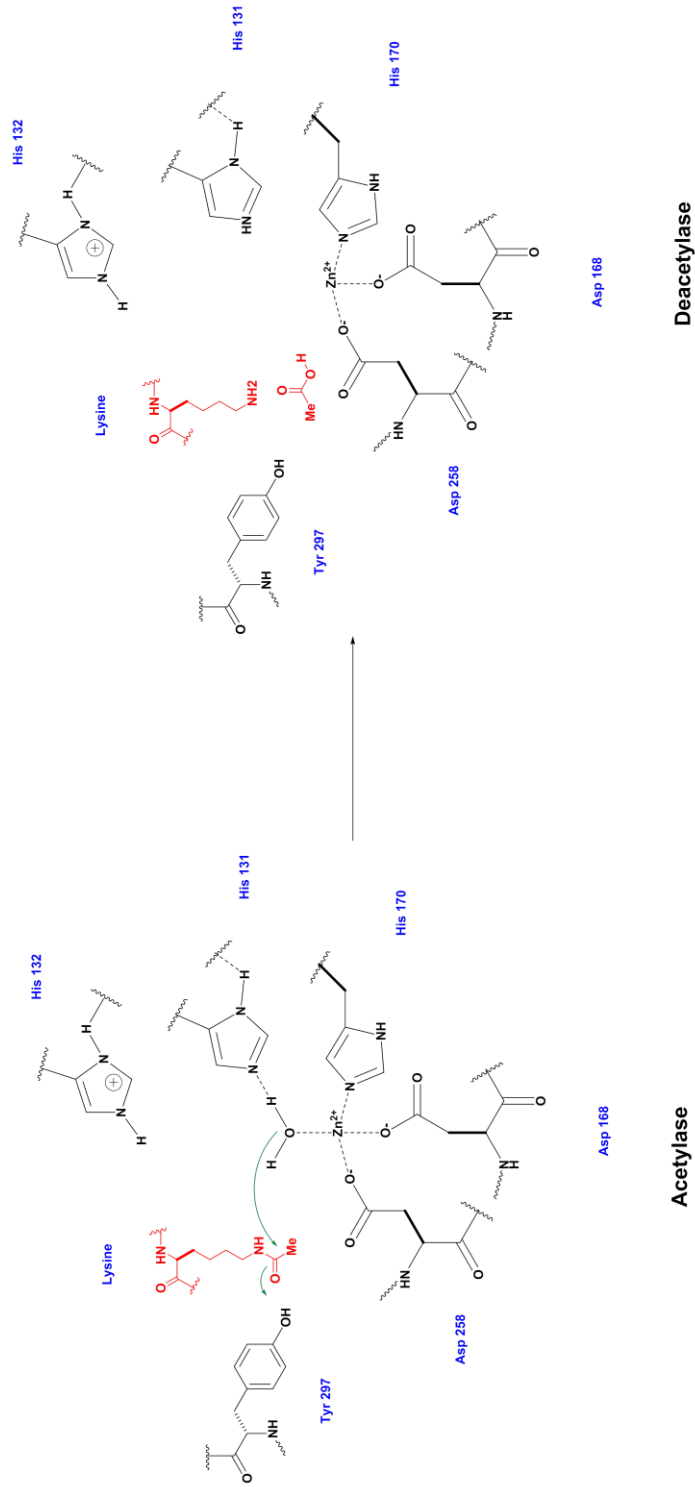


Figure 3.4. Cocrystal structure of **SAHA** in HDAC8.

The role of zinc in HDACs (Scheme 3.1) is to activate water, which attacks an acetyl group leading to a deacetylated lysine. Designing an inhibitor to bind to zinc will block this deacetylation and leave an acetylated lysine.



Scheme 3.1. Mechanism of deacetylation of histones by HDACs.

Transition metal-based anticancer agents are increasing rapidly because of the ability of a metal atom to help solve protein x-ray crystal structures, undergo redox and ligand exchange reactions and the variety of coordination numbers to provide different geometries and oxidation states that cannot be achieved with organic therapeutics.¹²⁻¹³ Many metal complexes have been synthesized and their applications have been studied such as platinum, ruthenium, rhodium, iridium, iron and so on.¹⁴ Polyoxometalate-based HDAC inhibitors have also been synthesized and studied.¹⁵

A novel anti-cancer platinum complex, *cis*-[Pt^{II}(NH₃)₂(malSAHAH₂)], **90** has been published as a bifunctional drug candidate (DNA binding, (Pt^{II}) and HDACi, (malSAHA)) and the results showed that the cytotoxicity of **90** (IC₅₀ 9 ± 3 μM) is comparable to cisplatin (IC₅₀ 2.9 ± 0.1 μM) against ovarian cancer cell lines A2780P and they found the presence of the HDACi, malSAHA (**89**) in **90**, is thus enhancing its cytotoxicity.¹⁶

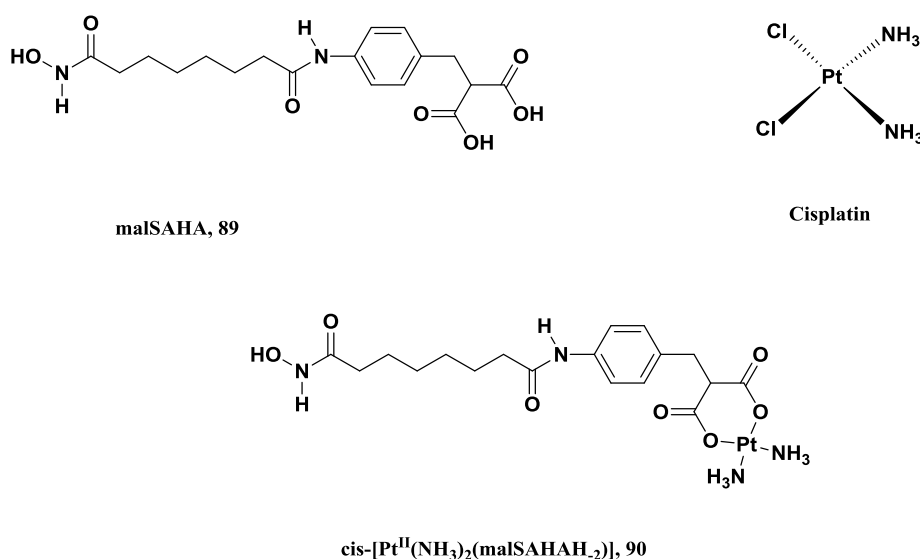


Figure 3.5. malSAHA **89**, Pt(II) complex **90** and cisplatin.

Ru^{II}, **91** and Rh^{III}, **92** complexes have been synthesized and their applications as HDAC inhibitors have been studied, which provided antiproliferative activity against H460 non-small cell lung carcinoma cells that is comparable to the clinically used HDAC inhibitor suberoylanilide hydroxamic acid (SAHA).¹⁷

A series of cyclometalated Ir(III) complexes as HDACis and photodynamic therapeutic agents have been studied. Compounds **97**, **98**, **99** and **100** showed potent cytotoxicity towards the cancer cell lines screened and show much lower phototoxicity against human normal cells. **97** induces apoptotic cell death and under UV light irradiation, the biological effects of **97** are significantly enhanced (Figure 3.8).¹⁹

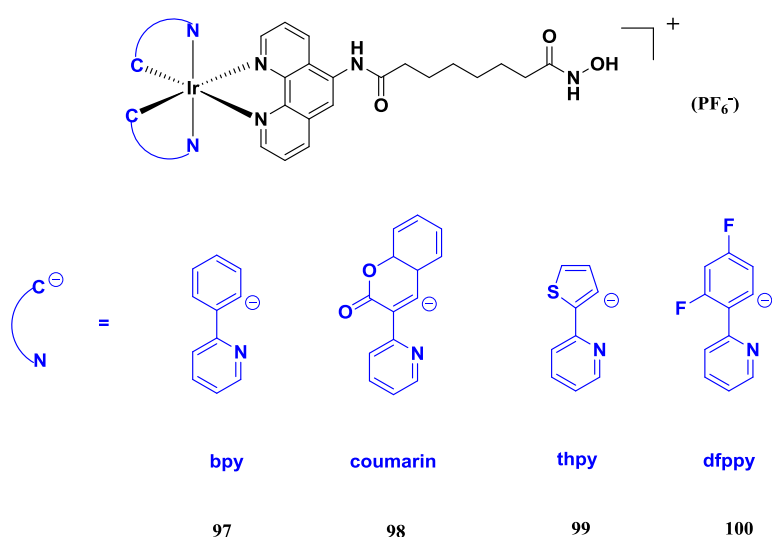


Figure 3.8. Cyclometalated Ir(III) complexes **97**, **98**, **99** and **100**.

Earlier work from Spencer and co-workers described *N*⁸-ferrocenyl-*N*¹-hydroxy-octanediamine (JAHA; “Jay Amin Hydroxamic Acid”), an analogue of SAHA, containing a ferrocenyl group as a phenyl bioisostere. JAHA analogues **35** displayed anticancer activity and inhibition of several HDACs.²⁰ “Click JAHA” **36** also had good HDAC inhibition, (Figure 3.9).²¹

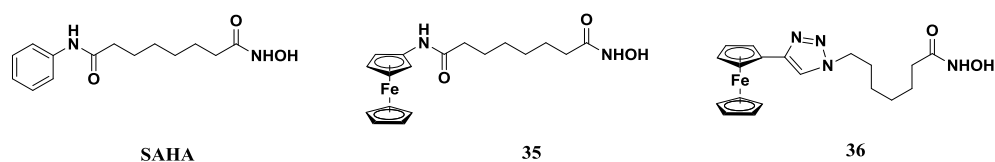


Figure 3.9. SAHA, JAHA **35** and click JAHA **36**.

Gasser's group has shown the synthesis of light activated organometallic HDAC inhibitors, p-Fc-SAHA (**41**), that release a JAHA-type HDAC inhibitor,²² as shown in the cleavable linker (Figure 3.10).

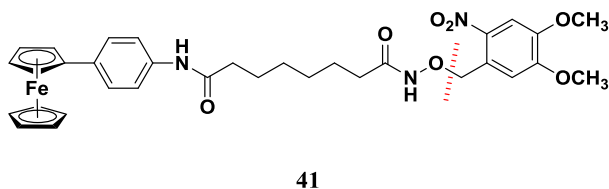


Figure 3.10. Light activatable organometallic HDAC inhibitor, p-Fc-SAHA.

A hydroxamic acid compound has been synthesized by replacing the phenyl ring in **SAHA** with a $[\text{Re}(\text{CO})_3(\text{Cp})]$ bioisostere (Figure 3.11) and its cytotoxicity is in the same range as **SAHA**.²³

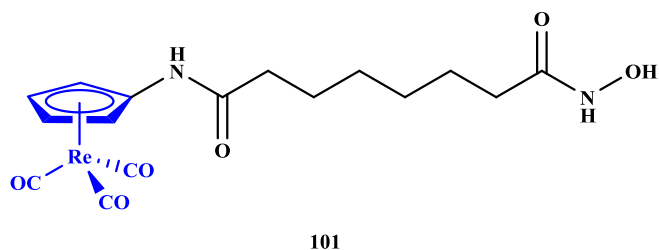
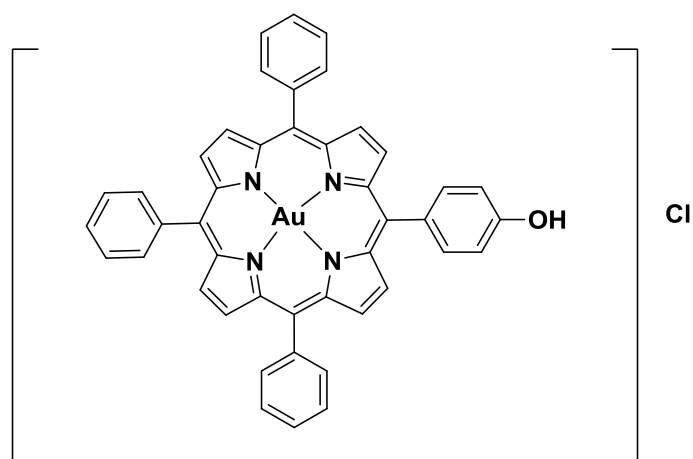


Figure 3.11. Re-HDACi **101**.

A gold (III) complex has been synthesized and its cytotoxicity was studied in a panel of human breast cancer cell lines, which was 100-fold to 3,000-fold higher than that of cisplatin (Figure 3.12).²⁴



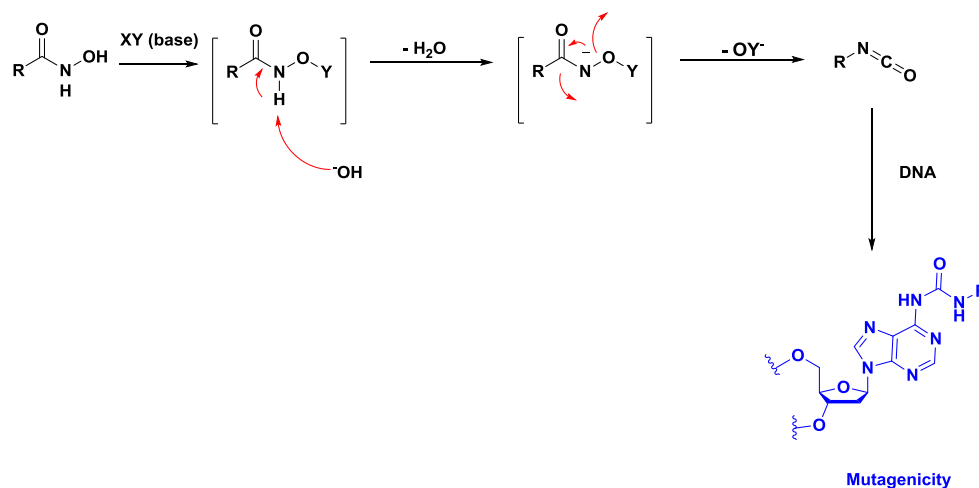
102

Figure 3.12. Au-HDACi 102.

Hence, metal based HDACis show much promise in cancer therapy. Our studies on the design of a HDAC3i are now described.

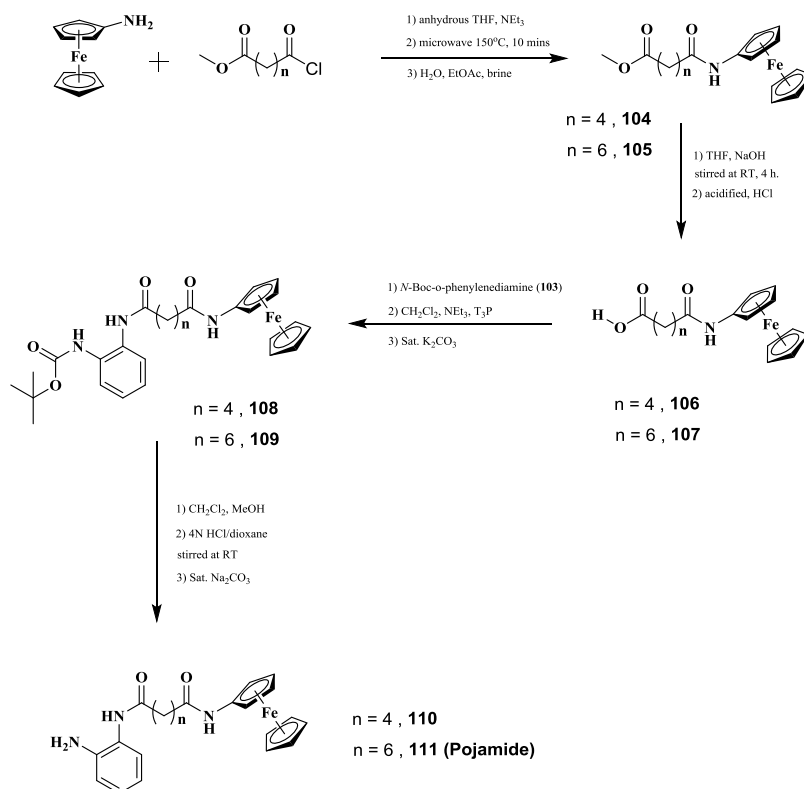
3.3 Results and Discussion

We wished to extend our JAHA chemistry to *ortho*-anilide (benzamide) analogues, hoping that this may lead to HDAC3-specificity and lower toxicity issues documented for hydroxamate ZBGs; for example, a Lossen rearrangement will transform an activated hydroxamate into isocyanate and lead to the known toxicity of hydroxamic acids (Scheme 3.2).²⁵



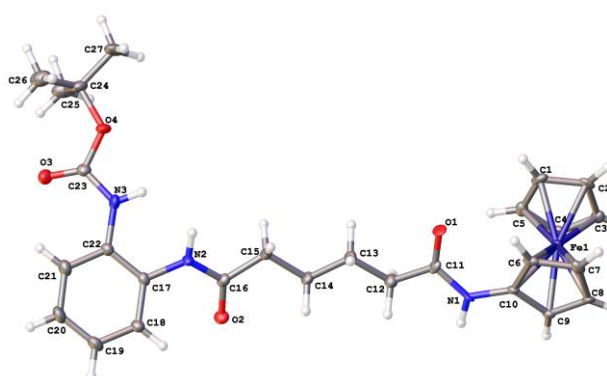
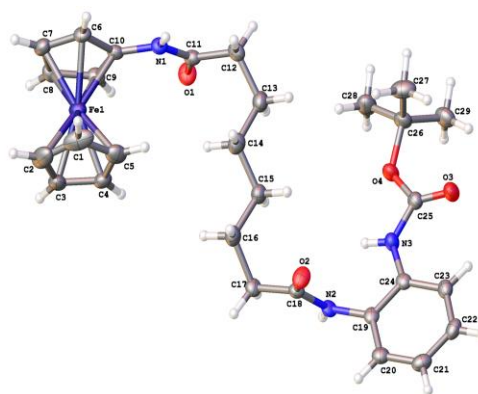
Scheme 3.2. Lossen rearrangement of hydroxamate.

The synthesis of the benzamides **110** and **111** (Pojamide) is shown in Scheme 3.3. Hence, the amide coupling of ferrocenyl amine with an acid chloride led to the amides **104** and **105**. Hydrolysis of the terminal ester groups led to the carboxylic acids **106** and **107** which were coupled to give the Boc-protected benzamides **108** and **109**. Acid deprotection gave the final benzamides **110** and **111**.



Scheme 3.3. Synthesis of **110** and Pojamide, **111**.

Compounds **108** and **109** were characterised in the solid state by X-ray crystallography (Figure 3.13).²⁶

**108****109****Figure 3.13.** X-ray structures of **108** and **109**.

We confirmed Pojamide's HDAC3-specificity on a panel of HDACs vs. **110**, SAHA and known HDAC3is (Table 3.1). Also both **110** and Pojamide displayed ca. 14- and 20-fold selectivity respectively towards HDAC3 over HDACs 1/2 and significantly greater selectivity over HDACs 4-8. Indeed, Pojamide showed an impressive IC₅₀ of 82 nM vs HDAC3. Pojamide's profile was similar to **TCH106**, but it was less active than **RGFP966** in its HDAC3-selectivity. Only SAHA displayed activity vs. HDAC8.

Table 3.1.

HDAC	IC ₅₀ (μ M)				
	SAHA ^[a]	110	Poj ^[a]	RGFP966	TCH106 ^[b]
1	0.005	8.94	1.19	0.611	0.389
2	0.015	13.79	1.64	0.576	1.262
3	0.009	0.606	0.082	0.015	0.049
4	11.23	>30	>30	>30	>30
5	9.82	>30	>30	>30	>30
6	0.02	>30	>30	>30	>30
7	>30	>30	>30	>30	>30
8	0.472	>30	>30	>30	>30

[a] Profiling done in duplicate, n=8. All others n=4; [b] Slow, tight-binding inhibitor, with inverted IC₅₀ and K_i values, causes IC₅₀ value to drop over longer pre-incubation periods.²⁹

Biochemical evaluation vs HDAC isoforms 1 – 8.

3.3.1 Modelling. (Contributed with help by Rhiannon Jones)

To explore the binding modes of **110** and **111** (Pojamide) in HDAC3 we performed docking studies using the recently published structure of HDAC3.²⁷ Docking was performed using molecular mechanics GLIDE 6.5 in Schrodinger Suite 2014-4.²⁸ The docking protocol uses molecular mechanics to predict the strength of non-covalent interactions and provides a scoring function. This was used to consider possible binding modes and the associated conformational changes within receptor active sites. We found that Pojamide bound the zinc active-site forming hydrogen bonds between the N-H of the amide and the carbonyl of Asp93, the (ortho-anilide) benzamide amide N-H and the carbonyl of Gly143, the aniline NH₂ and the nitrogen of His134 and the carbonyl of Asp170 as well as the characteristic benzamide-zinc interaction. **110** is docked slightly shifted from Pojamide. It forms hydrogen bonds with Asp93 and Gly143. However, the substitution of the 6-carbon aliphatic chain for a 4-carbon chain results in a rotation of the benzamide group leading to a loss of key interactions, namely, hydrogen bonding with His134 and Asp170 as well as forcing zinc coordination from the benzamide aniline to the amide carbonyl. Docking poses of **111**(Pojamide) and **110** in HDAC3 (PDB code: 4A69). Top docking poses of **111** (slate, A) and **110** (teal, B) in HDAC3. C) Superposition of the active site of HDAC3 (grey) and HDAC8^{6,29} (PDB code: 1T69, green) showing key residues overlaid with **111** top docking pose in HDAC3. Colour Scheme: Hydrogen bonds shown in black dashed lines, π - π interactions shown in green dashed lines.

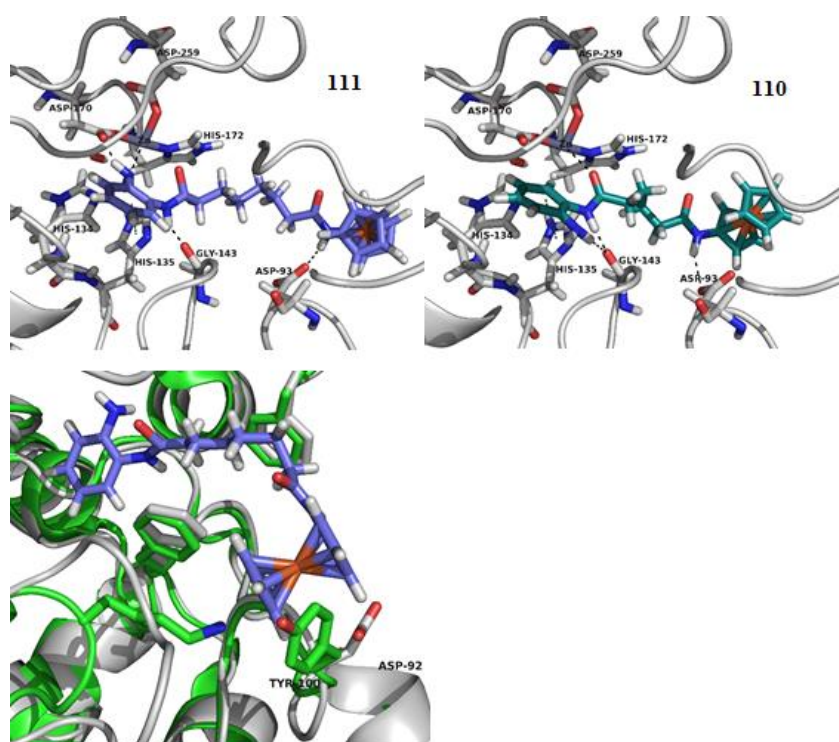


Figure 3.14. Docking poses of **111** (Pojamide) and **110** in HDAC3.

3.4 Biological Results (contributed by Dr Cory A. Ocasio)

We attempted to explore the inhibitory activity of the benzamides in HDAC3 overexpressing cervical and colorectal cancer cell lines. HeLa, HT-29 and HCT116 cells are tumour forming cell lines that have been used previously as model systems to characterise HDAC3s.^{8,30} We confirmed in this study the malignant cancer cell lines HeLa, HT-29 and HCT116 had high HDAC3 expression levels (Figure 3.15A). However, immortalised Retinal Pigment Epithelium (RPE) cells, which do not form tumours and have a longer lifespan, and cannot form tumours, had low HDAC3 levels.

Based on these data, this small panel of cell lines was treated with increasing concentrations of **110**, **111** (Pojamide) and the control HDAC3i **RGFP966** and **TCH106**. **RGFP966** shows a 5.5-fold greater potency than Pojamide in blocking HDAC3 activity (Table 3.1), yet it was found that **RGFP966** and Pojamide are comparable at inhibiting HCT116 cellular proliferation, displaying GC_{50} values of 8.9 and 8.6 μ M respectively (Figure 3.15B). RPE cells were as sensitive to Pojamide as HCT116 cells, but were not inhibited by **RGFP966**. **TCH106** displayed superior potency against all cell lines with

GC₅₀ values ranging from 1 – 2 μM and completely blocked colony formation at 10 μM in HCT116 colony formation assays compared to 75 and 60% inhibition of colony formation by Pojamide and **RGFP966** respectively (Figures 3.15B-F). Interestingly, **TCH106** is 1.5- and 3-fold more potent toward HDAC1 inhibition over **RGFP966** and Pojamide respectively and proliferating RPE cells have been shown to overexpress HDACs 1, 2 and 5,³¹ suggesting that HDAC1 inhibition is in part responsible for the anti-proliferative effects of Pojamide and **TCH106** in these cell lines. In fact, cellular proliferation and colony formation assays using Romidepsin, a very potent and selective HDAC1/2 inhibitor (reported IC₅₀ values of 36 and 47 nM respectively),³² revealed a GC₅₀ value of 0.52 ± 0.02 nM and near complete inhibition of colony formation at 0.5 nM; clearly the most potent anti-proliferative HDACi tested in this study. HeLa and HT-29 cells were only mildly inhibited by Pojamide and **RGFP966** showing maximal growth inhibition of ~40 and 30% at 10 μM respectively, and in all cases compound **110** was ineffective at inhibiting cellular proliferation.

Next, to establish the anti-invasive properties of Pojamide against known HDACis, we investigated the effects of **RGFP966**, **TCH106** and Pojamide on HCT116 cellular invasion. In this assay, we decided to test compounds at 1x and 0.1x of their GC₅₀ value determined using the HCT116 cellular proliferation assay. At the lowest concentrations tested, only Pojamide demonstrated robust inhibition of invasion, with about 70% inhibitory activity; however, at the 1x concentrations both **RGFP966** and Pojamide, exhibiting ca. 40 and 15-fold selectivity for HDAC3 inhibition compared to HDAC1, inhibited invasion by about 90% compared to 70% for **TCH106**, which showed only 7-fold selectivity for HDAC3 vs. HDAC1 inhibition (Figures 3.15H-J).

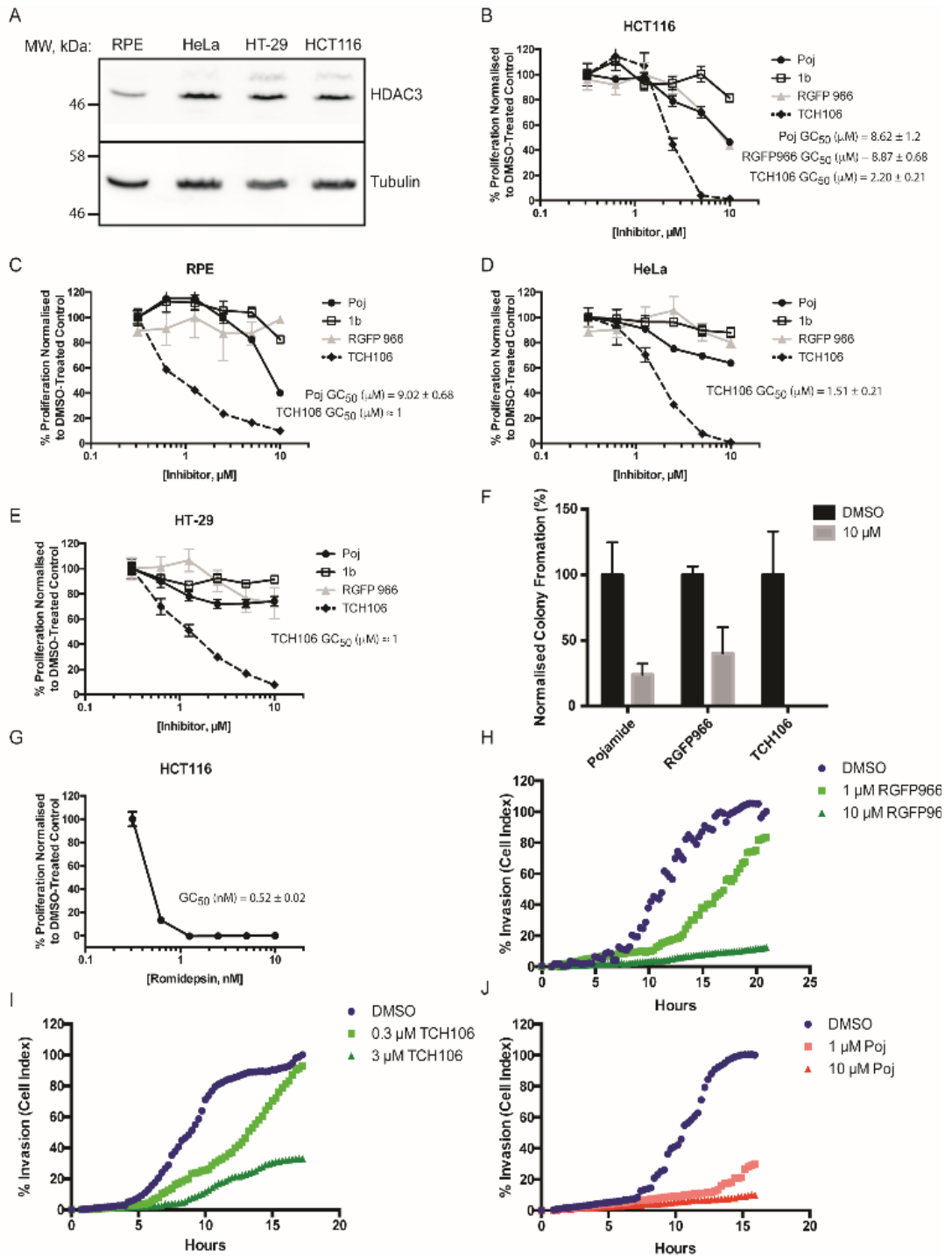


Figure 3.15. A) Western blot analysis of HDAC3 and α -Tubulin in Retinal Pigment Epithelium (RPE) cells and HeLa, HT-29 and HCT116 cells. B-E) HCT116 (B), RPE (C), HeLa (D) and HT-29 (E) CellTiter-Blue proliferation assays. F) HCT116 colony formation assays; % Colony formation (normalised to DMSO control) was quantitated manually and the average \pm S.D. was plotted. G) Inhibitory activity of Romidepsin on HCT116 cellular proliferation. H-J) HCT116 cellular invasion assays in the presence of RGFP966 (H), TCH106 (I) and Pojamide (J).

Pojamide appears more efficacious in preventing HCT116 cellular invasion, particularly at lower concentrations (*i.e.* 1 μM). In addition, we wanted to look to oxidise the iron atom in the ferrocene unit to offer a unique advantage at targeting cancer cells. In Ehrlich ascites tumour (EAT) cells and HPB (human leukemic T lymphocytes) it was shown that treatment with ferrocenium salts (*e.g.* $\text{Fe(III)Cp}_2\text{PF}_6$) inhibited tumour growth, whereas their ferrocene (II) derivatives were inactive. Indeed, ferrocenium's toxicity involves the generation of OH^\bullet radicals and the rapid induction of DNA-damage.³³ Pojamide was also studied by cyclic voltammetry and its voltammogram is shown in Figure 3.17 (contributed with help by Nikolaos Tsoureas). It shows a reversible process at 0.39V *vs* Fc^{*+0} (Fc = Ferrocene, Fc^* = $\text{Fe(Cp}^*)_2$), which is attributed to the reversible oxidation of the ferrocenyl moiety. We used Fc^* as the internal reference standard as attempts to use Fc hampered proper referencing of the observed process. Nevertheless, given that the Fc^* redox couple is found -0.59V *vs.* ferrocene (Fc),⁸ one can extrapolate an approximate value of the depicted in Figure 3.16 ; an observed process of -0.20V *vs* Fc . CV scans with different scan rates were also recorded (200, 100, 150, 50 $\text{mV}\cdot\text{s}^{-1}$) with no observed change in the reversibility of the process or the i_a/i_c ratio. Given the observed value for the oxidation of Pojamide and calculating approximately its value at 280 mV *vs.* the $\text{Ag/AgCl.KCl}_{(\text{sat.})}$ reference electrode, we find that the neutral Pojamide undergoes facile oxidation by SNP ($[\text{Fe(II)(CN)}_5\text{NO}]/[\text{Fe(III)(CN)}_5\text{NO}]$) 760 mV *vs.* $\text{Ag/AgCl.KCl}_{(\text{sat.})}$.

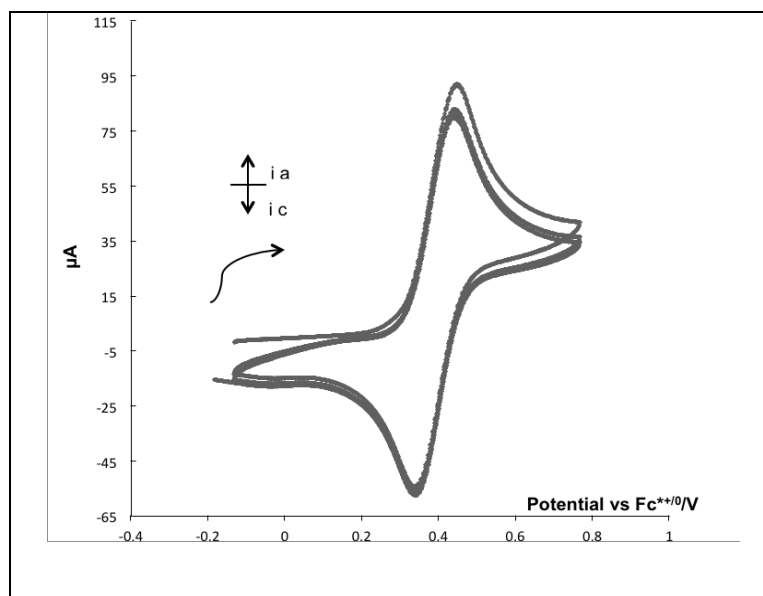
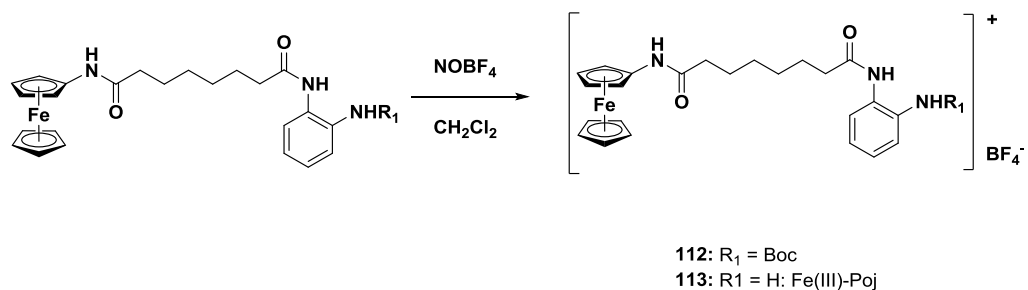


Figure 3.16. Overlaid CV scans (6) of Pojamide in DMSO (0.05M $[N(n\text{-Bu})_4]PF_6$ electrolyte) in the anodic direction. Scan rate: $300 \text{ mV}\cdot\text{s}^{-1}$; $i_a/i_c = 1$ (Working electrode: Glassy C; Reference Electrode: Ag; Counter Electrode: Pt). The voltamogram was referenced by adding a CH_2Cl_2 solution (ca. 0.5 ml) of Fc^* (1-2 crystals) in the DMSO analyte solution, resulting in no change in the characteristics of the observed voltamogram.

In order to take advantage of ferrocenium cytotoxicity, we generated the ferrocenium species **113** (Fe(III)-Poj) by reacting Pojamide with nitrosonium (NO^+) tetrafluoroborate and this was confirmed by cyclic voltammetry³⁴ (Scheme 3.3). Hence, we hypothesised that intracellular generation of NO^+ in the presence of Pojamide might also lead to Fe(III)-Poj in cells.



Scheme 3.3. Synthetic ferrocenium Pojamides.

It has previously been reported that sodium nitroprusside (SNP) leads to intracellular NO^+ release,³⁵ and neuronal PC12 cells have shown that SNP alone triggers apoptosis at very high concentrations $> 30 \mu\text{M}$.³⁶ To develop a cell-based assay utilising SNP as an NO^+ donor, we conducted cytotoxicity studies using the colony formation assay. At $25 \mu\text{M}$ SNP, HCT116 colony formation is reduced by about 30%; however, addition of $500 \mu\text{M}$ GSH completely eliminated SNP cytotoxicity. GSH is a free radical scavenger and its cytoprotective effects were demonstrated in our assay at concentrations of 50 and $500 \mu\text{M}$, whereby GSH treatments enhanced colony formation by about 4 and 10% respectively. Reacting with GSH to form innocuous NO may further reduce SNP cytotoxicity.³⁶ After identifying the optimal conditions for SNP/GSH treatment, we treated HCT116 cells with increasing concentrations of inhibitor in the presence and absence of SNP/GSH. The generation of Fe(III)-Po_j was monitored by blotting for the DNA-damage marker phospho- γH2AX (pH2AX) (Figure 3.17A-D). Without SNP/GSH, increasing concentrations of **RGFP966** and Pojamide reduced pH2AX levels, but addition of SNP/GSH to cells treated with Pojamide led to an initial decrease in pH2AX, with appearance of the DNA-damage marker at concentrations greater than $2 \mu\text{M}$ (Figure 3.17A-D). In a longer time-course (6-d) with $4 \mu\text{M}$ inhibitor (\pm SNP/GSH), only the Pojamide/SNP/GSH combination led to significant DNA-damage in comparison to the DNA-damage caused by cisplatin ($4 \mu\text{M}$) (Figure 3.17E).

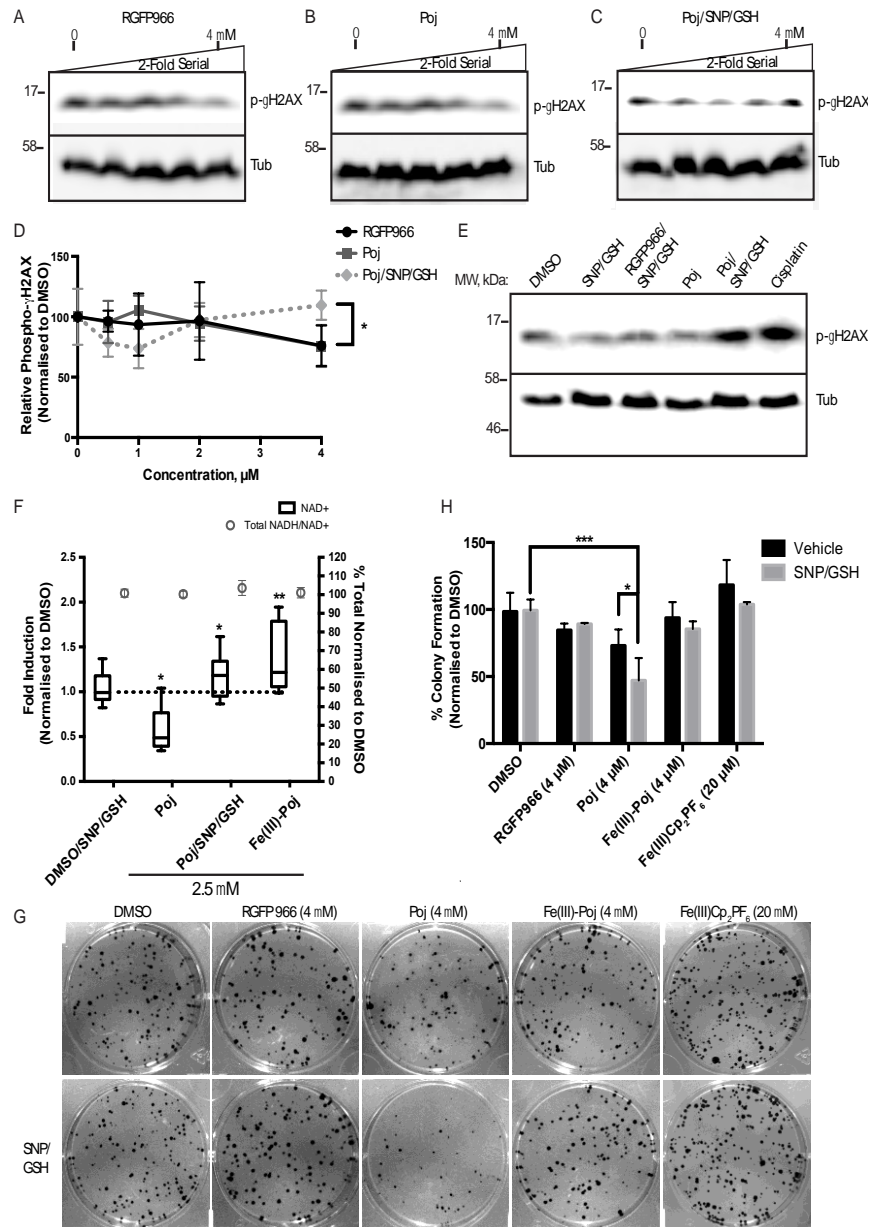
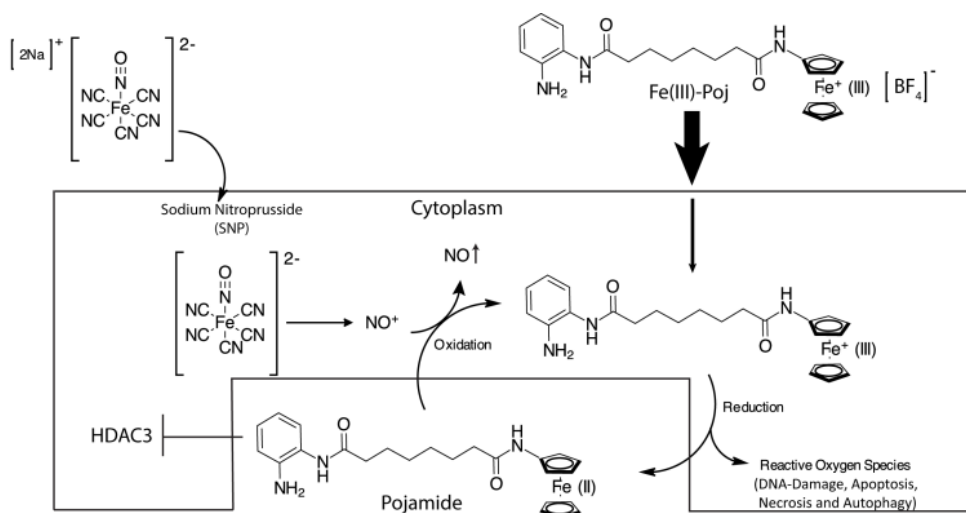


Figure 3.17. A-C) Western analysis of pH2AX and α -tubulin (Tub) in HCT116 cells treated for 3-d with (A) RGFP966, (B) Poj and (C) Poj + SNP/GSH. D) The pH2AX/Tub ratio was determined via densitometry and the average ratio normalised to DMSO control was plotted as the mean \pm S.D. E) Western analysis of pH2AX and α -tubulin (Tub) in HCT116 cells treated for 6-d as indicated above. F) NAD⁺ and total NAD⁺/NADH levels normalised to the DMSO control; the average (n=10) was plotted \pm S.D. G,H) HCT116 colony formation assays; % Colony formation (H) (normalised to DMSO control) was quantitated manually and the average \pm S.D. was plotted. The t-test statistical module of Prism 6.0 was used to determine p-values (ns (not statistically significant): P > 0.05; *: P \leq 0.05; **: P \leq 0.01; ***: P \leq 0.001).

To further support that our SNP/GSH treatment in the presence of Pojamide leads to production of Fe(III)-Poj, we assessed the levels of NAD⁺ in cells using the NAD/NADH-Glo Assay since the one one-electron transfer from NADH to ferrocenium oxidants such as Fe(III)Cp₂PF₆ shows that ferrocenium salts can successfully oxidise NADH to NAD⁺ *in vitro*.³⁷ To show this in cells, we treated HCT116 cells with DMSO/SNP/GSH and 2.5 μM Pojamide with and without SNP/GSH. For each condition, total NAD⁺/NADH levels remained the same, but Pojamide in the presence of SNP/GSH led to an increase in NAD⁺ levels; similar to those obtained with synthetic Fe(III)-Poj. In contrast, Pojamide treatment alone decreased NAD⁺ levels (Figure 3.18F). With cellular validation of Fe(III)-Poj generation, we tested our system in the HCT116 colony formation assay (Figures 3.18G,H). Pojamide alone caused a significant decrease in colony formation, which was enhanced by the addition of SNP/GSH; 27 and 53% inhibition respectively. At 4 μM, RGFP966, with and without SNP/GSH, displayed a 10 – 15% reduction in colony formation; however, like Pojamide, both ferrocenium salts were less effective without SNP/GSH. In combination with SNP/GSH, Fe(III)-Poj and Fe(III)Cp₂PF₆ caused a slight, about 10%, reduction in colony formation (Figure 3.18G,H). Interestingly, colonies resulting from treatment with ferrocenium salts and SNP/GSH were larger, but overall fewer colonies formed; a result similar to RGFP966 treatment. Although the cytotoxicity of ferrocenium salts is well documented, their activity is ~100-fold reduced compared to Pojamide,³⁸ perhaps due to limited membrane permeability, and explains their weak inhibition at the 4 and 20 μM concentrations tested.

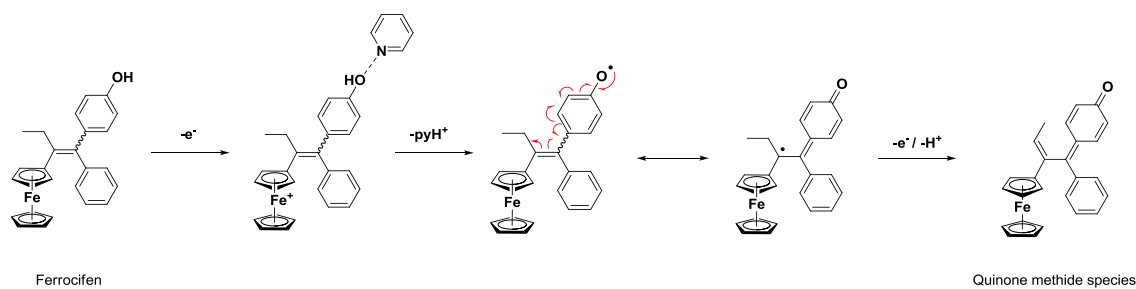
3.5 Conclusion

In summary, the SNP/GSH combination treatment is an ideal system for increasing the intracellular ferrocenium concentration from a Pojamide precursor. Also, when Fe(III)-Poj is reduced back to the Fe(II) species, it would be available to act upon HDACs. In this way, Pojamide is advantageous compared to other similarly potent HDACis: it is doubly toxic to cancer cells due to its facile conversion to the cytotoxic Fe(III) species in cells, whilst the reduced species inhibits cellular invasion through potently targeting HDAC3 and proliferation, to a lesser extent, due to its low micromolar HDAC1 inhibitory activity (Scheme 3.4).

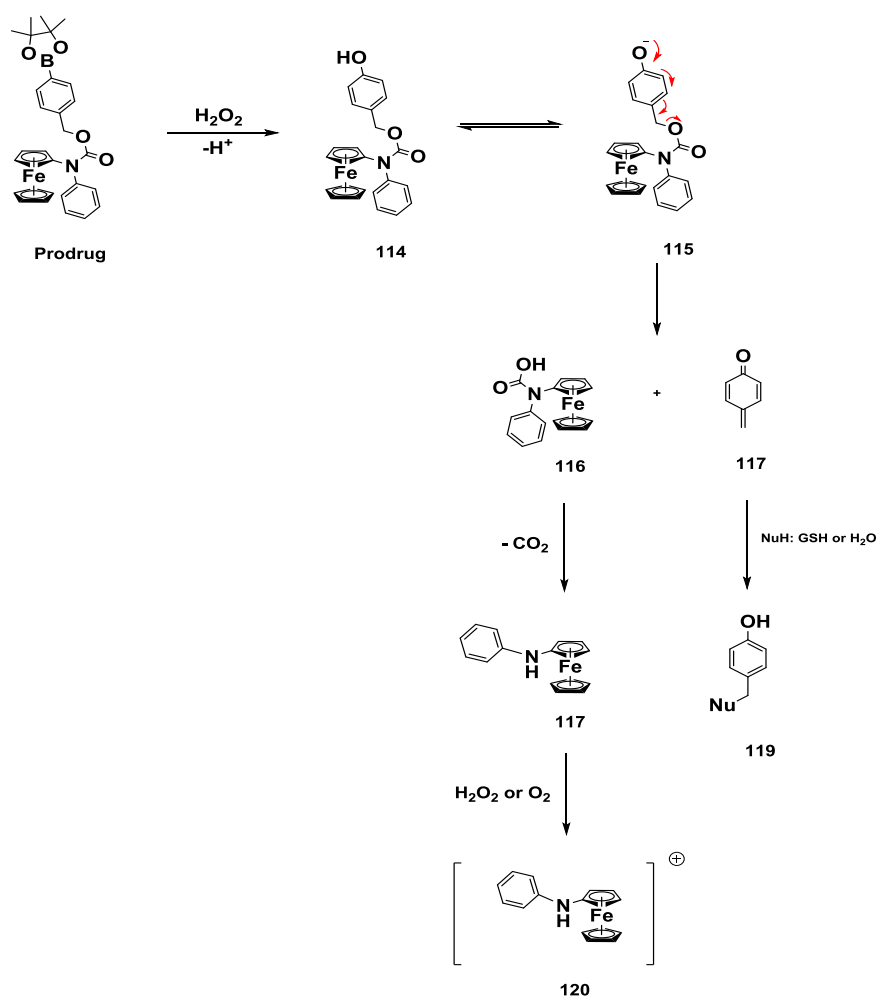


Scheme 3.4. Model for the enhanced redox-triggered cytotoxicity of Pojamide.

Lastly, co-treatments of intravenous SNP injection along with Pojamide administration might have application when used with pharmacologically distinct Fe(II)Cp₂-containing drugs (*e.g.* ferrocifens, hypoxia-induced prodrugs such as the prodrug of **114** (Schemes 3.5, 3.6)).³⁹⁻⁴⁰



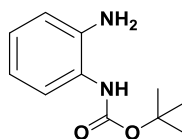
Scheme 3.5. The activation process of ferrocifen.



Scheme 3.6. Other Fe(II)Cp_2 – containing drugs and their activation process.

3.6 Experimental

Solvents and reagents were purchased from commercial suppliers and were used without purification. Ferrocenylamine was purchased from TCI, UK, and used as such. All reactions were performed in a fume hood. NMR spectra were recorded on Varian 500 MHz or 400 MHz spectrometers and chemical shifts are reported in ppm, usually referenced to TMS as an internal standard. LCMS was performed using a Shimadzu LCMS-2020 equipped with a Gemini® 5µm C18 110Å column and percentage purities were ran over 30 minutes in water/acetonitrile with 0.1% formic acid (5 min at 5%, 5%-95% over 20 min, 5 min at 95%) with the UV detector at 254 nm. High-resolution mass spectrometry (HRMS) was performed by the EPSRC National Mass Spectrometry Facility, University of Swansea. Elemental analyses were conducted by Stephen Boyer (London Metropolitan University). FT-IR spectra were recorded on a PerkinElmer Spectrum Version 10.03.06.

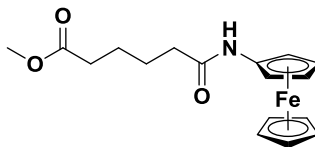


N-Boc-*o*-phenylenediamine, 103.

The title compound was prepared by using *o*-phenylenediamine (1.18 g, 10.95 mmol) in anhydrous dioxane (12 mL) and added 1M sodium hydroxide (5.90 mL), followed by tert-butyldicarbonate (1.1 equiv., 12.05 mmol) as a solution in dioxane (6 mL). The reaction mixture was stirred at room temperature overnight (18-h). Extraction was performed with dichloromethane. The organic layer was washed with brine, dried (MgSO₄) and then purification by column chromatography (ethyl acetate : hexane, 7:3) yielded a beige solid (1.371 g, 60%).

¹H NMR (DMSO-d₆, 500 MHz): δ = 8.23 (1H, s, NH), 7.17 (1H, d, J=8.0 Hz, CH), 6.84-6.81 (1H, m, CH), 6.67 (1H, d, J=8.0 Hz, CH), 6.53-6.50 (1H, m, CH), 4.79 (2H, s, NH₂), 1.45 (9H, s, 3CH₃).

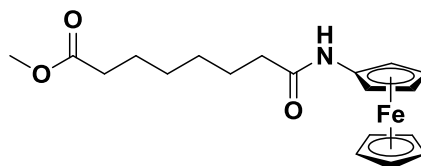
¹³C NMR (DMSO-d₆, 126 MHz). δ = 154.1, 141.7, 125.4, 125.0, 124.2, 116.7, 116.2, 79.1, 28.7.

**Methyl-6-oxo-6-(ferrocenylamino)hexanoate, 104.**²⁰

The title compound was prepared by using a microwave tube equipped with a magnetic stirrer and ferrocenylamine (0.3g, 1.5 mmol, 1 equiv.), methyl-6-chloro-6-oxohexanoate (0.30 mL, 1.94 mmol, 1.3 equiv, $d=1.144$) and anhydrous THF (5 mL). Dry triethylamine (0.83 mL, 6.00 mmol, 4 equiv., $d=0.73$) was added dropwise at rt. The reaction mixture was placed in a (CEM Explorer) microwave and the temperature was ramped to 150 °C with an initial power of 150 W for 10 mins. The cooled crude reaction mixture was diluted with distilled water (20 mL), extracted with ethyl acetate (20 mL). The organic layer was washed with brine (2 x 10 mL, sat.). The separated organic layer was dried using magnesium sulphate, filtered through a cotton wool plug. The dry organic extract was concentrated under reduced pressure and then purified by column chromatography (hexane : EtOAc = 1:1) to give an orange solid (0.369g, 72% yield).

¹H NMR (DMSO- d_6 , 500 MHz): δ = 9.20 (1H, s, NH), 4.58-4.55 (2H, m, 2CH), 4.08 (5H, s, Cp), 3.94-3.90 (2H, m, 2CH), 3.58 (3H, s, CH₃), 2.38-2.32 (2H, m, CH₂), 2.17-2.14 (2H, m, CH₂), 1.57-1.54 (4H, m, 2CH₂).

¹³C NMR (DMSO- d_6 , 126 MHz): δ = 173.6, 170.9, 96.1, 69.2, 64.1, 61.1, 51.6, 39.7, 36.0, 33.5, 25.2, 24.5.

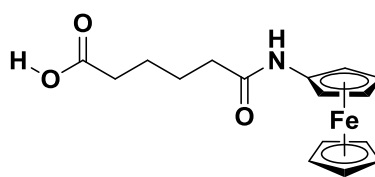


Methyl-8-oxo-8-(ferrocenylamino)octanoate, 105.²⁰

To a microwave tube equipped with a magnetic stirrer was added ferrocenylamine (0.3 g, 1.5 mmol, 1 equiv.), methyl-8-chloro-8-oxooctanoate (0.28 mL, 1.94 mmol, 1.3 equiv, $d=1.156$) and anhydrous THF (5 mL). Reagent grade triethylamine (0.83 mL, 6.00 mmol, 4 equiv., $d=0.73$) was added drop wise at room temperature. The reaction mixture was placed in a CEM Explorer microwave and the temperature was ramped to 150 °C at an initial power of 150 W for 10 mins. The cooled crude reaction mixture was diluted first with distilled water (20 mL), then extracted with ethyl acetate (20 mL) and the organic layer was washed with brine (2 x 10 mL, sat.). The separated organic layer was dried using magnesium sulphate and then filtered through a cotton wool plug. The dry organic extract was concentrated under reduced pressure and then purified by column chromatography (hexane : EtOAc = 1:1) to give an orange solid (0.360g, 65% yield).

¹H NMR (DMSO- d_6 , 500 MHz): δ = 9.17 (1H, s, NH), 4.58-4.55 (2H, m, 2CH), 4.08 (5H, s, Cp), 3.93-3.91 (2H, m, 2CH), 3.57 (3H, s, CH₃), 2.29 (2H, t, $J=7.3$ Hz, CH₂), 2.13 (2H, t, $J=7.3$ Hz, CH₂), 1.58-1.52 (4H, m, 2CH₂), 1.32-1.28 (4H, m, 2CH₂).

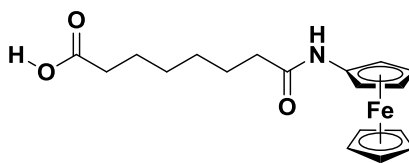
¹³C NMR (DMSO- d_6 , 126 MHz): δ = 173.7, 171.2, 96.2, 69.1, 64.1, 61.0, 51.6, 36.4, 33.7, 28.7, 28.6, 25.5, 24.8.

**6-Oxo-6-(ferrocenylamino)hexanoic acid, 106.**²⁰

The methyl ester precursor (344 mg, 1.00 mmol, 1 equiv.) was suspended in THF (10 mL). To this was added a solution of sodium hydroxide (2 equiv., 80 mg) in water (1 mL). The reaction mixture was stirred at room temperature for 4 h. After that, the organic volatiles were removed *in vacuo*, the reaction mixture was diluted with water and acidified with conc. HCl to pH ~ 4. A precipitate formed which was filtered under vacuum, washed with water and air-dried to give the expected product as an orange solid (220 mg, 67%).

¹H NMR (DMSO-d₆, 500 MHz): δ = 11.95 (1H, s, OH), 9.20 (1H, s, NH), 4.57-4.55 (2H, m, 2CH), 4.08 (5H, s, Cp), 3.95-3.90 (2H, m, 2CH), 2.23 (2H, t, J=6.9 Hz, CH₂), 2.15 (2H, t, J=6.9 Hz, CH₂), 1.57-1.50 (4H, m, 2CH₂).

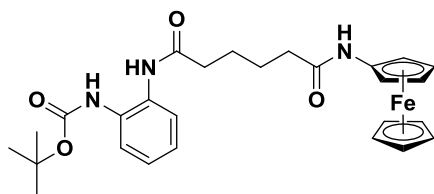
¹³C NMR (DMSO-d₆, 126 MHz): δ = 174.7, 171.0, 96.1, 69.4, 69.2, 64.1, 61.1, 39.6, 36.1, 33.9, 25.3, 24.6.

**8-Oxo-8-(ferrocenylamino)octanoic acid, 107.**²⁰

The methyl ester precursor (371 mg, 1.00 mmol, 1 equiv.) was suspended in THF (10 mL). A solution of sodium hydroxide (2 equiv., 80 mg) in water (1 mL) was next added. The reaction mixture was stirred at room temperature for 4 h, after which, the organic volatiles were removed *in vacuo*. The reaction mixture was diluted with water and acidified with conc. HCl to pH ~ 4. A precipitate formed which was filtered under vacuum, washed with water and air-dried to give the expected product as an orange solid (236 mg, 66%).

¹H NMR (DMSO-d₆, 500 MHz): δ = 11.93 (1H, s, OH), 9.18 (1H, s, NH), 4.56 (2H, s, 2CH), 4.08 (5H, s, Cp), 3.92 (2H, s, 2CH), 2.20-2.14 (4H, m, 2CH₂), 1.58-1.52 (4H, m, 2CH₂), 1.36-1.24 (4H, m, 2CH₂).

¹³C NMR (DMSO-d₆, 126 MHz): δ = 173.7, 171.2, 96.2, 69.1, 64.1, 61.0, 51.6, 36.4, 33.7, 28.7, 28.6, 25.5, 24.8.

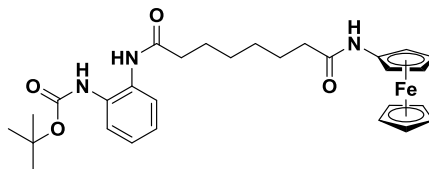


***Tert*-butyl-2-(6-oxo-6-(phenylamino)hexanamido)ferrocenylcarbamate, 108.**⁴¹

6-Oxo-6-(ferrocenylamino)hexanoic acid (493.6 mg, 1.5 mmol, 1 equiv.) and *N*-Boc-*o*-phenylenediamine (343.4 mg, 1.65 mmol, 1.1 equiv.) were dissolved in dichloromethane (18 mL). To this triethylamine (1.17 mL, 9 mmol) was added and the mixture was cooled in an ice bath. Next, propane phosphonic acid anhydride T3P (50% solution in DMF, 1.38 mL, 1.1 mmol)² was added and the reaction mixture was allowed to warm up to room temperature overnight. Then the mixture was poured into a saturated solution of K₂CO₃, stirred for 30 min. and extracted into CH₂Cl₂ (DCM). The organic layer was dried (MgSO₄), filtered and evaporated *in vacuo*. The residue was purified by trituration with DCM to give an orange solid (576.3 mg, 74%). Crystallization by solvent evaporation of DCM provided yellow crystals.

¹H NMR (DMSO-d₆, 500 MHz): δ = 9.44 (1H, s, NH), 9.22 (1H, s, NH), 8.31 (1H, s, NH), 7.53 (1H, d, J=7.8 Hz, CH), 7.41 (1H, d, J=7.8 Hz, CH), 7.12-7.04 (1H, m, CH), 7.06 (1H, d, J=7.8 Hz, CH), 4.57 (2H, s, 2CH), 4.08 (5H, s, Cp), 3.93 (2H, s, 2CH), 2.37 (2H, d, J=8.3 Hz, CH₂), 2.19 (2H, t, J=6.1 Hz, CH₂), 1.65-1.56 (4H, m, 2CH₂), 1.45 (9H, s, 3CH₃).

¹³C NMR (DMSO-d₆, 126 MHz): δ = 171.0, 153.5, 130.1, 125.4, 125.3, 124.3, 124.1, 96.1, 79.8, 69.2, 64.1, 61.1, 36.2, 28.7, 28.5, 25.3.

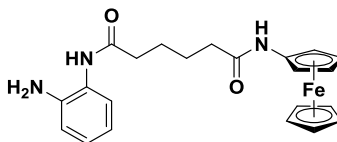


***Tert*-butyl-2-(8-oxo-8-(phenylamino)octanamido)ferrocenylcarbamate, 109.**⁴¹

Methyl-8-oxo-8-(ferrocenylamino)octanoic acid (215 mg, 0.6 mmol, 1 equiv.) and *N*-Boc-*o*-phenylenediamine (137.4 mg, 0.66 mmol, 1.1 equiv.) were dissolved in dichloromethane (7.7 mL). To this triethylamine (0.5 mL, 3.6 mmol) was added and the mixture was cooled in an ice bath. Next, propane phosphonic acid anhydride T3P (50% solution in DMF, 0.59 mL, 0.66 mmol) was added and the reaction mixture was allowed to warm up to room temperature overnight. Then the mixture was poured into saturated solution of K₂CO₃, stirred for 30 min. and extracted into CH₂Cl₂. The organic layer was dried (MgSO₄), filtered and evaporated *in vacuo*. The residue was purified by trituration with DCM to give the orange solid (233.1 mg, 71%). Crystallization by solvent evaporation of DCM provided yellow crystals.

¹H NMR (DMSO-*d*₆): 9.40 (1H, s, NH), 9.15 (1H, s, NH), 8.26 (1H, s, NH), 7.54-7.48 (1H, m, CH), 7.42-7.35 (1H, m, CH), 7.13-7.09 (1H, m, CH), 7.08-7.03 (1H, m, CH), 4.55 (2H, s, 2CH), 4.06 (5H, s, Cp), 3.91 (2H, s, 2CH), 2.33 (2H, t, *J*=7.4 Hz, CH₂), 2.14 (2H, t, *J*=7.4 Hz, CH₂), 1.62-1.54 (4H, m, 2CH₂), 1.44 (9H, s, 3CH₃), 1.38-1.26 (4H, m, 2CH₂).

¹³C NMR (DMSO-*d*₆, 126 MHz): δ = 171.6, 171.2, 142.3, 126.1, 125.7, 124.1, 116.6, 116.3, 96.1, 69.1, 64.1, 61.0, 39.7, 39.5, 36.4, 36.2, 29.0, 28.9, 25.7, 25.6.



N¹-(2-Aminophenyl)-N⁶-ferrocenyladipamide, 110.

Tert-butyl-2-(6-oxo-6-(phenylamino)hexanamido)ferrocenylcarbamate (520 mg, 1.00 mmol, 1 equiv.) was suspended in dichloromethane (40 mL) and MeOH (4 mL). To this mixture 4N HCl/dioxane (8 mL) was added and the mixture was stirred at room temperature overnight. The volatiles were removed *in vacuo*, then sat. Na₂CO₃ (aq.) was added to the residue and the mixture was sonicated. The precipitate was collected by suction and washed on the frit with water, dried, triturated with CH₂Cl₂ to give the title compound as a brown solid (318 mg, 76%).

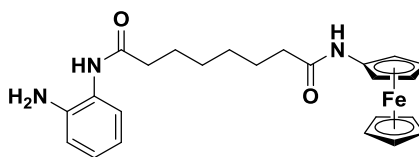
¹H NMR (DMSO-d₆): 9.21 (1H, s, NH), 9.09 (1H, s, NH), 7.15 (1H, d, J=7.8 Hz, CH), 6.78-6.73 (1H, m, CH), 6.70 (1H, dd, J=7.8, 1.4 Hz, CH), 6.53 (1H, dd, J=7.8, 1.4 Hz, CH), 4.80 (2H, s, NH₂), 4.56 (2H, s, 2CH), 4.08 (5H, s, Cp), 3.92 (2H, s, 2CH), 2.36-2.32 (2H, m, CH₂), 2.25-2.10 (2H, m, CH₂), 1.68-1.54 (4H, m, 2CH₂).

¹³C NMR (DMSO-d₆, 126 MHz): δ = 171.4, 171.1, 142.3, 126.1, 125.7, 124.1, 116.6, 116.3, 96.1, 69.2, 64.1, 61.1, 36.3, 36.1, 25.5.

HRMS-ESI (m/z): found 420.1366, calc. for [C₂₂H₂₆FeN₃O₂]⁺ 420.1369.

Anal. calcd (%) for C₂₂H₂₅FeN₃O₂: C, 63.02; H, 6.01; N, 10.02.

Found (%): C, 62.85; H, 6.05; N, 9.84.



N¹-(2-Aminophenyl)-N⁸-ferrocenyloctanediamide, 111.

Tert-butyl-2-(8-oxo-8-(phenylamino)octanamido)ferrocenyl carbamate (136.8 mg, 0.25 mmol, 1 equiv.) was suspended in dichloromethane (10 mL) and MeOH (1 mL). To this mixture 4N HCl/dioxane (2 mL) was added and the mixture was stirred at room temperature overnight. The volatiles were removed *in vacuo*, then sat. Na₂CO₃ (aq.) was added to the residue and the mixture was sonicated. The precipitate was collected by suction and washed on the frit with water, dried, triturated with CH₂Cl₂ to give the title compound as a brown solid (82 mg, 73%).

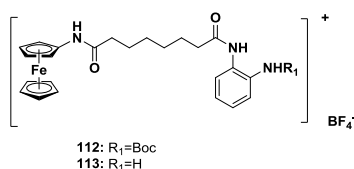
¹H NMR (DMSO-d₆): 9.18 (1H, s, NH), 9.05 (1H, s, NH), 7.14 (1H, dd, J=8.0, 1.5 Hz, CH), 6.91-6.84 (1H, m, CH), 6.70 (1H, dd, J=8.0, 1.5 Hz, CH), 6.54-6.48 (1H, m, CH), 4.78 (2H, s, NH₂), 4.57 (2H, t, J=1.9 Hz, 2CH), 4.08 (5H, s, Cp), 3.92 (2H, t, J=1.9 Hz, 2CH), 2.31 (2H, t, J=7.4 Hz, CH₂), 2.15 (2H, t, J=7.4 Hz, CH₂), 1.68-1.53 (4H, m, 2CH₂), 1.35-1.29 (4H, m, 2CH₂).

¹³C NMR (DMSO-d₆, 126 MHz): δ = 171.6, 171.2, 142.3, 126.1, 125.7, 124.1, 116.6, 116.3, 96.1, 69.1, 64.1, 61.0, 39.7, 39.5, 36.4, 36.2, 29.0, 28.9, 25.7, 25.6.

HRMS-ESI (m/z): found 448.1675, calc. for [C₂₄H₃₀FeN₃O₂]⁺ 448.1682.

Anal. Calcd (%) for C₂₄H₂₉FeN₃O₂: C, 64.44; H, 6.53; N, 9.39.

Found (%): C, 64.23; H, 6.60; N, 9.29.



Tert-butyl-2-(8-oxo-8-(phenylamino)octanamido)ferroceniumcarbamate tetrafluoroborate, 112.

Tert-butyl-2-(8-oxo-8-(phenylamino)octanamido)ferrocenylcarbamate (109.5 mg, 0.2 mmol, 1 equiv.) was suspended in dry DCM (5 mL). To this NOBF₄ (37.4 mg, 0.32 mmol, 1.6 equiv.) was added.³⁴ The colour of the solution changed from yellow to dark brown. Filtration afforded the title compound as a dark brown solid (89 mg, 70%).

¹⁹F NMR (DMSO-d₆): -29.53.

¹¹B NMR (DMSO-d₆): -2.56.

C₂₉H₃₇BF₄FeN₃O₄: C, 54.92; H, 5.88; N, 6.62.

Found (%): C, 55.08; H, 5.84; N, 6.57.

FTIR (cm⁻¹): 992 (BF₄⁻).

N¹-(2-Aminophenyl)-N⁸-ferroceniumoctanediamide tetrafluoroborate, 113.

N¹-(2-Aminophenyl)-N⁸-ferrocenyloctanediamide (100 mg, 0.2 mmol, 1 equiv.) was suspended in dry DCM (5 mL). To this NOBF₄ (37.4 mg, 0.32 mmol, 1.6 equiv.) was added. The colour of the solution changed from yellow to dark brown. Filtration afforded the title compound as a dark brown solid (78 mg, 73%).

¹⁹F NMR (DMSO-d₆): -29.53.

¹¹B NMR (DMSO-d₆): -1.34.

C₂₄H₂₉BF₄FeN₃O₂: C, 67.12; H, 5.80; N, 9.49.

Found (%): C, 66.97; H, 5.84; N, 9.31.

FTIR (cm⁻¹): 1038 (BF₄).

HDAC isoform inhibition assay/profiling.

(contributed by colleges from Harvard University)

The inhibitory effect of compounds on the function of HDACs 1–9 was determined in vitro using an optimised homogenous assay performed in 384-well plate format as previously described.⁴²

Pojamide		SAHA		TC-H106		RGFP966	
HDAC	IC50 (uM)	HDAC	IC50 (uM)	HDAC	IC50 (uM)	HDAC	IC50 (uM)
1	1.000	1	0.006	1	0.389	1	0.611
2	1.029	2	0.016	2	1.262	2	0.576
3	0.111	3	0.007	3	0.049	3	0.015
4	>30	4	26.230	4	>30	4	>30
5	>30	5	9.651	5	>30	5	>30
6	>30	6	0.004	6	>30	6	>30
7	>30	7	>30	7	>30	7	>30
8	>30	8	0.286	8	>30	8	>30
9	>30	9	>30	9	>30	9	>30

3.7 References

- 1 A. C. West and R. W. Johnstone, *J Clin Invest.*, 2014, **124**, 30–39.
- 2 M. Weïwer, M. C. Lewis, F. F. Wagner and E. B. Holson, *Future Med. Chem.*, 2013, **5**, 1491–508.
- 3 S. E. Bates, R. Eisch, A. Ling, D. Rosing, M. Turner, S. Pittaluga, H. M. Prince, M. H. Kirschbaum, S. L. Allen, J. Zain, L. J. Geskin, D. Joske, L. Popplewell, E. W. Cowen, E. S. Jaffe, J. Nichols, S. Kennedy, S. M. Steinberg, D. J. Liewehr, L. C. Showe, C. Steakley, J. Wright, T. Fojo, T. Litman and R. L. Piekarz, *Br. J. Haematol.*, 2015, **170**, 96–109.
- 4 L. Marquard, L. M. Gjerdrum, I. J. Christensen, P. B. Jensen, M. Sehested and E. Ralfkiaer, *Histopathology*, 2008, **53**, 267–277.
- 5 B. S. Mann, J. R. Johnson, M. H. Cohen, R. Justice and R. Pazdur, *Oncologist*, 2007, **12**, 1247–52.
- 6 M. Malvaez, S. C. McQuown, G. a Rogge, M. Astarabadi, V. Jacques, S. Carreiro, J. R. Rusche and M. a Wood, *Proc. Natl. Acad. Sci. U. S. A.*, 2013, **110**, 2647–2652.
- 7 C. M. Marson, C. J. Matthews, S. J. Atkinson, N. Lamadema and N. S. B. Thomas, *J. Med. Chem.*, 2015, **58**, 6803–6818.
- 8 A. J. Wilson, D. S. Byun, N. Popova, L. B. Murray, K. L’Italien, Y. Sowa, D. Arango, A. Velcich, L. H. Augenlicht and J. M. Mariadason, *J. Biol. Chem.*, 2006, **281**, 13548–13558.
- 9 H. Lehrmann, L. L. Pritchard and A. Harel-Bellan, *Adv. Cancer Res.*, 2002, **86**, 41–65.
- 10 T. L. Newkirk, A. A. Bowers and R. M. Williams, *Nat. Prod. Rep.*, 2009, **26**, 1293–1320.

- 11 J. R. Somoza, R. J. Skene, B. A. Katz, C. Mol, J. D. Ho, A. J. Jennings, C. Luong, A. Arvai, J. J. Buggy, E. Chi, J. Tang, B. C. Sang, E. Verner, R. Wynands, E. M. Leahy, D. R. Dougan, G. Snell, M. Navre, M. W. Knuth, R. V. Swanson, D. E. McRee and L. W. Tari, *Structure*, 2004, **12**, 1325–1334.
- 12 E. Meggers, *Curr. Opin. Chem. Biol.*, 2007, **11**, 287–292.
- 13 K. J. Kilpin and P. J. Dyson, *Chem. Sci.*, 2013, **4**, 1410–1419.
- 14 C. H. Leung, L. J. Liu, K. H. Leung and D. L. Ma, *Coord. Chem. Rev.*, 2016, **319**, 25–34.
- 15 Z. Dong, R. Tan, J. Cao, Y. Yang, C. Kong, J. Du, S. Zhu, Y. Zhang, J. Lu, B. Huang and S. Liu, *Eur. J. Med. Chem.*, 2011, **46**, 2477–2484.
- 16 D. Griffith, M. P. Morgan and C. J. Marmion, *Chem. Commun.*, 2009, 6735.
- 17 J. M. Cross, T. R. Blower, N. Gallagher, J. H. Gill, K. L. Rockley and J. W. Walton, *Chempluschem*, 2016, **81**, 1276–1280.
- 18 R. R. Ye, Z. F. Ke, C. P. Tan, L. He, L. N. Ji and Z. W. Mao, *Chem. A Eur. J.*, 2013, **19**, 10160–10169.
- 19 R. R. Ye, C. P. Tan, L. He, M. H. Chen, L. N. Ji and Z. W. Mao, *Chem Commun*, 2014, **50**, 10945–10948.
- 20 J. Spencer, J. Amin, M. Wang, G. Packham, S. S. S. Alwi, G. J. Tizzard, S. J. Coles, R. M. Paranal, J. E. Bradner and T. D. Heightman, *Med. Chem. Lett.*, 2011, 358–362.
- 21 J. Spencer, J. Amin, R. Boddiboyena, G. Packham, B. E. Cavell, S. S. S. Alwi, R. M. Paranal, T. D. Heightman, M. Wang, B. Marsden, P. Coxhead, M. Guille, G. J. Tizzard, S. J. Coles and J. E. Bradner, *Medchemcomm*, 2012, **3**, 1–5.
- 22 A. Leonidova, C. Mari, C. Aebbersold and G. Gasser, *Organometallics*, 2016, **35**, 851–854.
- 23 D. Can, H. W. Peindy N'Dongo, B. Spingler, P. Schmutz, P. Raposinho, I. Santos and R. Alberto, *Chem. Biodivers.*, 2012, **9**, 1849–1866.
- 24 K. H. M. Chow, R. W. Y. Sun, J. B. B. Lam, C. K. L. Li, A. Xu, D. L. Ma, R. Abagyan, Y. Wang and C. M. Che, *Cancer Res.*, 2010, **70**, 329–337.

- 25 S. Shen and A. P. Kozikowski, *ChemMedChem*, 2016, **11**, 15–21.
- 26 S. J. Coles and P. A. Gale, *Chem. Sci.*, 2012, **3**, 683–689.
- 27 F. Thaler and C. Mercurio, *ChemMedChem*, 2014, **9**, 523–536.
- 28 R. A. Friesner, R. B. Murphy, M. P. Repasky, L. L. Frye, J. R. Greenwood, T. A. Halgren, P. C. Sanschagrín and D. T. Mainz, *J. Med. Chem.*, 2006, **49**, 6177–6196.
- 29 M. Rai, E. Soragni, C. J. Chou, G. Barnes, S. Jones, J. R. Rusche, J. M. Gottesfeld and M. Pandolfo, *PLoS One*, 2010, **5**, e8825.
- 30 G. Alcarraz-Vizán, J. Boren, W. N. P. Lee and M. Cascante, *Metabolomics*, 2010, **6**, 229–237.
- 31 W. Xiao, X. Chen, X. Liu, L. Luo, S. Ye and Y. Liu, *J. Cell. Mol. Med.*, 2014, **18**, 646–655.
- 32 R. Furumai, A. Matsuyama, N. Kobashi, K. H. Lee, M. Nishiyama, H. Nakajima, A. Tanaka, Y. Komatsu, N. Nishino, M. Yoshida and S. Horinouchi, *Cancer Res.*, 2002, **62**, 4916–4921.
- 33 C. Y. Acevedo-Morantes, E. Meléndez, S. P. Singh and J. E. Ramírez-Vick, *J. Cancer Sci. Ther.*, 2012, **4**, 271–275.
- 34 J. Y. Chung, C. Schulz, H. Bauer, Y. Sun, H. Sitzmann, H. Auerbach, A. J. Pierik, V. Schünemann, A. Neuba and W. R. Thiel, *Organometallics*, 2015, **34**, 5374–5382.
- 35 L. Grossi and S. D'Angelo, *J. Med. Chem.*, 2005, **48**, 2622–2626.
- 36 M. Kayahara, U. Felderhoff, J. Pocock, N. Hughes and H. Mehmet, *Biochem. Soc. Trans.*, 1998, **26**, 42.
- 37 P. O. Danis, C. Wesdemiotis and F. W. McLafferty, *J. Am. Chem. Soc.*, 1983, **105**, 7454–7456.
- 38 D. Osella, M. Ferrali, P. Zanello, F. Laschi, M. Fontani, C. Nervi and G. Cavigliolo, *Inorganica Chim. Acta*, 2000, **306**, 42–48.
- 39 H. Hagen, P. Marzenell, E. Jentsch, F. Wenz, M. R. Veldwijk and A. Mokhir, *J. Med. Chem.*, 2012, **55**, 924–934.

- 40 G. Jaouen, A. Vessières and S. Top, *Chem. Soc. Rev.*, 2015, **44**, 8802–17.
- 41 J. R. Dunetz, Y. Xiang, A. Baldwin and J. Ringling, *Org. Lett.*, 2011, **13**, 5048–5051.
- 42 J. E. Bradner, N. West, M. L. Grachan, E. F. Greenberg, S. J. Haggarty, T. Warnow and R. Mazitschek, *Nat Chem Biol*, 2010, **6**, 238–243.

Chapter 4

Synthesis of ferrocene-based kinase inhibitors containing a pentafluorosulfanyl moiety.

4.1 Overview

A series of SF₅-oxindole analogues has been synthesized by a Knoevenagel condensation reaction and were tested for biological activity testing versus a panel of cell lines and protein kinases. The resulting compounds were characterized by elemental analyses, NMR spectroscopy, mass spectrometry, LC-MS and X-ray crystallography studies.

4.2 Introduction

Kinases are a group of enzymes responsible for phosphorylation of proteins, which are key steps in a number of biological processes. There are over 500 in humans. The phosphorylation step uses ATP to transfer the phosphate group (Scheme 4.1) usually to a serine, threonine or tyrosine residue, leading to a structural change in the protein and an intracellular signal. In disease, this step is uncontrolled and is responsible for a number of inflammatory disorders and cancers. Phosphorylation can modify the function of a protein in many ways. The structure of ATP is shown in Figure 4.1 and the phosphorylation diagram is shown in Scheme 4.1.¹

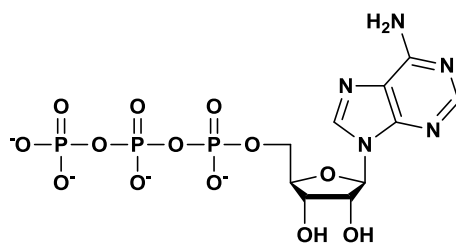
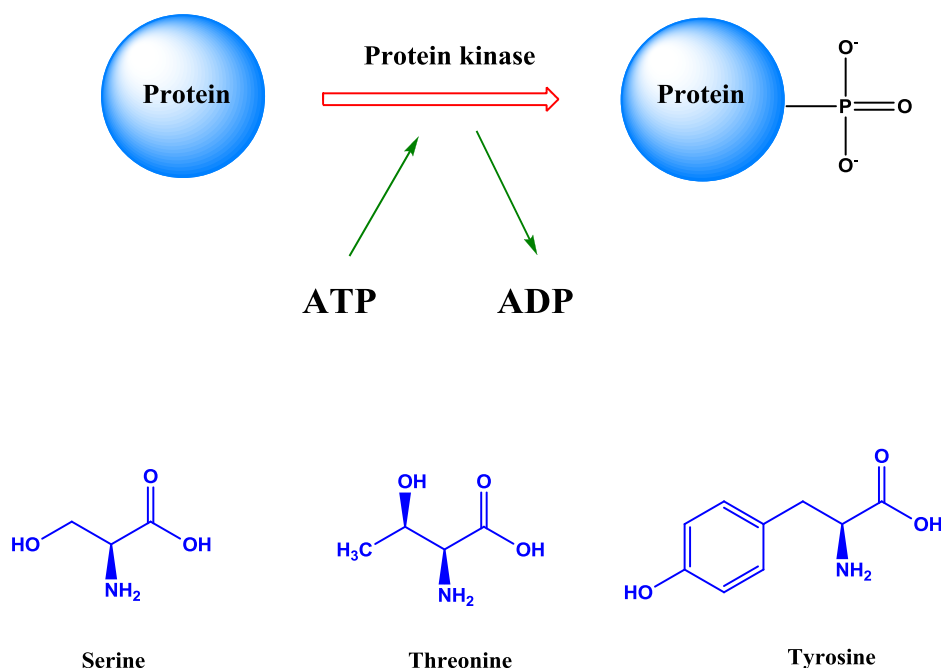
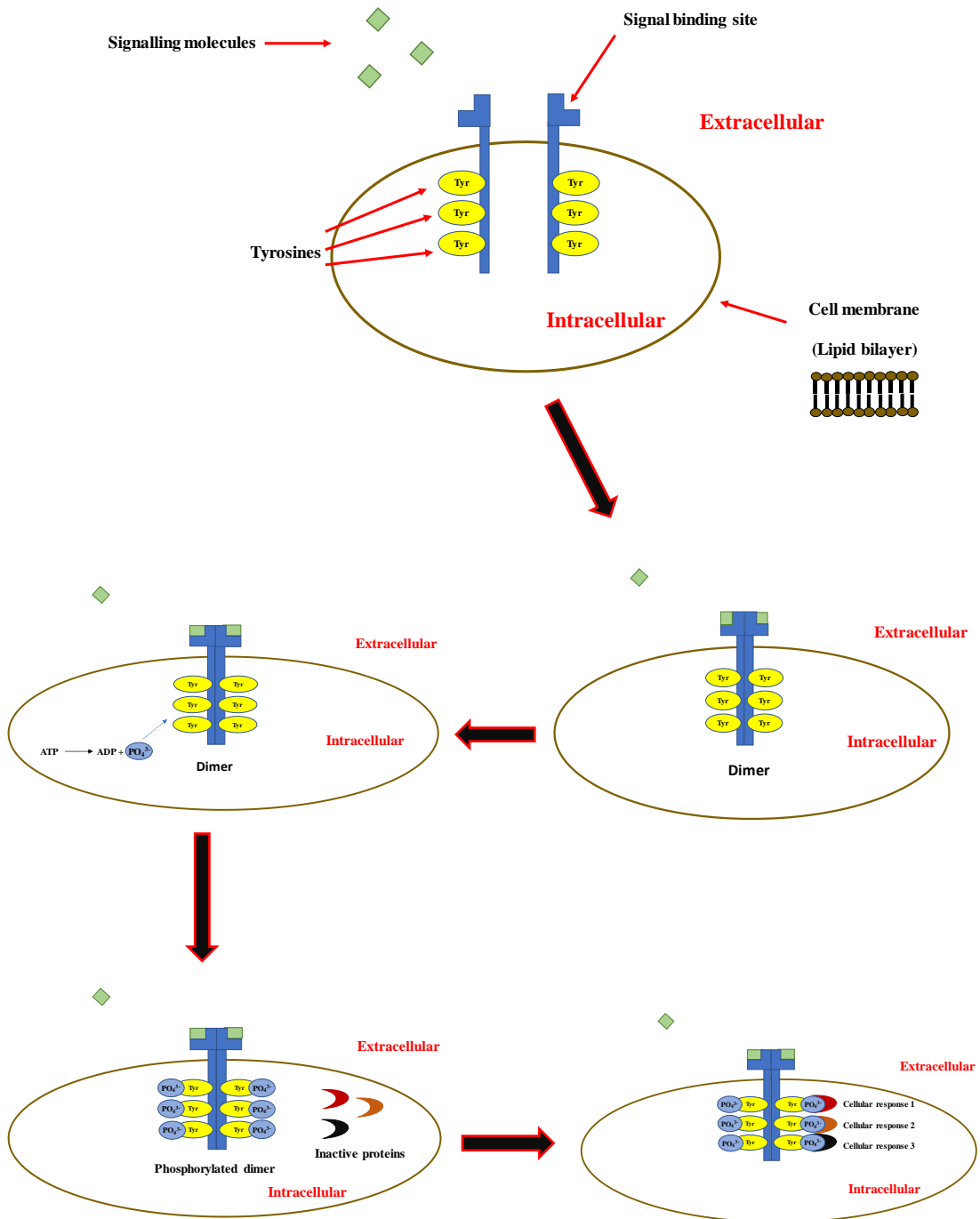


Figure 4.1. Adenosine triphosphate (ATP).



Scheme 4.1. Phosphorylation process with 3 examples of amino acids in the protein.

Many human cancers are related to the dysregulation of protein kinases because of mutations. Protein kinases are an important target class for developing treatments. Phosphorylation is often a required step in the growth of some cancers and inflammatory disorders; hence the enzyme inhibitors that block the action of protein kinases will provide the treatment of diseases. Scheme 4.2 shows the receptor tyrosine kinase phosphorylation mechanism. In the first step an extracellular signalling molecule will attach to the signal binding site then each monomer will bind together and form a dimer, then the phosphate group from the ATP will attach to the tyrosine forming a “phosphorylated dimer”. In the next step, inactive protein will come to the molecule and attach to a phosphorylated tyrosine and this change will lead to the signal transduction pathway which leads to the cellular response.



Scheme 4.2. Receptor tyrosine kinase mechanism.

The epidermal growth factor receptor (EGFR) belongs to the ErbB family of receptor tyrosine kinases (RTK). ErbB is a gene of a protein family containing 4 receptor tyrosine kinases; ErbB-1 or EGFR, ErbB-2, ErbB-3 and ErbB-4. In the early 1990s, chloroanilinoquinazoline or CAQ (**121**) was studied and confirmed to be a potent inhibitor of EGFR tyrosine kinase by ICI Pharmaceuticals²⁻³ and a further structural study showed that the anilinoquinazoline acts as a mimic of ATP. The replacement of the methoxy groups at positions 6 and 7 on the quinazoline ring provided an increase in potency, 4-(3-chloro-benzyl)-6,7-dimethoxy-quinazoline (**122**).²

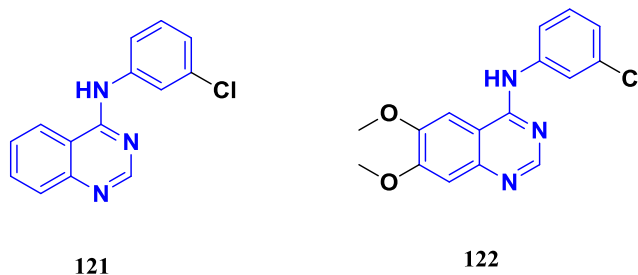
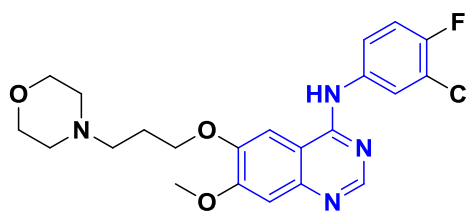


Figure 4.2. CAQ, **121** and methoxy-CAQ, **122**.

The discovery of **121** and **122** led to the drug gefitinib (or Iressa), which is an EGFR inhibitor used for non-small-cell lung cancer (NSCLC)⁴ but had limited effects on patients.⁵



Erlotinib or Tarceva is also a drug used to treat non-small cell lung cancer (NSCLC), which acts on the epidermal growth factor receptor (EGFR).⁶

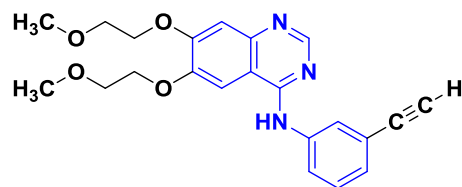


Figure 4.4. Erlotinib or Tarceva.

There are a number of quinazoline-based inhibitors, which are now in active clinical development such as AZD0530 (**123**), AZD0424 (**124**), AZD3759 (**125**), AZD1522 (**126**) and AZD2811 (**127**).²

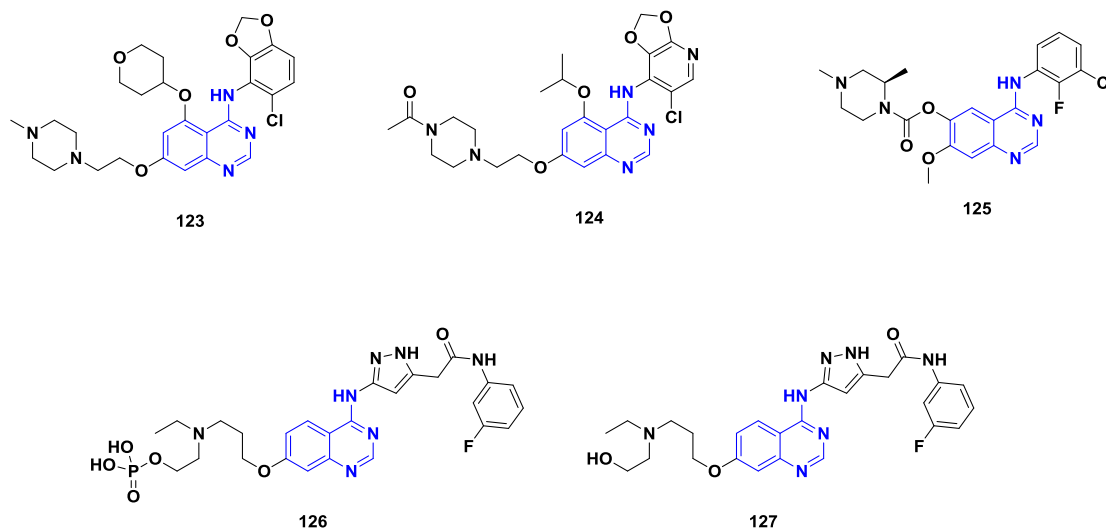


Figure 4.5. Some quinazoline-based inhibitors.

Kinase drugs for example, Imatinib (Gleevec, **128**), Nilotinib (**129**), Bosutinib (**130**) and Ponatinib (**131**) have been approved for the treatment of chronic myelogenous leukemia (CML).⁷

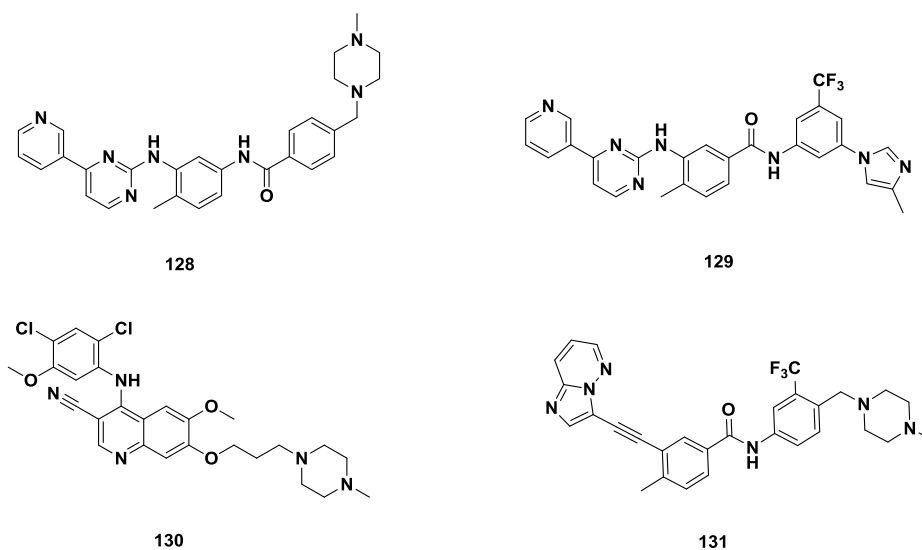


Figure 4.6. Some kinase drugs for CML.

Whereas sunitinib (**132**), sorafenib (**133**), axitinib (**134**) and pazopanib (**135**) are used for treating various stages of renal cell cancer.⁷

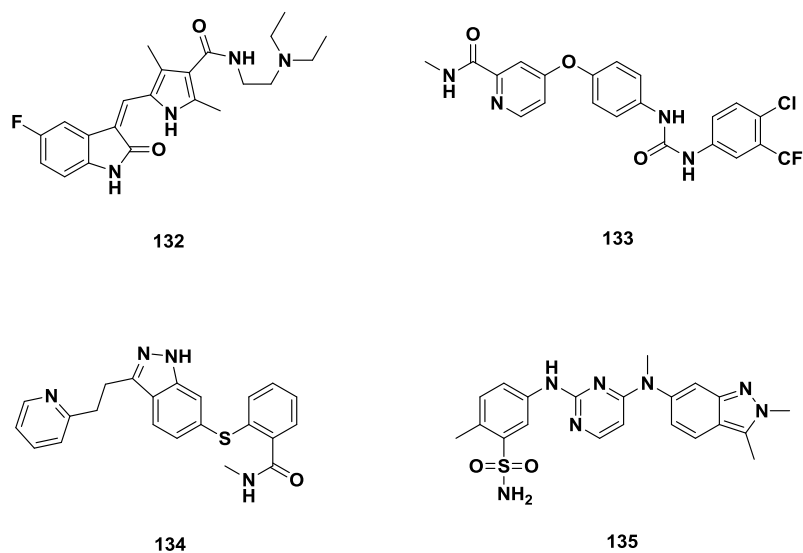


Figure 4.7. Some kinase drugs for renal cancer cell.

Staurosporine⁸ is an alkaloid compound that exhibits activity against a wide range of protein kinases by the prevention of ATP binding with IC_{50} 's in the nanomolar range but it is a non-specific protein kinase inhibitor and has high toxicity.⁹ Meggers's group were interested in synthesizing Ru and Pt complexes (**136**, **137** and **138**) where the sugar unit was replaced by square planar and octahedral complexes. These complexes made use of "hypervalent" carbon mimics (e.g. up to 6-valent Ru) compared to the staurosporine structure and their biological activity has been studied. These complexes are potent, selective inhibitors of protein kinases, attributed to the geometry enabled by the metal complexes compared with a tetrahedral carbon in the sugar unit.¹⁰⁻¹¹

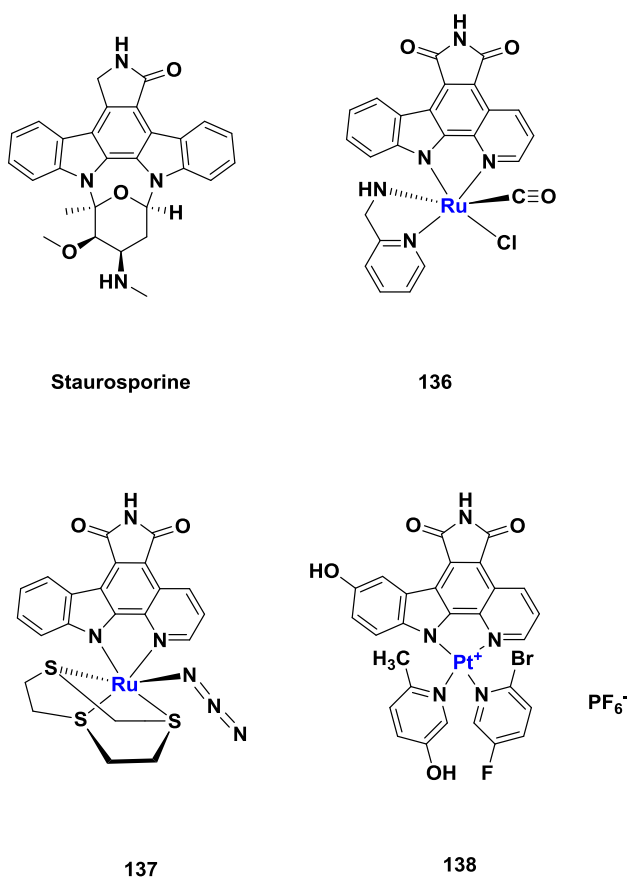


Figure 4.8. Staurosporine, Ru and Pt complexes (**136**, **137** and **138**).

Moreover, Meggers's group has synthesized the Ir complex, **139** based on staurosporine's structure and the result showed that **139** proved to be potent and selective towards the Flt4 kinase (protein encoded with gene Flt4 related to lymphangiogenesis and maintenance of the lymphatic endothelium).¹²

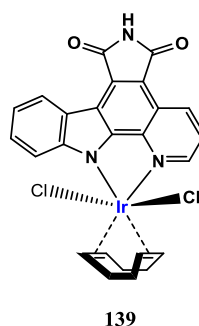


Figure 4.9. Ir complex **139**.

3-Substituted oxindole analogues, **140**, **141** and **142** (oxindole or indolin-2-one is an aromatic heterocyclic compound) have been investigated for their inhibitory properties against various RTKs (receptor tyrosine kinases). The results showed **140** and **142** to be potent and selective inhibitors of the vascular endothelial growth factor (VEGF), Flk-1 while **141** was shown to be unselective for RTK inhibition. In this study, it was shown that the 3-[(substituted pyrrolyl-, thienyl- and pyrazolyl)methylidene]indolin-2-ones (for example **143**, **144** and **145** in Figure 4.11) exhibiting a Z configuration had high selectivity to VEGF (Flk-1) and/or PDGF (platelet-derived growth factor receptors) RTK activity, among them **143** showed the highest potency towards VEGF (Flk-1) and PDGF RTK.¹³

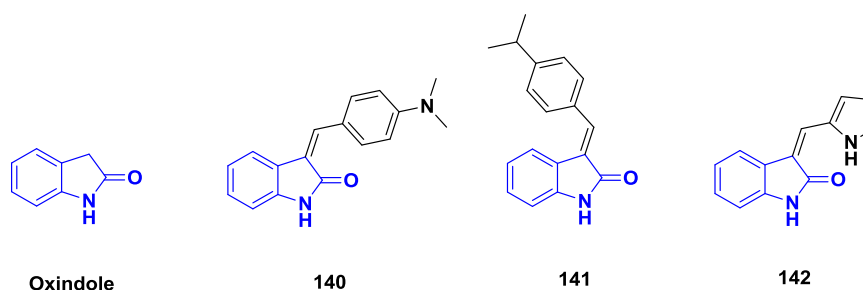


Figure 4.10. Oxindole and 3-substituted oxindole analogues **140**, **141** and **142**.

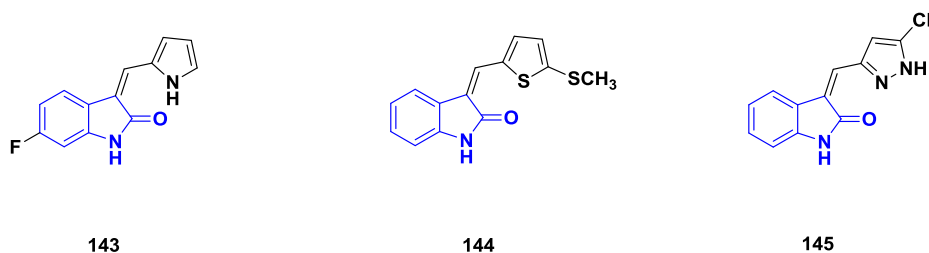


Figure 4.11. Oxindole analogues of **143**, **144** and **145**.

The reaction between oxindole and ferrocene carboxaldehyde has been studied and the biological activities of the resulting compounds were tested against a number of kinases. The resulting products (*E*)- and (*Z*)-3-ferrocenylmethylidene-1,3-dihydro-2*H*-indol-2-one **146** (*E*, major product and *Z*, minor product) displayed similar and significant activity against VEGFR and PDGFR-RTKs.¹⁴

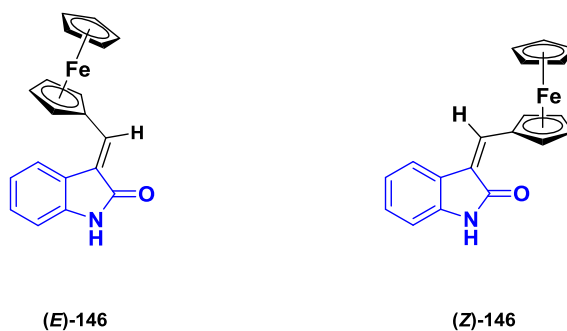


Figure 4.12. Oxindole analogues *E* and *Z*-146.

Later work showed the synthesis of similar derivatives and biological evaluation, versus kinases, of oxindole and ferrocene/ruthenocene analogues (compounds **146-156**, including the previous *E* and *Z*-146 compounds) by using the Knoevenagel condensation reaction. The inhibition data showed some derivatives to have activity against different targets such as CLK1, DYRK3, VEGFR2 and DYRK4 but not on DYRK1 and DYRK2 (DYRK is dual specificity tyrosine-phosphorylation-regulated kinase).¹⁵

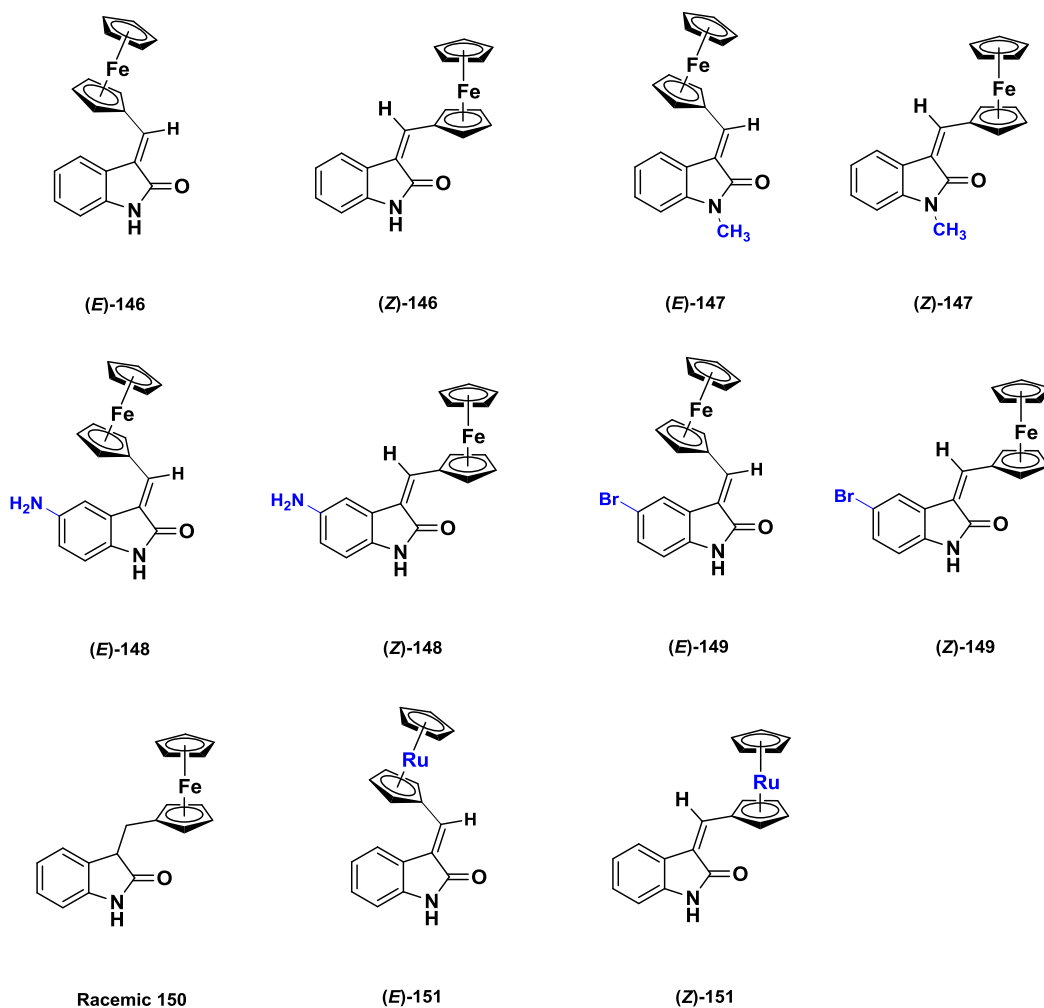


Figure 4.13. Oxindole analogues *E* and *Z*-146-151.

A number of small molecule kinase inhibitors have been approved by the FDA, also structural and binding information have been presented, which is extremely useful for studying new kinase inhibitors in the future. Figure 4.14 shows the structural binding mode of some small molecule kinase inhibitors (erlotinib, gefitinib and sunitinib).¹⁶

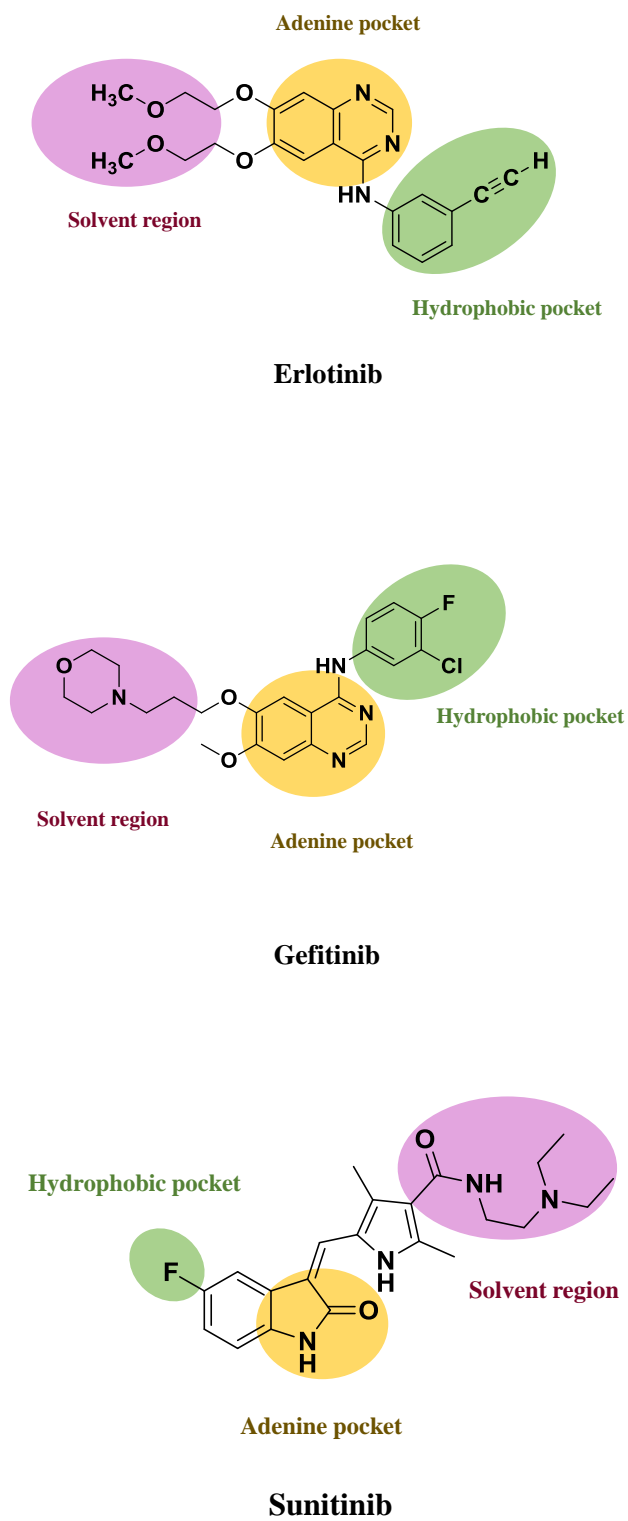


Figure 4.14. Structures and binding mode of some kinase inhibitors.

In this work, we aimed to synthesize kinase inhibitors based on an oxindole scaffold with a SF₅ group to occupy the hydrophobic pocket.

SF₅, or pentafluorosulfanyl, is a stable group and it has led to multiple applications in material sciences and medicinal chemistry. A SF₅ group is interesting as it has strong polarity, good physicochemical and biological activities, high density and high lipophilicity. SF₅ and CF₃ (trifluoromethyl) share many features for example; high electronegativity, lipophilicity, chemical and thermal stability, high stability under physiological conditions. The SF₅ group has been shown to behave often like a CF₃ group.¹⁷⁻¹⁸ Although the two groups share similarities they are not always biologically equivalent.¹⁹⁻²⁰

Altomonte's group have synthesized two series of -CF₃ and -SF₅ aniline-pyrazoles compounds and their CB₁ receptor affinities (K_i) were studied. *In vitro* assay results showed the -SF₅ compound (**152**, K_i = 11.2 nM) had the lower K_i value than the -CF₃ ones (**153**, K_i = 26 nM).¹⁹

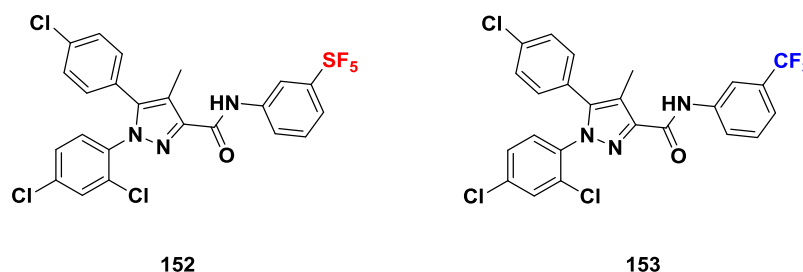


Figure 4.15. -CF₃ and -SF₅ aniline-pyrazoles compounds **152** and **153**.

The pentafluorosulfanyl analogues of fluoxetine (**154**), fenfluramine (**155**) and nonfenfluramine (**156**) have been synthesized by replacing the CF_3 group (**157**, **158** and **159**, respectively) with a SF_5 group, then the potency against the 5-HT_{2b} , 5-HT_{2c} and 5-HT_6 receptors was studied (5-HT receptors or 5-hydroxytryptamine receptors are a group of G protein-coupled receptors). The literature results showed **159** had enhanced potency against 5-HT_{2b} , 5-HT_{2c} and 5-HT_6 receptors.²⁰

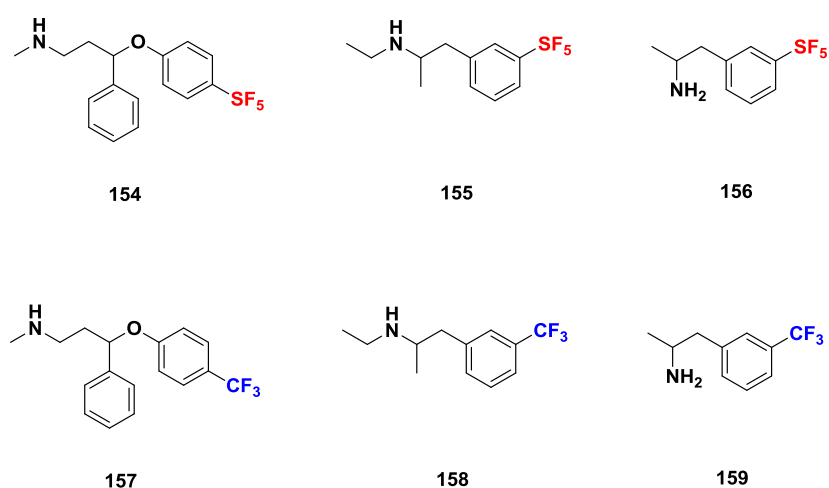


Figure 4.16. SF_5 group of fluoxetine **154**, fenfluramine **155** and nonfenfluramine **156**.

Other work from Wipf's group published the synthesis of SF_5 analogues of the antimalarial agent mefloquine, **160** and **161** then evaluated their biological activities against malaria parasites (mefloquine, **162** is medication used to prevent and treat malaria²¹ but there are many side effects of mefloquine such as anxiety, depression, hallucinations and seizures, etc.).²² The results showed **160** and **161** had improved activities compared to the parent CF_3 - mefloquine compound.²³

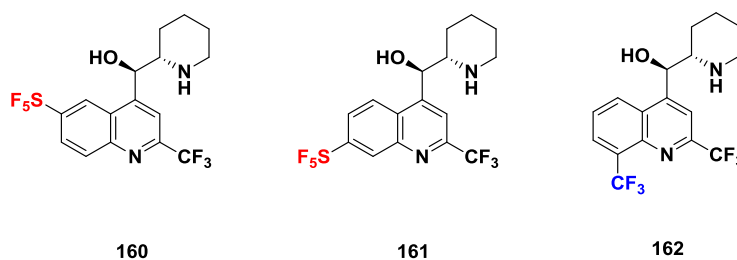
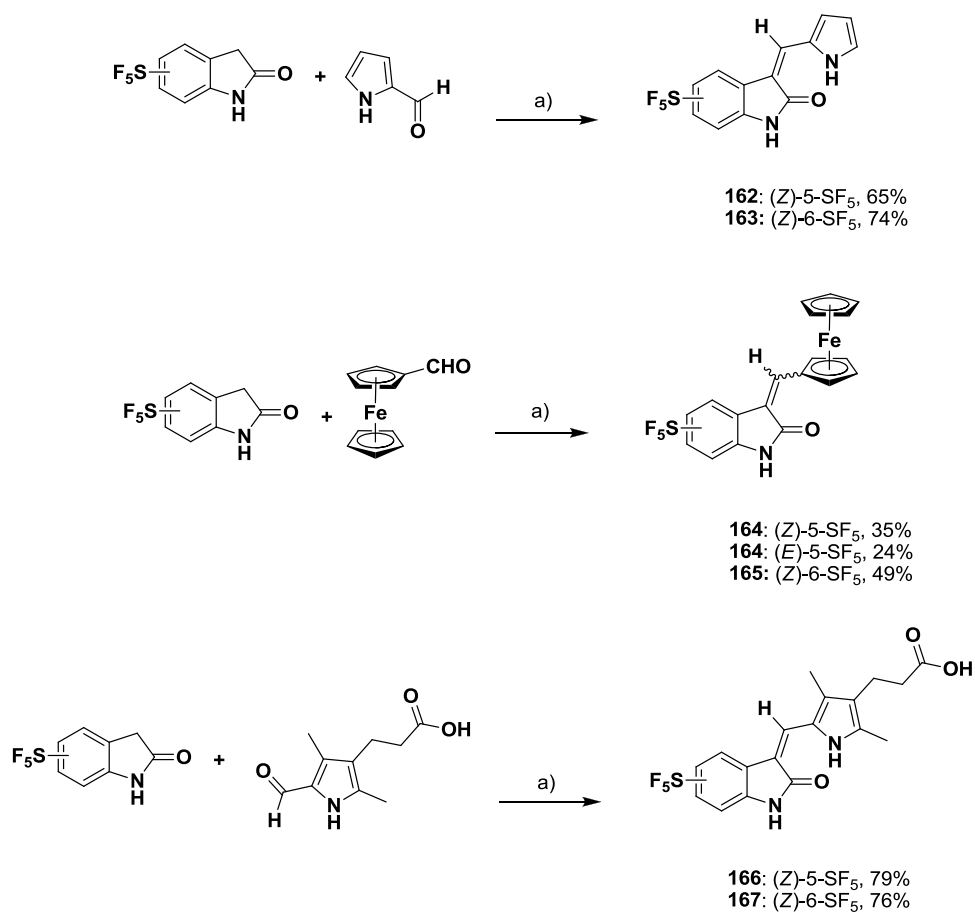


Figure 4.17. SF_5 group of mefloquine **160**, **161** and mefloquine **162**.

4.3 Results and Discussion

We synthesized pyrrole and ferrocene compounds by using a Knoevenagel condensation reaction according to the published literature¹⁵ and explored SAR against a wide range of kinases. The previous oxindole compounds (*Z*)-**146** and (*E*)-**146** showed biological activity against PDGFR and VEGFR isoforms (Table 4.1)



a) Piperidine, EtOH, μ W 150 C 30 mins.

Scheme 4.3. Synthesis of SF₅-oxindole analogues.

Table. 4.1. % Inhibition of (Z)-**146** and (E)-**146** vs VEGFR and PDGFR. – denotes inactive.¹⁴

Compound	% Inhibition			
	<i>h</i> VEGFR-1	<i>h</i> VEGFR-2	<i>h</i> PDGFR- α	<i>h</i> PDGFR- β
(Z)- 146	13	88	-	12
(E)- 146	15	91	-	10

The structures of the pyrrole compounds **162** and **163** were confirmed by ¹H NMR, ¹³C NMR spectroscopy, elemental analysis, mass spectrometry and X-ray crystallography. The yields of the products were between 65-74%. The ¹H NMR spectra showed the most downfield signals were assigned to the 2 –NH groups (δ 11.10-13.40 ppm (the latter being an intramolecular NH-O=C hydrogen bond)). The results from elemental analysis and mass spectrometry corresponded to the calculated values and the solid state molecular structures of the two compounds were determined by X-ray crystallography and showed, as with ¹H NMR, an intramolecular H- bond between the –NH of the pyrrole ring and the C=O of the indole-2-one moiety.

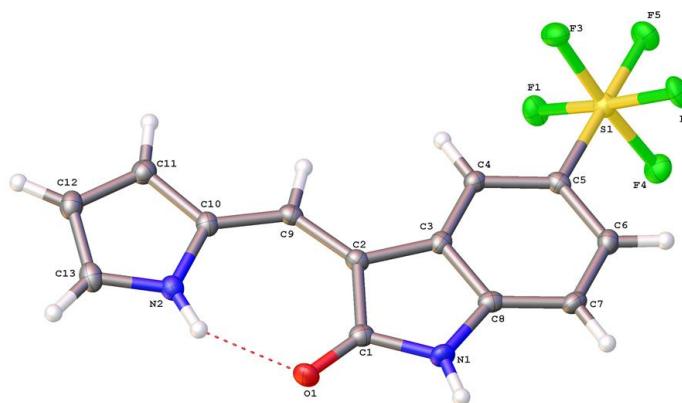


Figure 4.18. X-ray structure of **162**.

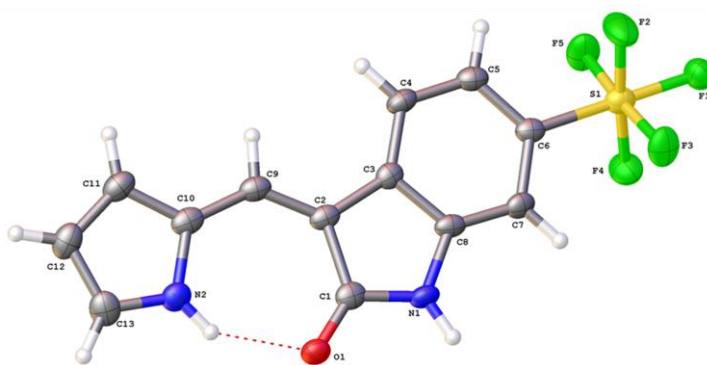


Figure 4.19. X-ray structure of **163**.

The structures of ferrocenyl compounds **164** and **165** were confirmed by ¹H NMR, ¹³C NMR, elemental analysis, mass spectrometry and X-ray crystallography. The total yields were between 49-59%. The ¹H NMR spectrum of the products showed the most downfield signal was assigned to -NH (δ 10.84-10.94 ppm). The solid state molecular structures of two compounds were determined by X-ray crystallography and the isomers could be determined in solution by NOESY NMR, for example Figure 4.20 shows the NOESY NMR of (*Z*)-**164** which is confirmed as the *Z*-isomer because as there is a proton at δ =6.92 ppm in proximity to another proton at δ =7.67 ppm.

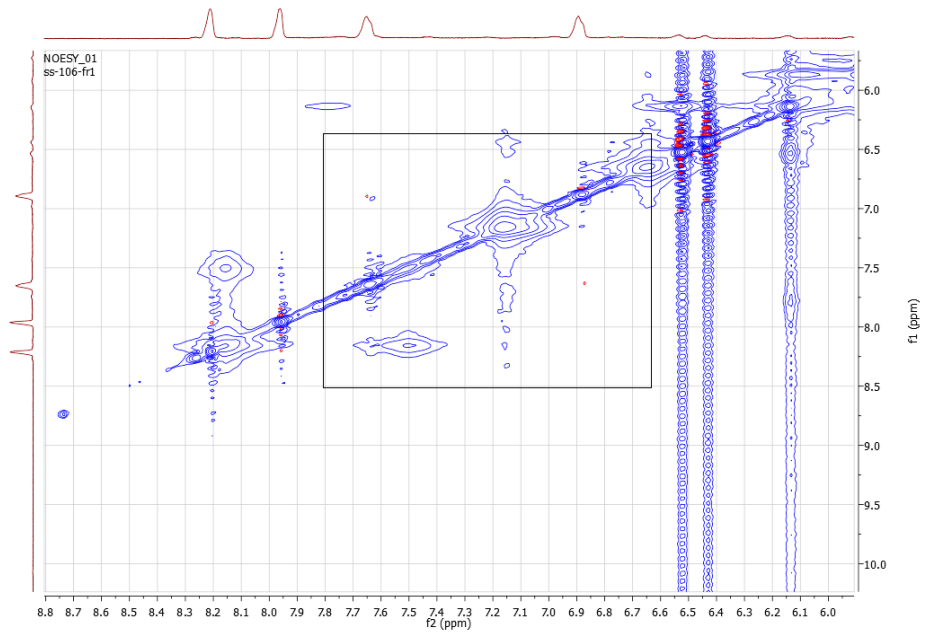
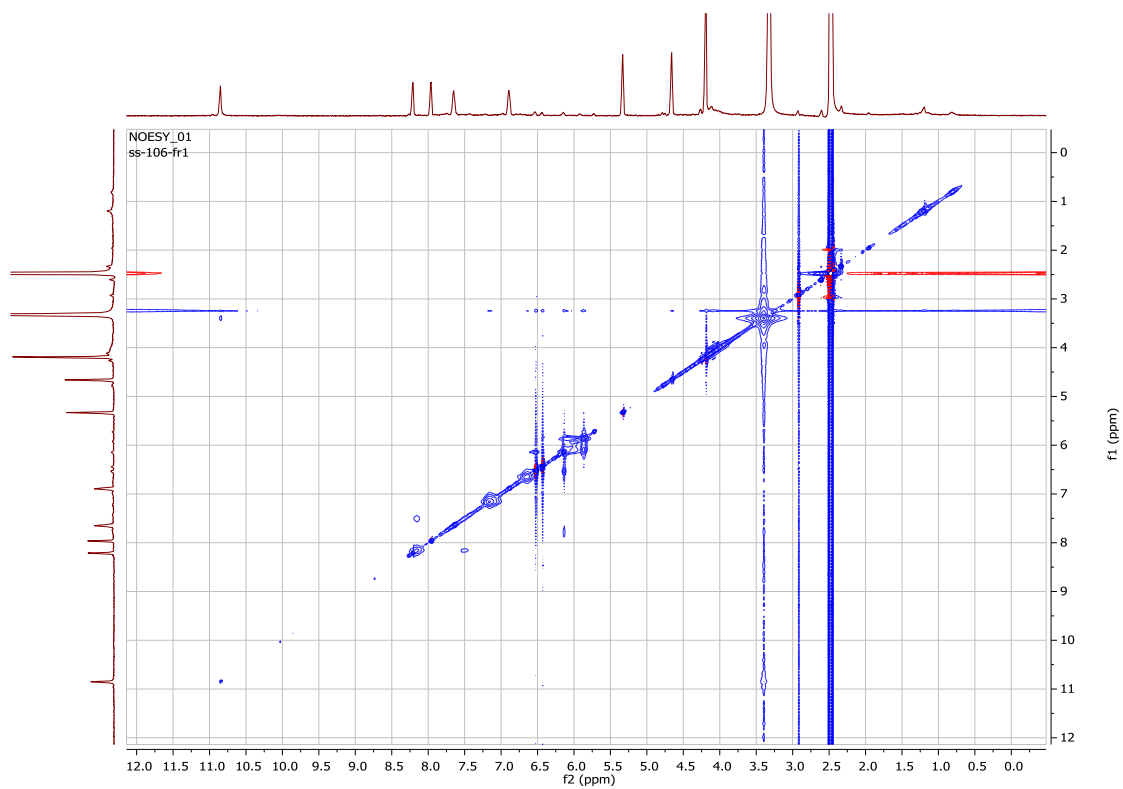


Figure 4.20. NOESY NMR of (Z)-164

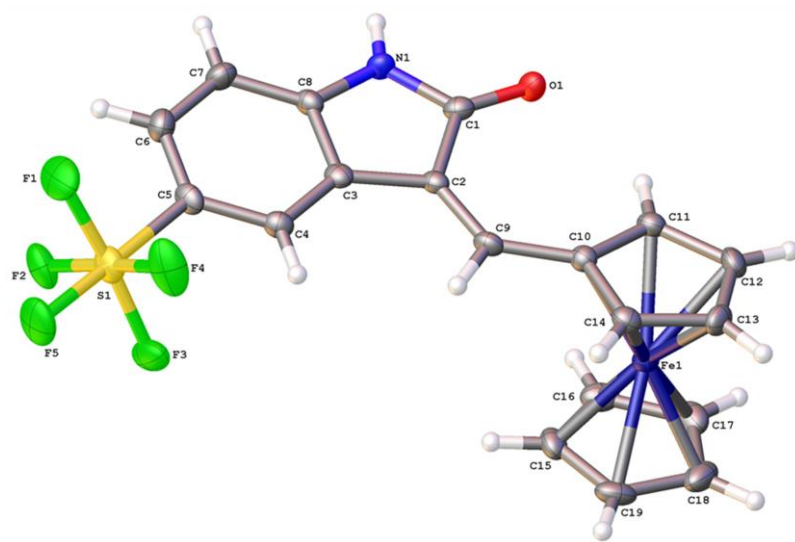


Figure 4.21. X-ray structure of (Z)-164.

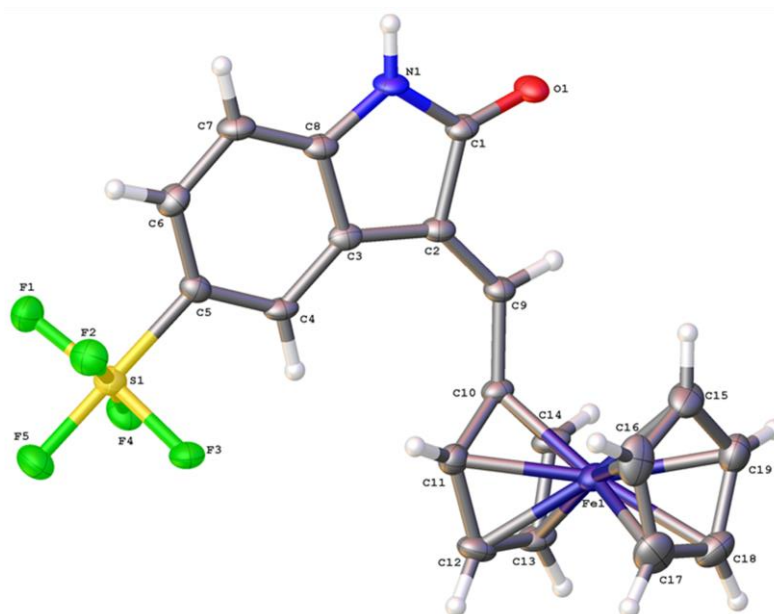


Figure 4.22. X-ray structure of (E)-164.

4.4 Biological Results

4.4.1 Biochemical assays

We tested all the above 7 compounds against a number of kinases that were inhibited by related ferrocene-based oxindoles (Figures 4.12, 4.13) in a biochemical assay (CEREP, commercial screen) i.e. VEGFR, PDGFR and DYRK family kinases. Any compounds that showed appreciable (approx. 50%) inhibition at 1 μ M were tested over a dose range for IC₅₀ values since these assays are relatively expensive.

Table 4.2 shows the IC₅₀ values against VEGFR3 (vascular endothelial growth factor receptor 3), PDGFR α (platelet-derived growth factor receptor), DYRK3 (dual specificity tyrosine-phosphorylation-regulated kinase 3), which were found to be hits from the initial screen.

These compounds were also tested, in biochemical assays vs. novel kinases including AAK1 (adaptor-associated protein kinase1), BMP2K (bone morphogenic protein-2-inducible kinase), GAK (cyclin G-associated kinase) and STK16 (serine/threonine-protein kinase16) by the Structural Genomics Consortium (SGC, Oxford) and results are found in the same table. Fortunately, whether active or not, IC₅₀ results were generated by our collaborators.

Table 4.2. IC₅₀ values of 7 compounds vs VEGFR3, PDGFR α , DYRK, AAK1, BMP2K, GAK and STK16. – denotes inactive.

Compound	IC ₅₀ (M)											
	FLT-1 kinase (h) (VEGFR1)	FLT-4 kinase (h) (VEGFR3)	KDR kinase (h) (VEGFR2)	PDGFR α kinase (h)	PDGFR β kinase (h)	DYRK1a (h)	DYRK2 (h)	DYRK3 (h)	AAK1	BMP2K	GAK	STK16
162	-	-	-	-	-	-	-	-	1.0 × 10 ⁻⁶	4.52 × 10 ⁻⁷	3.42 × 10 ⁻⁵	1.76 × 10 ⁻⁵
163	-	2.3 × 10 ⁻⁷	-	9.8 × 10 ⁻⁸	-	-	-	-	1.0 × 10 ⁻³	1.87 × 10 ⁻⁴	4.76 × 10 ⁻⁷	1.35 × 10 ⁻⁴
<i>(Z)</i> - 164	-	-	-	-	-	-	-	1.7 × 10 ⁻⁶	-	-	-	-
<i>(E)</i> - 164	-	-	-	-	-	-	-	2.4 × 10 ⁻⁶	-	-	-	-
<i>(Z)</i> - 165	-	-	-	-	-	-	-	-	-	-	-	-
166	-	5.3 × 10 ⁻⁷	-	-	-	-	-	-	-	-	-	-
167	-	1.8 × 10 ⁻⁸	-	3.1 × 10 ⁻⁹	-	-	-	-	-	-	-	-
Staurosporine	2.8 × 10 ⁻⁸	7.8 × 10 ⁻¹⁰	2.3 × 10 ⁻⁹	1.2 × 10 ⁻⁹	2.5 × 10 ⁻⁹	3.2 × 10 ⁻⁸	8.3 × 10 ⁻⁷	4.5 × 10 ⁻⁸	2.47 × 10 ⁻⁹	3.17 × 10 ⁻⁹	1.89 × 10 ⁻⁸	1.14 × 10 ⁻⁷

The position of the SF₅ group is important for activity; (*Z*)-**162** is inactive whereas (*Z*)-**163** shows sub micromolar activity vs. VEGFR3 (230 nM) and PDGFR α (98 nM, IC₅₀). Both (*E*)- and (*Z*)-**164** have low μ M activity vs. DRYK3 whereas (*Z*)-**165** is inactive. Again, the position of the SF₅ group appears to be important; **166** has an IC₅₀ of 530 nM whereas **167** has an IC₅₀ of 18 nM vs. VEGFR3 and a very impressive 3.1 nM activity vs. PDGFR α . While both compounds of (*Z*)-**162** and (*E*)-**163** showed the activity vs. protein kinases; AAK1, BMP2K, GAK and STK16 but not on the remaining 5 compounds.

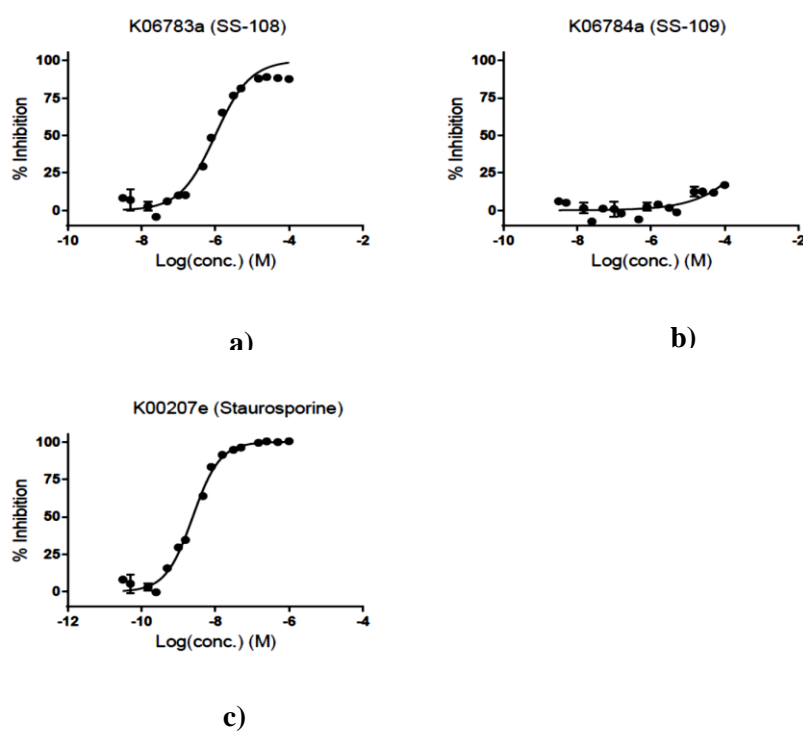


Figure 4.23. Activity of a) **162**, b) **163** and c) staurosporine in AAK1.

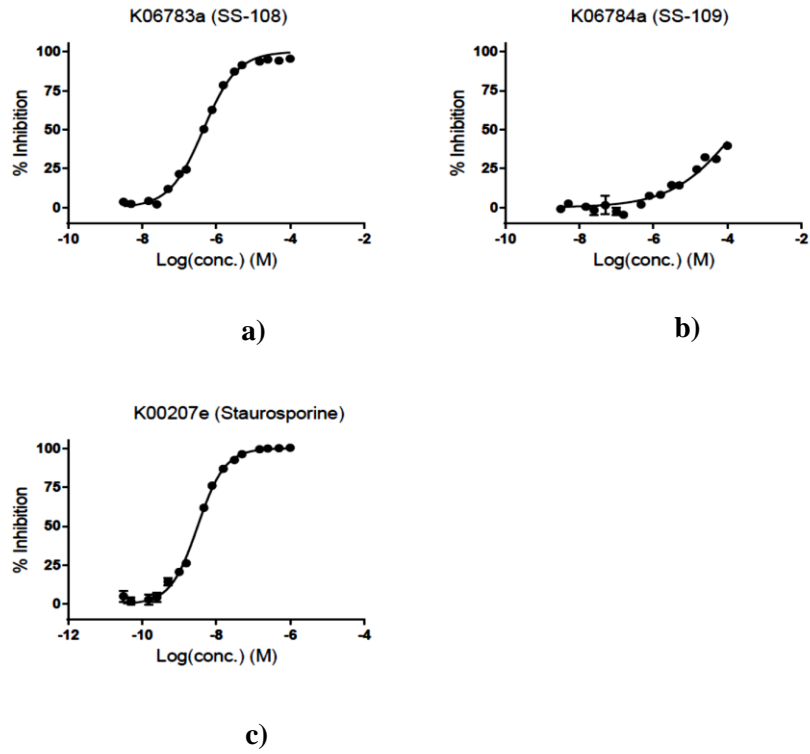


Figure 4.24. Activity of a) **162**, b) **163** and c) staurosporine in BMP2K.

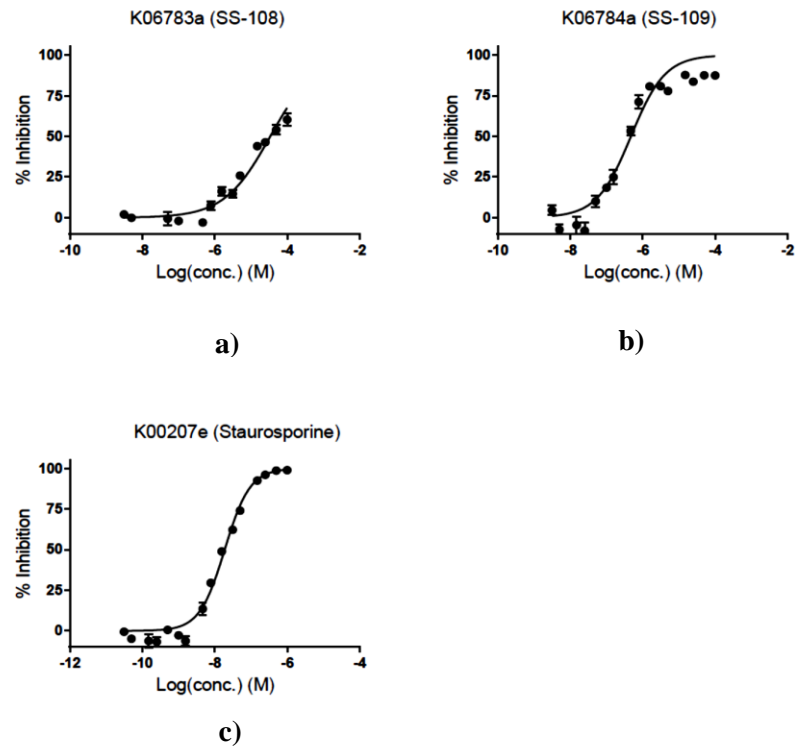


Figure 4.25. Activity of a) **162**, b) **163** and c) staurosporine in GAK.

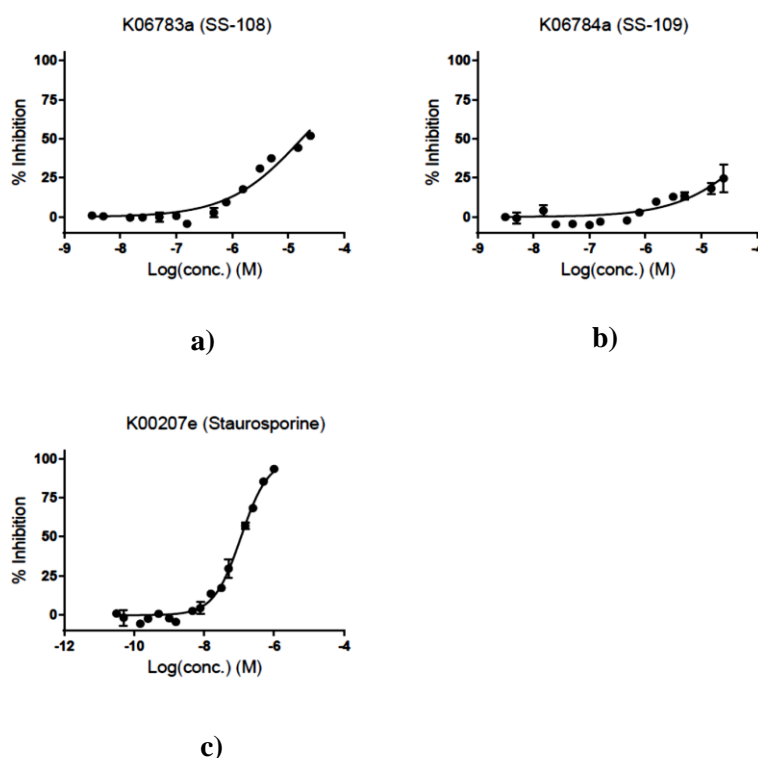


Figure 4.26. Activity of a) **162**, b) **163** and c) staurosporine in STK16.

4.4.2 Cell-based assays

Compounds **162-167** were next tested in breast cancer and normal healthy cells. The cell lines chosen were: MCF10A, which are breast cells, which are non-transformed, does not form tumours and are considered to be benign. These, as well as RPE cells (retinal pigment epithelium), would allow us to test the effects of our compounds on healthy cells, i.e. toxicity. MCF7, which are Luminal A, ER + and PR + (responsive to estrogen and progesterone, hence, estrogen and progesterone receptor positive) yet Her2 negative (unresponsive to human epidermal growth factor receptor 2). Such cell lines could normally respond to e. g. tamoxifen, **16**. T47D (Luminal A, ER +, PR +, Her2 -), MDA-MB-436 (abbreviated as MM36) and MDA-MB-231 (abbreviated as MM231) cell lines, both of which are triple negative (---) and cannot be treated with hormones or EGFR (HER2) inhibitors. These can be considered to be the most challenging to treat in the clinic.

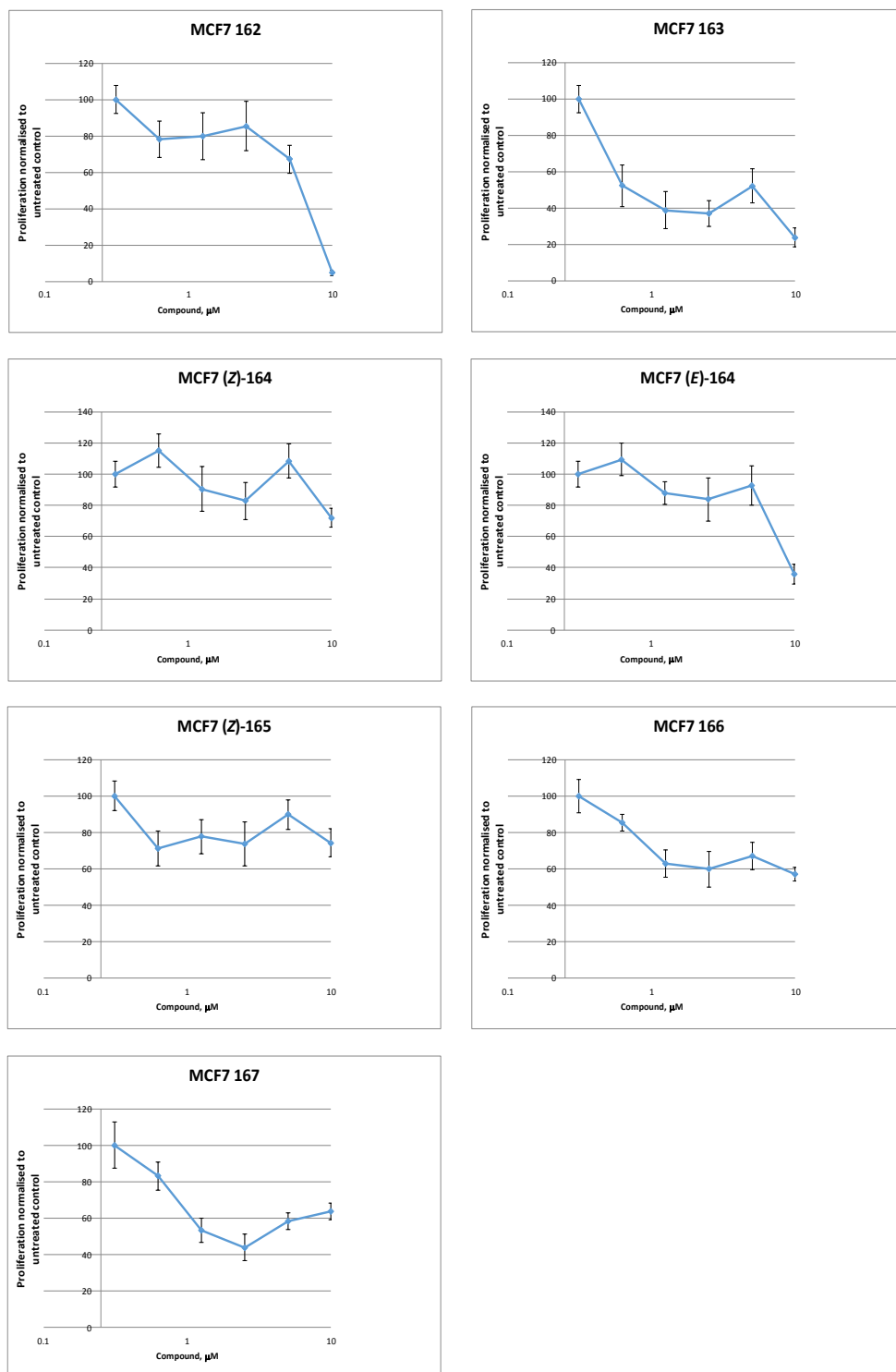


Figure 4.27. Toxicity of compounds on MCF7 cells.

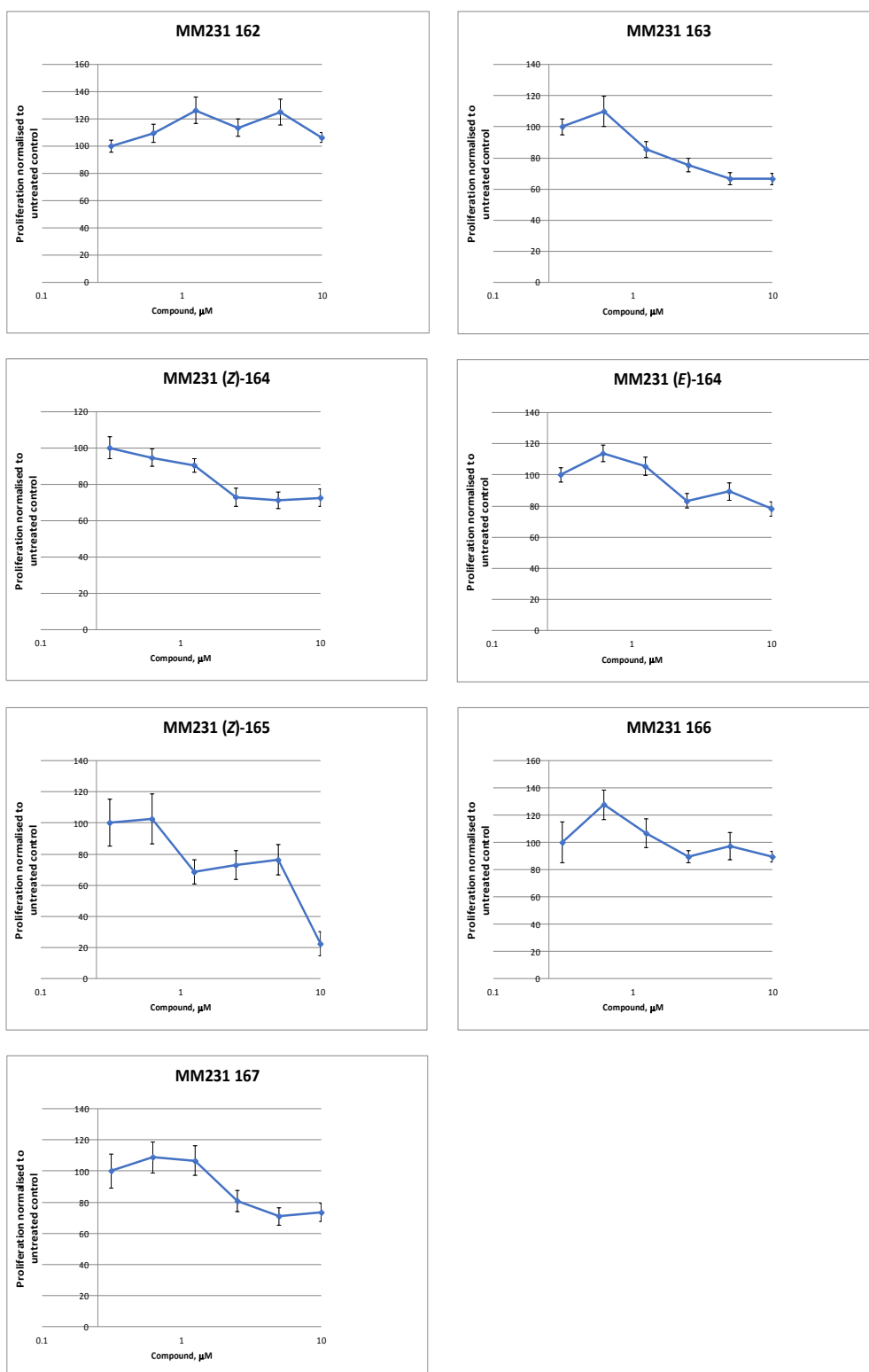


Figure 4.28. Toxicity of compounds on MM231 cells.

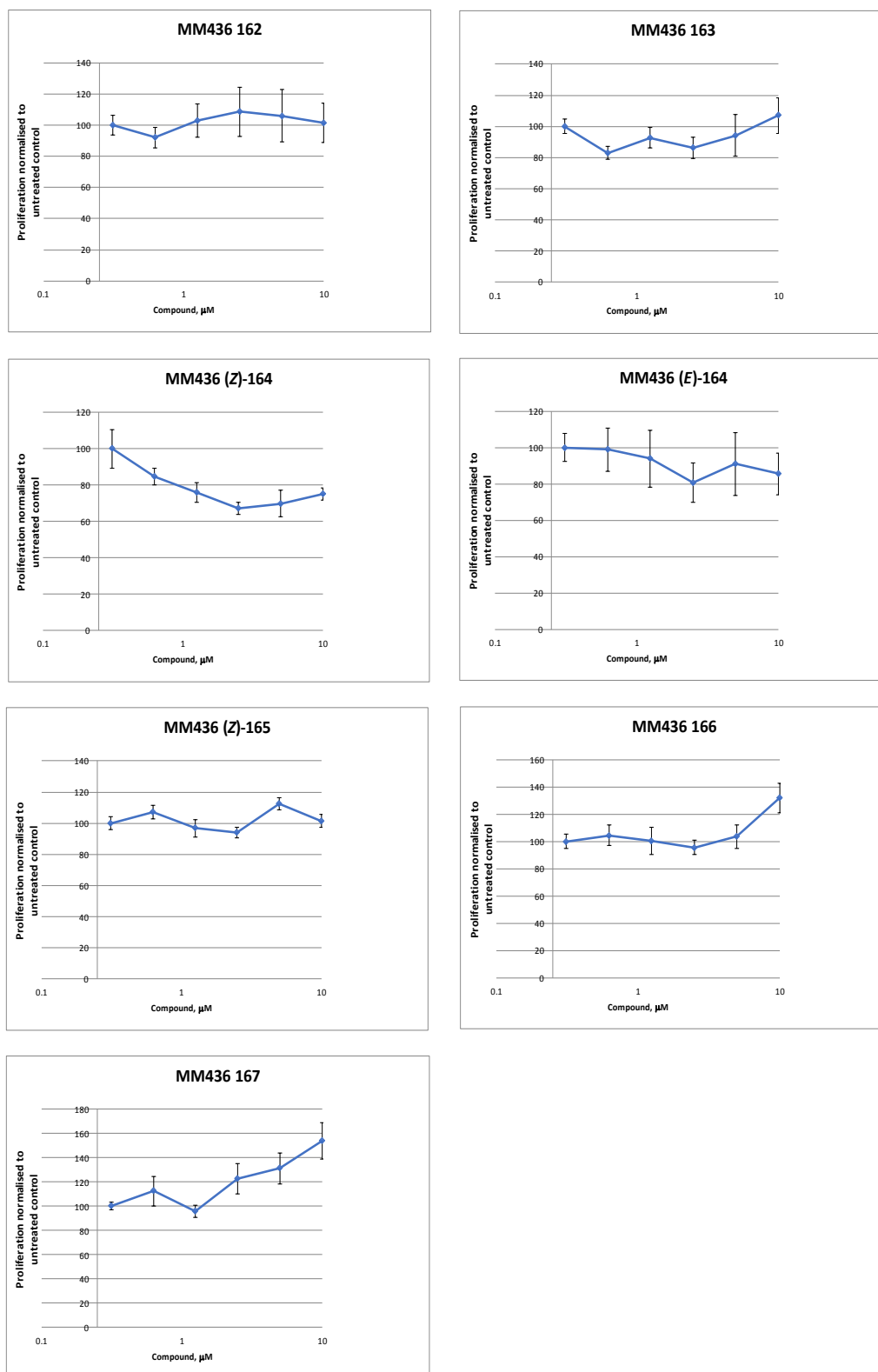


Figure 4.29. Toxicity of compounds on MM436 cells.

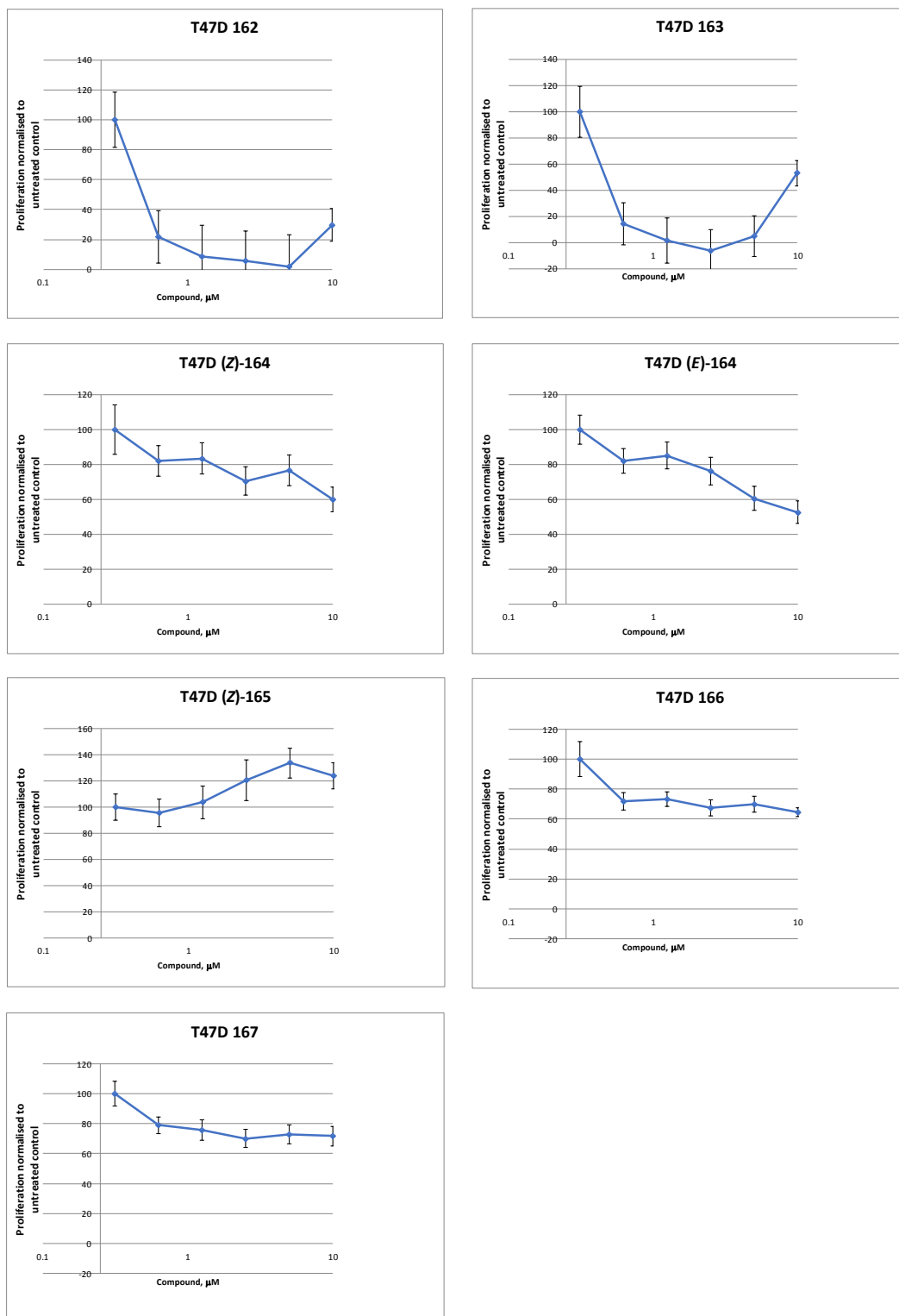


Figure 4.30. Toxicity of compounds on T47D cells.

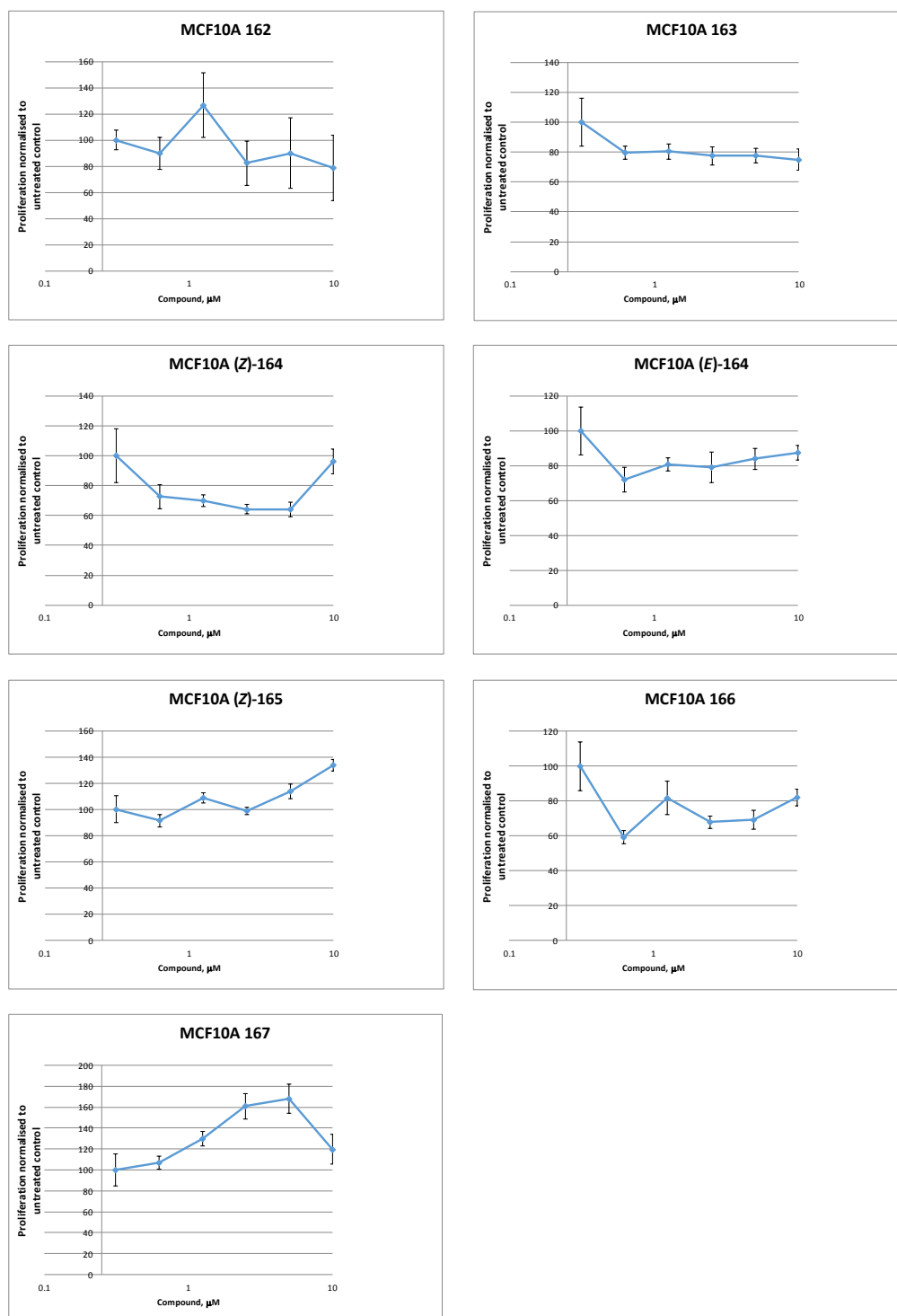


Figure 4.31. Toxicity of compounds on non-cancerous MCF10A cells.

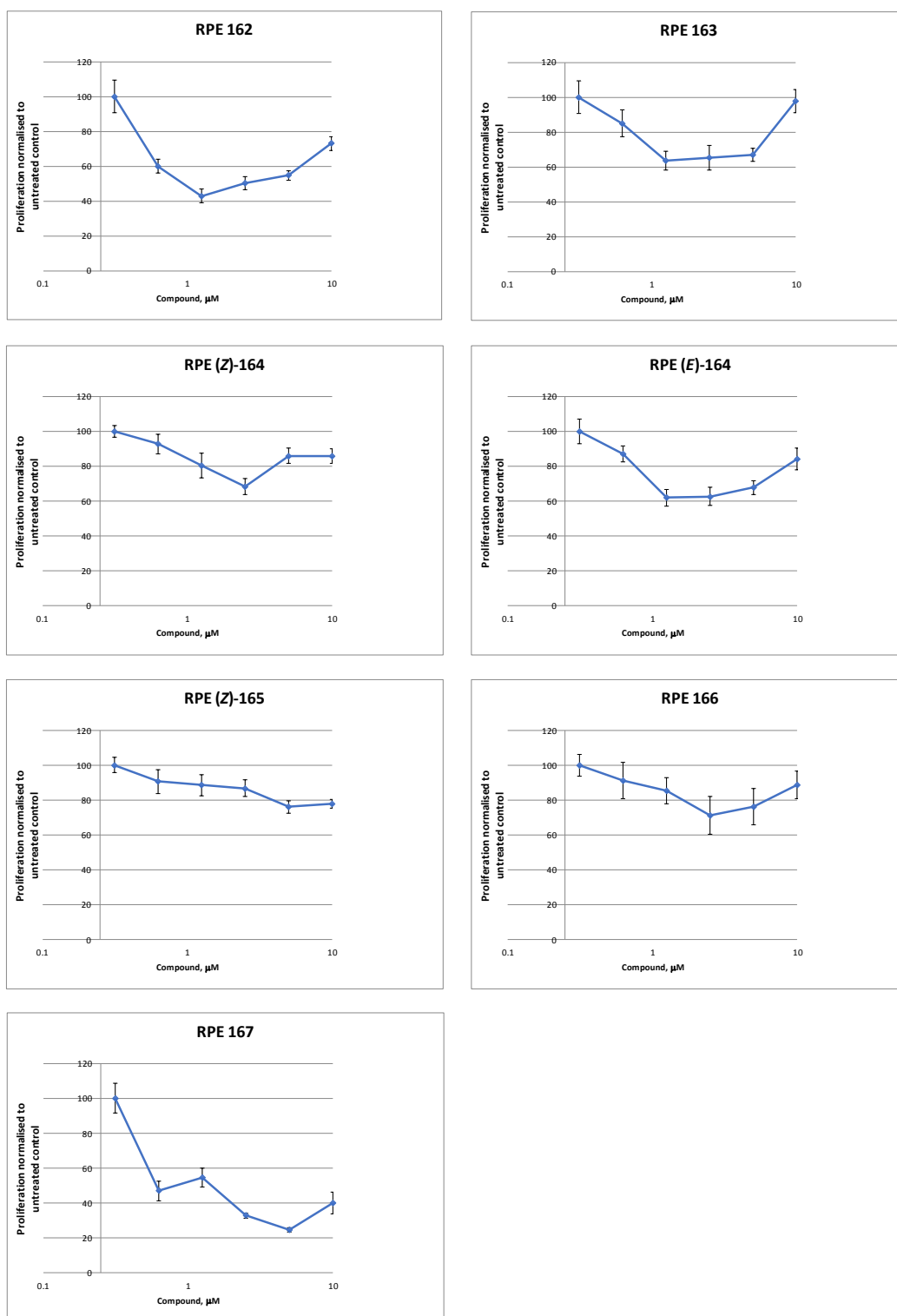


Figure 4.32. Toxicity of compounds on non-cancerous RPE cells.

Table 4.3 shows the GC_{50} values of compounds **162** and **163** in MCF7 and T47D.

Compound	GC_{50} (μ M)			
	MCF7	\pm standard deviation	T47D	\pm standard deviation
162	3.75	2.70	0.49	0.40
163	0.69	0.40	0.35	0.05

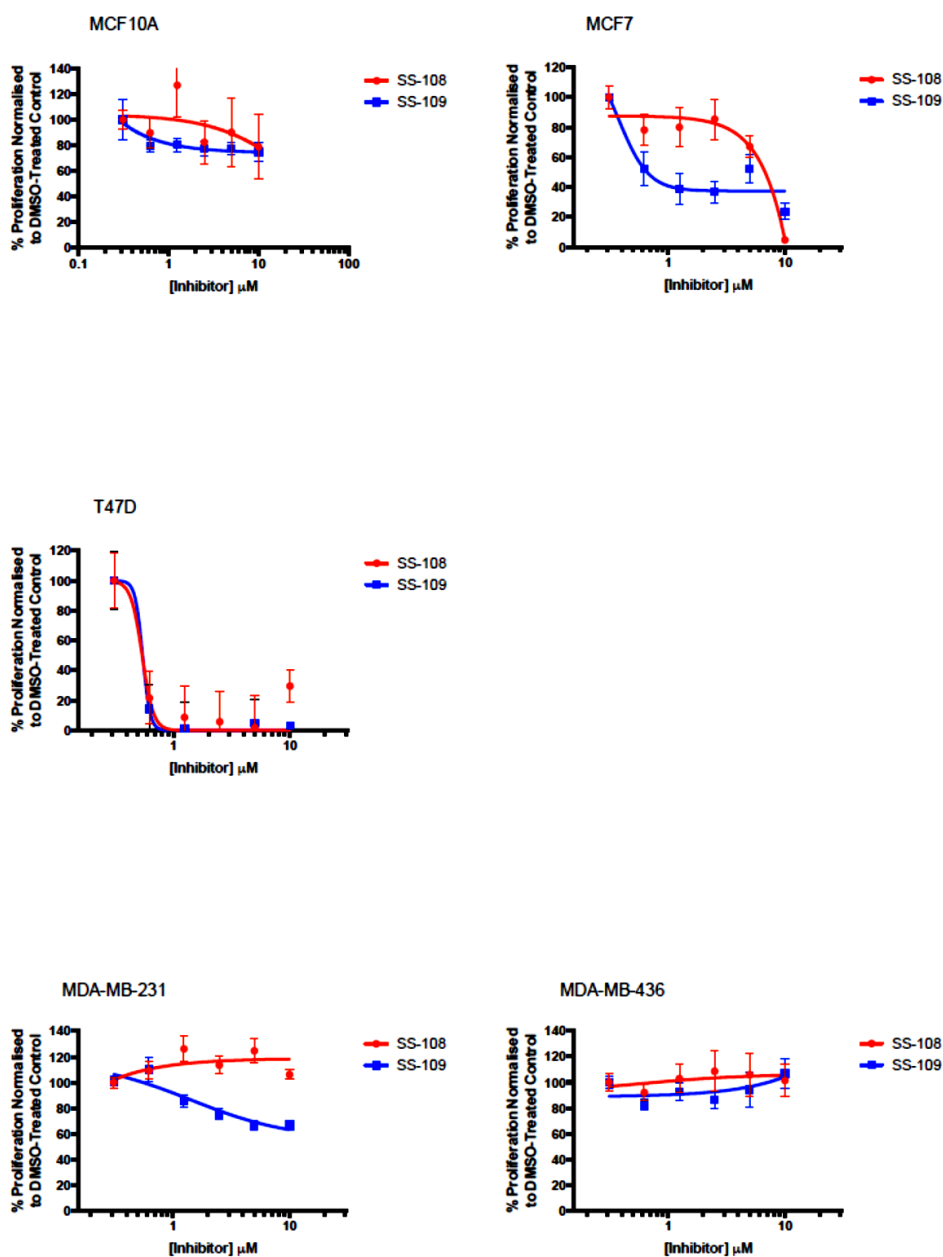


Figure 4.33. Activity of **162** (red) and **163** (blue) in different cell lines.

Figure 4.33 displays MCF7 and T47D, which are very similar breast cancer cell lines and it is encouraging that the **162** and **163** have similar potency against both, with GC_{50} s in the low micromolar range. While MDA-MB-231 and MDA-MB-436 are not affected (these are usually the most difficult to treat). The normal cell lines MCF10 are not affected.

4.4.3 Modelling

To explore the binding modes of **162** and **163** in PDGFR α (PDB: 5K5X) we performed docking studies and it showed both compounds bind to the ATP pocket. Docking was performed using molecular mechanics (AutoDock 4.2.6. using the Lamarckian Genetic Algorithm and empirical free energy scoring function). PDB format files for the ligand and kinase domain were pre-processed using AutoDock Tools 1.5.6.²⁴ We found **163** binds deeply in a predominantly hydrophobic pocket where **162** is shown in blue and **163** is shown in green colour. The carbonyl group of **163** binds to the Asp backbone as shown in Figure 4.34. Also in Figure 4.35 are shown the zoom-in docking poses where the carbonyl group of **162** binds to the Cys backbone. The oxindole binds to the hinge region. **163** fits nicely deep into the hydrophobic pocket. **163** has a higher potency compared to **162** and Figure 4.36 shows the clash of **162** in PDGFR α .

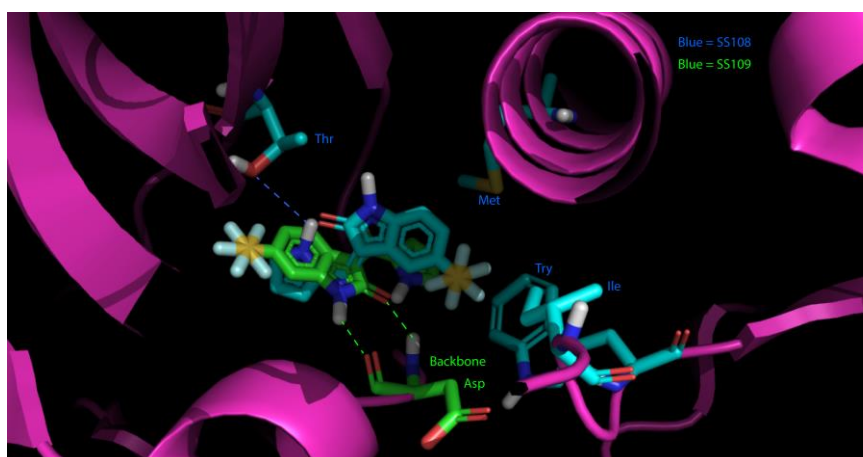


Figure 4.34. Docking poses of **162** (blue) and **163** (green) in PDGFR α .

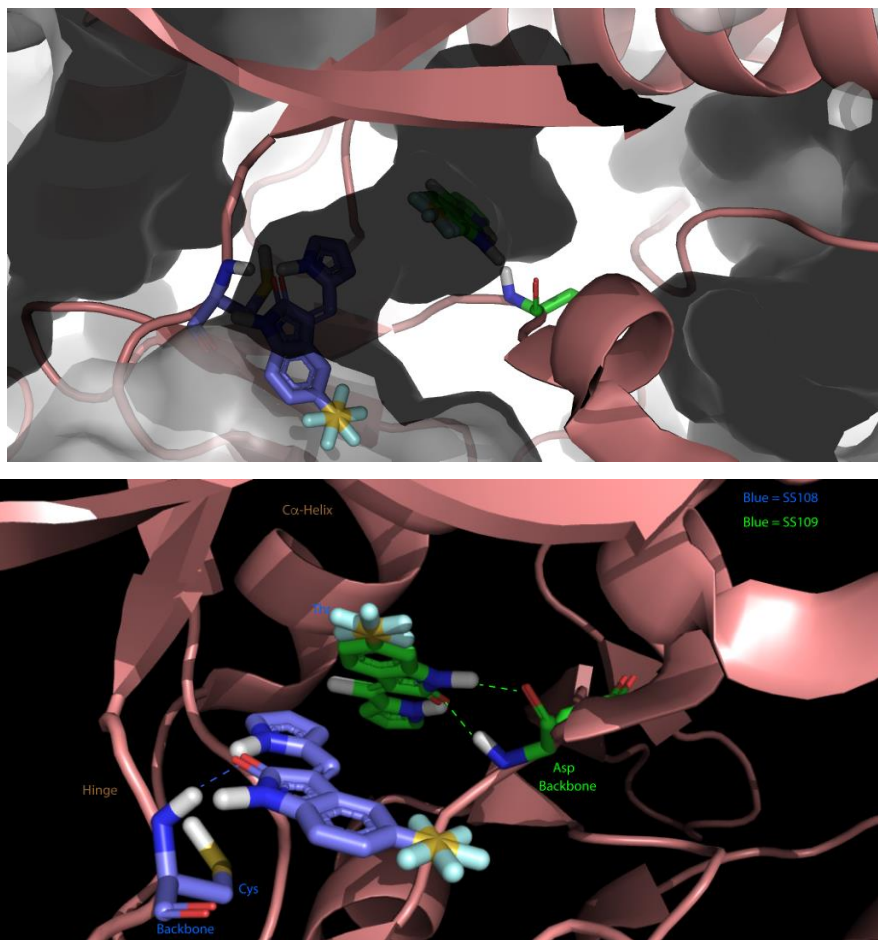


Figure 4.35. Docking poses of **162** (blue) and **163** (green) in PDGFR α (zoom-in).

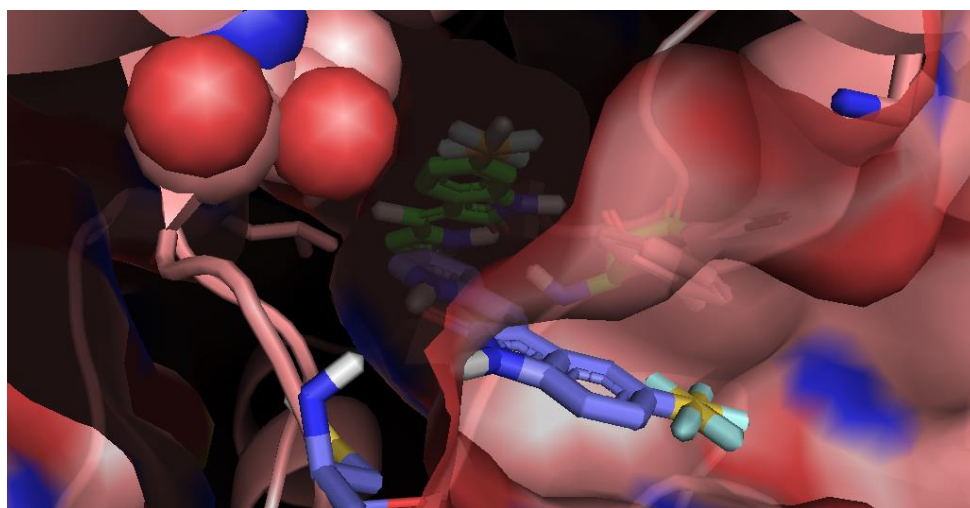


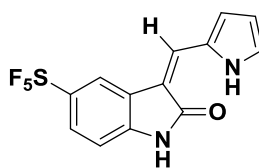
Figure 4.36. Docking poses of SF₅ group clashing in **162** (blue) in PDGFR α .

4.5 Conclusion

SF₅-oxindole compound analogues have been synthesized, characterized by a number of spectroscopic techniques in solution and by X-ray crystallography in the solid state. They were tested for biological activity testing versus a panel of kinases and in cancer cell lines. Compounds **163** displayed good activity and by docking studies we showed that **163** nicely fits in the protein PDGFR α and more effectively than **162**. Preliminary studies show these to have good activity in breast cancer cell lines. However, we need to further explore these inhibitors in order to gain an understanding of their mechanism of action. More kinase screens are needed to explore their selectivity and promiscuity as well as more cancer cell line work is needed. Are the cell line effects due to kinase inhibition, what are the expression levels of such kinases in cells, or are the cell effects due to the inhibition of other targets in the cell for example?

4.6 Experimental

5-(Pentafluorosulfanyl)-1,3-dihydro-indol-2-one and 6-(pentafluorosulfanyl)-1,3-dihydro-indol-2-one were obtained from SpiroChem. Ferrocene carboxaldehyde, pyrrole-2-carboxaldehyde, piperidine and sodium chloride were obtained from Sigma-Aldrich. Magnesium sulfate was obtained from Fisher Scientific. Preparative TLC was obtained from Analtech. Solvents and reagents were purchased from commercial suppliers and were used without purification. All reactions were performed in a fume hood. NMR spectra were recorded on Varian 500 MHz or 400 MHz spectrometers and chemical shifts are reported in ppm, usually referenced to TMS as an internal standard. LCMS were performed by Shimadzu LCMS-2020 equipped with a Gemini® 5 μ m C18 110Å column and percentage purities were ran over 30 minutes in water/acetonitrile with 0.1% formic acid (5 min at 5%, 5%-95% over 20 min, 5 min at 95%) with the UV detector at 254 nm. Mass spectrometry: ESI mass spectra were obtained using a Bruker Daltonics Apex III, using Apollo ESI as the ESI source. For EI mass spectra, a Fissions VG Autospec instrument was used at 70 eV. All analyses were run by Dr. Alla .K. Abdul-Sada. Analyses are for the molecular ion peak [M]⁺ and are given in m/z, mass to charge ratio. Elemental analyses were conducted by Stephen Boyer (London Metropolitan University). The reactions for synthesis and purity of product were monitored by thin layer chromatography using TLC plates.



(Z)-3-((1H-pyrrol-2-yl)methylene)-5-pentafluorosulfanylindoline-2-one, 162.

The title compound was prepared by a Knoevenagel condensation reaction. 5-(Pentafluorosulfanyl)1,3-dihydro-indol-2-one (129.6 mg, 0.5 mmol), pyrrole-2-carboxaldehyde (57.06 mg, 0.6 mmol), ethanol (5 mL) and piperidine 3 drops were subjected to the microwave irradiation by ramping to 150°C and were held at that temperature for 30 minutes. TLC analysis of the cooled reaction mixture monitored consumption of starting materials. The crude reaction mixture was extracted with ethyl acetate (2×10 cm³) and washed with deionised water (10 mL) and brine (2×10 mL), the organic layer was dried using magnesium sulphate then filtered through a cotton wool plug. The crude mixture was concentrated in vacuo and purified using silica gel column chromatography using 3:7 hexane/diethyl ether to give an orange solid. The yield was 105 mg, 65%. Crystallization by mixed solvents, CH₂Cl₂ and hexane, provided orange crystals.

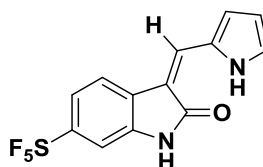
¹H NMR (DMSO-d₆, 500MHz): δ = 13.22 (1H, s, NH), 11.30 (1H, s, NH), 8.24 (1H, d, *J* = 2.3 Hz, CH), 8.11 (1H, s, CH), 7.65 (1H, dd, *J* = 8.6, 2.2 Hz, CH), 7.44 (1H, d, *J* = 2.2 Hz, CH), 7.02 (1H, d, *J* = 8.6 Hz, CH), 6.92 (1H, d, *J* = 3.6 Hz, CH), 6.41 (1H, dd, *J* = 3.6, 2.2 Hz, CH).

¹³C NMR (DMSO-d₆, 126 MHz): δ = 169.9, 147.5, 141.5, 130.0, 129.5, 127.6, 125.9, 124.7, 122.5, 116.7, 115.2, 112.3, 109.6.

HRMS-ESI (m/z) found: 337.0431, calc. for [C₁₃H₉F₅N₂OS + H]⁺ 337.0429.

Anal. Calcd (%) for C₁₃H₉F₅N₂OS: C, 46.43; H, 2.70; N, 8.33.

Found (%): C, 46.55; H, 2.61; N, 8.21.



(Z)-3-((1H-pyrrol-2-yl)methylene)-6-pentafluorosulfanylindoline-2-one, 163.

The title compound was prepared by a Knoevenagel condensation reaction. 6-(Pentafluorosulfanyl)1,3-dihydro-indol-2-one (129.6 mg, 0.5 mmol), pyrrole-2-carboxaldehyde (57.06 mg, 0.6 mmol), ethanol (5 mL) and piperidine 3 drops were subjected to the microwave irradiation by ramping to 150°C and were held at that temperature for 30 minutes. TLC analysis of the cooled reaction mixture monitored consumption of starting materials. The crude reaction mixture was extracted with ethyl acetate (2×10 mL) and washed with deionised water (10 mL) and brine (2×10 mL), the organic layer was dried using magnesium sulphate then filtered through a cotton wool plug. The crude mixture was concentrated in vacuo and purified using silica gel column chromatography using 3:7 hexane/ethyl acetate and trituration with hexane to give brown-orange solid. The yield was 142 mg, 74%. Crystallization by DCM provided orange crystals.

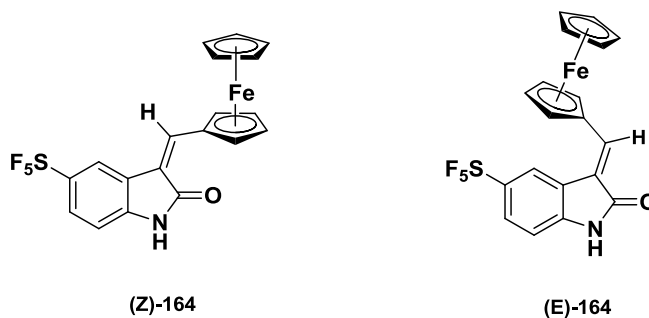
¹H NMR (DMSO-d₆, 500MHz): δ = 13.31 (1H, s, NH), 11.14 (1H, s, NH), 7.99 (1H, s, CH), 7.81 (1H, d, *J* = 8.6 Hz, CH), 7.53 (1H, dd, *J* = 8.6, 2.0 Hz, CH), 7.48 (1H, s, CH), 7.26 (1H, d, *J* = 2.0 Hz, CH), 6.93 (1H, m, CH), 6.43 (1H, dd, *J* = 3.7, 2.1 Hz, CH).

¹³C NMR (DMSO-d₆, 126 MHz): δ = 169.5, 138.8, 130.2, 130.0, 129.6, 128.3, 123.1, 119.1, 118.7, 114.7, 112.7, 107.0.

HRMS-ESI (m/z) found: 337.0432, calc. for [C₁₃H₉F₅N₂OS + H]⁺ 337.0429.

Anal. Calcd (%) for C₁₃H₉F₅N₂OS: C, 46.43; H, 2.70; N, 8.33.

Found (%): C, 46.59; H, 2.61; N, 8.17.



5-Pentafluorosulfonyl-3-ferrocenylindolin-2-one, 164.

5-Pentafluorosulfonyl-3-ferrocenylindolin-2-one was prepared by a Knoevenagel condensation reaction. 5-(Pentafluorosulfonyl)1,3-dihydro-indol-2-one (259.2 mg, 1.0 mmol), ferrocenecarboxaldehyde (256.8 mg, 1.2 mmol), ethanol (10 mL) and piperidine 6 drops were subjected to the microwave irradiation by ramping to 150°C and were held at that temperature for 30 minutes. TLC analysis of the cooled reaction mixture monitored consumption of starting materials. The crude reaction mixture was extracted with ethyl acetate (2×10 mL) and washed with deionised water (10 mL) and brine (2×10 mL), the organic layer was dried using magnesium sulphate then filtered through a cotton wool plug. The crude mixture was concentrated in vacuo and purified using preparative TLC using 3:7 hexane/ethyl acetate to give fraction 1 (purple solid 160 mg, 35%) and fraction 2 (red solid 109 mg, 24%). Crystallization of fraction 1 was by mixed solvents CH₂Cl₂ and hexane and fraction 2 was by CH₂Cl₂.

(Z)-164: (Z)-5-pentafluorosulfonyl-3-ferrocenylindolin-2-one.

¹H NMR (DMSO-d₆, 500MHz): δ = 10.84 (1H, s, NH), 8.23 (1H, s, CH), 7.98 (1H, s, CH), 7.68 (1H, d, J=8.6, CH), 6.92 (1H, d, J = 8.6 Hz, CH), 5.37 (2H, s, 2CH), 4.69 (2H, s, 2CH), 4.22 (5H, s, Cp)

¹³C NMR (CDCl₃-d, 126 MHz): δ = 167.7, 141.9, 125.1, 119.3, 116.0, 110.0, 108.4, 74.0, 73.3, 70.0, 60.3, 14.2.

HRMS-ESI (m/z) found: 455.0065, calc. for [C₁₉H₁₄F₅FeNOS]⁺ 455.0060.

Anal. Calcd (%) for C₁₉H₁₄F₅FeNOS: C, 50.13; H, 3.10; N, 3.08.

Found (%): C, 50.22; H, 3.03; N, 3.07.

(E)-164: (*E*)-5-Pentafluorosulfanyl-3-ferrocenylindolin-2-one.

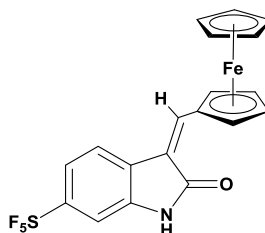
^1H NMR (DMSO- d_6 , 500MHz): δ = 10.94 (1H, s, NH), 8.30 (1H, s, CH), 7.76(1H, d, $J=8.4$, CH), 7.65-7.71 (1H, m, CH), 7.01 (1H, d, $J=8.4$, CH), 4.79-7.81 (4H, m, 4CH), 4.29 (5H, m, Cp).

^{13}C NMR (CDCl_3 - d , 126 MHz): δ = 171.1, 141.8, 109.0, 88.2, 72.6, 71.7, 70.2, 60.3, 31.5, 29.6, 22.6, 20.9, 19.0, 14.1, 14.0.

HRMS-ESI (m/z) found: 455.0064, calc. for $[\text{C}_{19}\text{H}_{14}\text{F}_5\text{FeNOS}]^+$ 455.0060.

Anal. Calcd (%) for $\text{C}_{19}\text{H}_{14}\text{F}_5\text{FeNOS}$: C, 50.13; H, 3.10; N, 3.08.

Found (%): C, 50.27; H, 3.23; N, 3.10.



(Z)-6-Pentafluorosulfanyl-3-ferrocenylindolin-2-one, 165.

The title compound was prepared by a Knoevenagel condensation reaction. 6-(Pentafluorosulfanyl)1,3-dihydro-indol-2-one (129.6 mg, 0.5 mmol), ferrocenecarboxaldehyde (128.4 mg, 0.6 mmol), ethanol (5 mL) and piperidine 3 drops were subjected to the microwave irradiation by ramping to 150°C and were held at that temperature for 30 minutes. TLC analysis of the cooled reaction mixture monitored consumption of starting materials. The crude reaction mixture was extracted with ethyl acetate (2×10 mL) and washed with deionised water (10 mL) and brine (2×10 mL), the organic layer was dried using magnesium sulphate then filtered through a cotton wool plug. The crude mixture was concentrated in vacuo and purified using preparative TLC using 3:7 hexane/diethyl ether to give a purple solid. The yield was 111.53 mg, 49%.

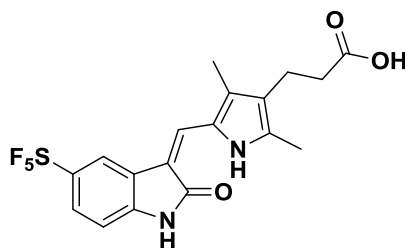
^1H NMR ($\text{CDCl}_3\text{-d}$, 500MHz): δ = 8.02 (1H, d, J = 8.6 Hz, CH), 7.84 (1H, s, NH), 7.72 (1H, s, CH), 7.54 (1H, m, CH), 7.40 (1H, dd, J = 8.6, 2.2 Hz, CH), 4.80 (2H, m, 2CH), 4.70 (2H, m, 2CH), 4.28 (5H, s, Cp).

^{13}C NMR ($\text{CDCl}_3\text{-d}$, 126 MHz): δ = 199.5, 163.1, 136.1, 130.8, 128.8, 121.9, 72.5, 71.8, 70.2, 29.3.

HRMS-ESI (m/z) found: 455.0064, calc. for $[\text{C}_{19}\text{H}_{14}\text{F}_5\text{FeNOS}]^+$ 455.0060.

Anal. Calcd (%) for $\text{C}_{19}\text{H}_{14}\text{F}_5\text{FeNOS}$: C, 50.13; H, 3.10; N, 3.08.

Found (%): C, 50.21; H, 2.99; N, 3.12.



(Z)-3-(2,4-Dimethyl-5-((5-pentafluorosulfanyl-2-oxoindolin-3-ylidene)methyl)-1H-pyrrol-3-yl)propanoic acid, 166.

The title compound was prepared by a Knoevenagel condensation reaction. 5-(Pentafluorosulfanyl)1,3-dihydro-indol-2-one (106 mg, 0.41 mmol), 3-(5-formyl-1H-pyrrole-3-yl)propanoic acid (97.6 mg, 0.5 mmol), ethanol (6 mL) and piperidine 5 drops were subjected to the microwave irradiation by ramping to 150°C and were held at that temperature for 30 minutes. TLC analysis of the cooled reaction mixture monitored consumption of starting materials. The crude reaction mixture was dried, washed with hexane and CH₂Cl₂ to give a brown solid. The yield was 141 mg, 79%.

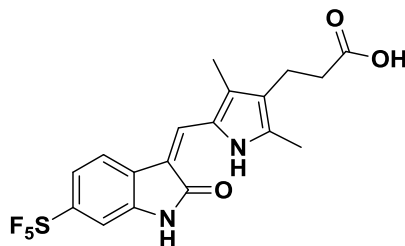
¹H NMR (DMSO-d₆, 500MHz): δ = 13.46 (1H, s, OH), 8.40 (1H, s, NH), 7.86 (1H, s, NH), 7.55 (1H, d, *J* = 8.6 Hz, CH), 6.98 (1H, *J* = 8.6 Hz, CH), 2.77-2.72 (2H, m, 2CH), 2.62 (2H, t, *J* = 7.7 Hz, CH₂), 2.31 (3H, s, CH₃), 2.28-2.22 (2H, s, CH₂), 1.48 (3H, s).

¹³C NMR (DMSO-d₆, 126 MHz): δ = 186.1, 174.6, 170.0, 140.1, 136.8, 132.7, 126.7, 126.3, 123.6, 116.2, 110.4, 109.0, 88.3, 88.2, 35.2, 20.0, 12.5, 10.1.

HRMS-ESI (m/z) found: 459.0772, calc. for [C₁₈H₁₇F₅N₂NaO₃S]⁺ 459.0772.

Anal. Calcd (%) for C₁₈H₁₇F₅N₂O₃S: C, 49.54; H, 3.93; N, 6.42.

Found (%): C, 49.63; H, 4.04; N, 6.48.



(Z)-3-(2,4-Dimethyl-5-((6-pentafluorosulfanyl-2-oxoindolin-3-ylidene)methyl)-1H-pyrrol-3-yl)propanoic acid, 167.

The title compound was prepared by a Knoevenagel condensation reaction. 6-(Pentafluorosulfanyl)1,3-dihydro-indol-2-one (106 mg, 0.41 mmol), 3-(5-formyl-1H-pyrrole-3-yl)propanoic acid (97.6 mg, 0.5 mmol), ethanol (6 mL) and piperidine 5 drops were subjected to the microwave irradiation by ramping to 150°C and were held at that temperature for 30 minutes. TLC analysis of the cooled reaction mixture monitored consumption of starting materials. The crude reaction mixture was dried, washed with hexane and CH₂Cl₂ to give a brown solid. The yield was 136 mg, 76%.

¹H NMR (DMSO-d₆, 500MHz): δ = 13.50 (1H, s, OH), 10.87 (1H, s, NH), 7.90 (1H, d, *J* = 8.6 Hz, CH), 7.74 (1H, s, NH), 7.46 (1H, dd, *J* = 8.6, 2.1 Hz, CH), 7.24 (1H, d, *J* = 2.1 Hz, CH), 2.78-7.69 (1H, m, CH), 2.66-2.61 (2H, m, CH₂), 2.34-2.27 (6H, m, 2CH₃), 2.25 (1H, s, CH), 1.5 (1H, s, CH).

¹³C NMR (DMSO-d₆, 126 MHz): δ = 174.5, 169.7, 137.8, 133.2, 130.4, 126.9, 123.9, 117.9, 109.8, 88.3, 88.2, 44.4, 35.1, 23.1, 22.5, 20.0, 12.5, 9.96.

HRMS-ESI (m/z) found: 459.0776, calc. for [C₁₈H₁₇F₅N₂NaO₃S]⁺ 459.0772.

Anal. Calcd (%) for C₁₈H₁₇F₅N₂O₃S: C, 49.54; H, 3.93; N, 6.42.

Found (%): C, 49.70; H, 4.09; N, 6.56.

4.7 References

- 1 M. K. Paul and A. K. Mukhopadhyay, *Int. J. Med. Sci.*, 2004, **1**, 101–115.
- 2 J. G. Kettle and D. M. Wilson, *Drug Discov. Today*, 2016, **21**, 1596–1608.
- 3 W. H. J. Ward, P. N. Cook, A. M. Slater, D. H. Davies, G. A. Holdgate and L. R. Green, *Biochem. Pharmacol.*, 1994, **48**, 659–666.
- 4 M. Maemondo, A. Inoue, K. Kobayashi, S. Sugawara, S. Oizumi, H. Isobe, A. Gemma, M. Harada, H. Yoshizawa, I. Kinoshita, Y. Fujita, S. Okinaga, H. Hirano, K. Yoshimori, T. Harada, T. Ogura, M. Ando, H. Miyazawa, T. Tanaka, Y. Saijo, K. Hagiwara, S. Morita and T. Nukiwa, *N. Engl. J. Med.*, 2010, **362**, 2380–8.
- 5 M. Fukuoka, S. Yano, G. Giaccone, T. Tamura, K. Nakagawa, J. Y. Douillard, Y. Nishiwaki, J. Vansteenkiste, S. Kudoh, D. Rischin, R. Eek, T. Horai, K. Noda, I. Takata, E. Smit, S. Averbuch, A. Macleod, A. Feyereislova, R. P. Dong and J. Baselga, *J. Clin. Oncol.*, 2003, **21**, 2237–2246.
- 6 Z. Li, M. Xu, S. Xing, W. T. Ho, T. Ishii, Q. Li, X. Fu and Z. J. Zhao, *J. Biol. Chem.*, 2007, **282**, 3428–3432.
- 7 D. Fabbro, S. W. Cowan-Jacob and H. Moebitz, *Br. J. Pharmacol.*, 2015, **172**, 2675–2700.
- 8 N. Funato, H. Takayanagi, Y. Konda, Y. Toda, Y. Harigaya, Y. Iwai and S. Omura, *Tetrahedron Lett.*, 1994, **35**, 1251–1254.
- 9 A. M. Lawrie, M. E. Noble, P. Tunnah, N. R. Brown, L. N. Johnson and J. A. Endicott, *Nat. Struct. Biol.*, 1997, **4**, 796–801.
- 10 D. S. Williams, P. J. Carroll and E. Meggers, *Inorg. Chem.*, 2007, **46**, 2944–2946.
- 11 E. Meggers, *Curr. Opin. Chem. Biol.*, 2007, **11**, 287–292.
- 12 C. Kunick and I. Ott, *Angew. Chemie - Int. Ed.*, 2010, **49**, 5226–5227.
- 13 L. Sun, N. Tran, F. Tang, H. App, P. Hirth, G. McMahon and C. Tang, *J. Med. Chem.*, 1998, **41**, 2588–2603.
- 14 J. Spencer, A. P. Mendham, A. K. Kotha, S. C. W. Richardson, E. A. Hillard, G. Jaouen, L. Male and M. B. Hursthouse, *Dalt. Trans.*, 2009, **9226**, 918–921.
- 15 J. Spencer, J. Amin, S. K. Callear, G. J. Tizzard, S. J. Coles, P. Coxhead and M. Guille, *Metallomics*, 2011, **3**, 600–608.
- 16 P. Wu, T. E. Nielsen and M. H. Clausen, *Trends Pharmacol. Sci.*, 2015, **36**, 422–

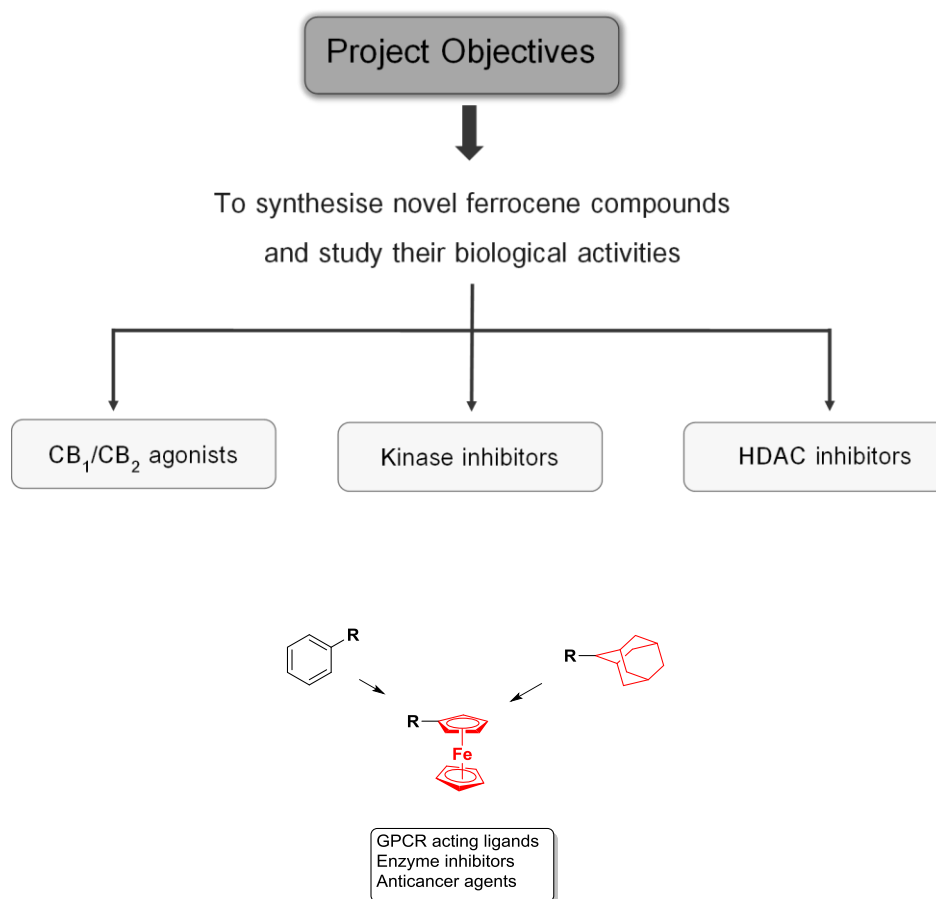
- 439.
- 17 B. Stump, C. Eberle, W. B. Schweizer, M. Kaiser, R. Brun, R. L. Krauth-Siegel, D. Lentz and F. Diederich, *ChemBioChem*, 2009, **10**, 79–83.
 - 18 S. Altomonte and M. Zanda, *J. Fluor. Chem.*, 2012, **143**, 57–93.
 - 19 S. Altomonte, G. L. Baillie, R. A. Ross, J. Riley and M. Zanda, *RSC Adv.*, 2014, **4**, 20164.
 - 20 J. T. Welch and D. S. Lim, *Bioorganic Med. Chem.*, 2007, **15**, 6659–6666.
 - 21 P. Schlagenhauf, M. Adamcova, L. Regep, M. T. Schaerer and H.-G. Rhein, *Malar. J.*, 2010, **9**, 357.
 - 22 E. C. Ritchie, J. Block and R. L. Nevin, *J. Am. Acad. Psychiatry Law*, 2013, **41**, 224–235.
 - 23 P. Wipf, T. Mo, S. J. Geib, G. S. Dow, L. Gerena and N. Roncalc, *Org. Biomol. Chem.*, 2009, **7**, 4163–4165.
 - 24 S. M. D. Rizvi, S. Shakil and M. Haneef, *EXCLI J.*, 2013, **12**, 830–857.

Chapter 5

Conclusion, future directions and thesis outcomes.

5.1 Conclusion

Ferrocene in medicinal chemistry has attracted attention as a benefit of its properties (mentioned in Chapter 1). Ferrocene complexes have been increasingly made and their activities have been studied. In this thesis, we aimed to synthesize the novel compounds by using the ferrocene molecule as a bioisostere and testing for different applications/targets (Scheme 5.1).



Scheme 5.1. Project objectives.

In Chapter 1 a review of ferrocenes and similar metal-based drugs is presented.

In Chapter 2, 10 novel compounds have been made by replacement of a 1-adamantyl group with ferrocene. Biological in vitro binding assay data show the new ferrocene compounds display good CB₂ affinity (cannabinoid receptor). Also, the CB₂ affinity of ferrocene derivatives is still maintained when compared with the 1-adamantyl compounds (Figure 5.1). The results showed many of our compounds displayed nM potency vs. the CB₁ and CB₂ receptors and that the intramolecular hydrogen bond is very important for their affinity.

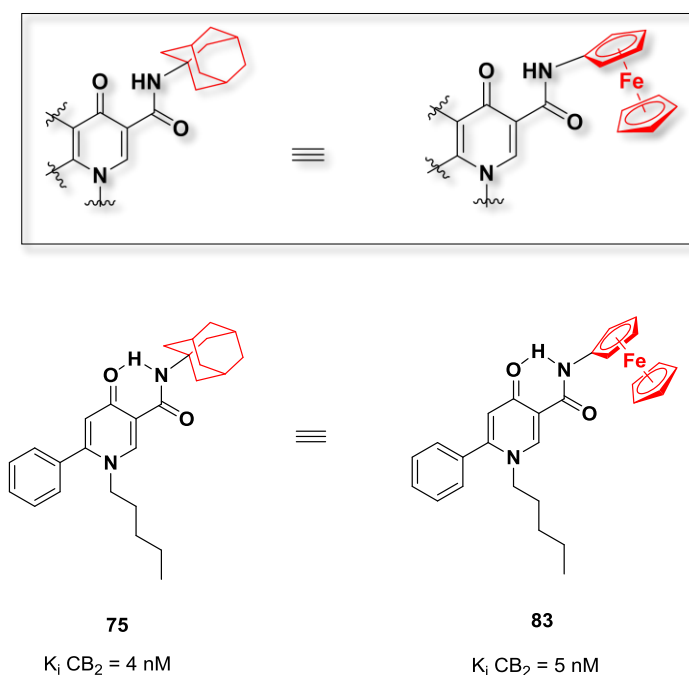


Figure 5.1. The replacement of a 1-adamantyl group by ferrocene.

In Chapter 3, benzamide compounds were made and biological data showed *N*¹-(2-aminophenyl)-*N*⁸-ferrocenyloctanediamide, (*Pojamide*) **111** to display nanomolar potency vs. HDAC3 compared to **RGFP966**. *Pojamide* and SNP (sodium nitroprusside) combinations led to greatly enhanced cytotoxicity and DNA damage attributed to activation to an Fe(III)-*Poj* species.

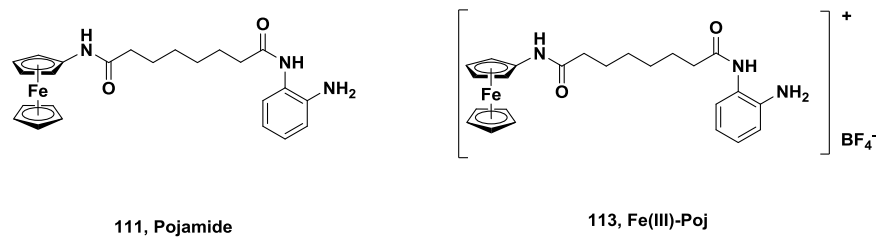


Figure 5.2. Pojamide, **111** and Fe(III)-Poj, **113**.

In Chapter 4, a series of oxindole compounds have been synthesized, by the Knoevenagel condensation reaction, for biological activity testing versus a panel of cell lines and protein kinases. Further studies are in progress to look at their effects on kinases in biochemical and cell assays.

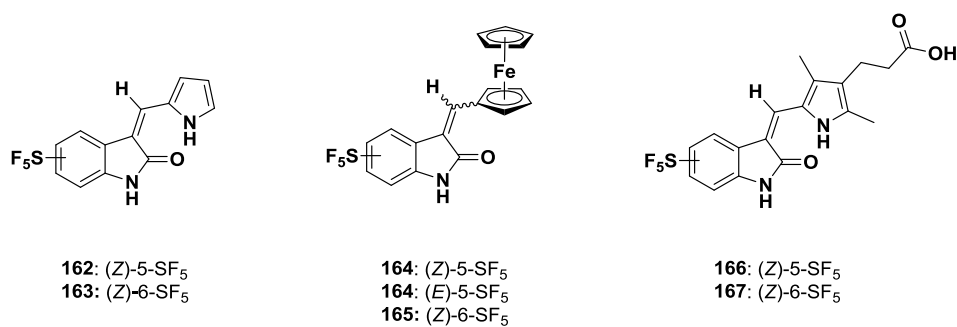
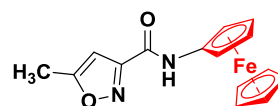
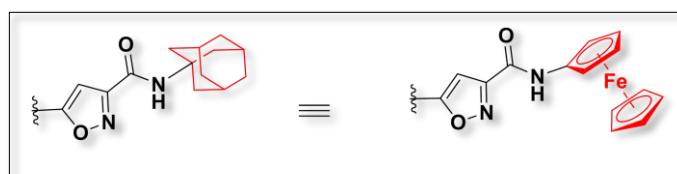


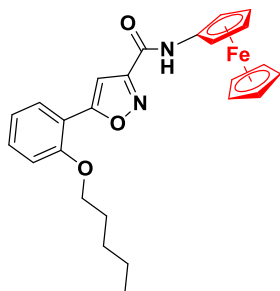
Figure 5.3. A series of oxindole compounds.

5.2 Future directions

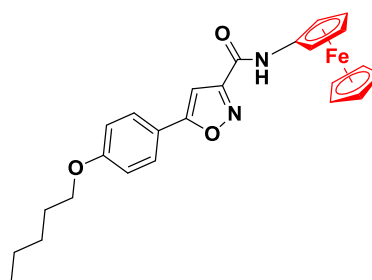
FAAH (fatty acid amide hydrolase) inhibitors based on an aminoferrocene backbone compounds have been synthesized by using ferrocene as a bioisostere of 1-adamantyl group and we are awaiting biological data.



84



85



86

Figure 5.3. Compound structures of **84**, **85** and **86**.

5.3 Thesis outcomes

Publications:

- 1 M. Librizzi, R. Chiarelli, L. Bosco, S. Sansook, J. Gascon, J. Spencer, F. Caradonna and C. Luparello “The Histone Deacetylase Inhibitor JAHA Down-Regulates pERK and Global DNA Methylation in MDA-MB231 Breast Cancer Cells” *Materials (Basel)*, 2015, 8, 7041–7047. DOI: 10.3390/ma8105358
- 2 S. Sansook, W. Tuo, L. Lemaire, A. Tourteau, A. Barczyk, X. Dezitter, F. Klupsch, N. Leleu-Chavain, G. J. Tizzard, S. J. Coles, R. Millet and J. Spencer “Synthesis of Bioorganometallic Nanomolar-Potent CB2 Agonists Containing a Ferrocene Unit” *Organometallics*, 2016, 35, 3361–3368. DOI: 10.1021/acs.organomet.6b00575
- 3 W. Tuo, N. Leleu-Chavain, J. Spencer, S. Sansook, R. Millet and P. Chavatte “Therapeutic Potential of Fatty Acid Amide Hydrolase, Monoacylglycerol Lipase, and N-Acylethanolamine Acid Amidase Inhibitors” *J. Med. Chem.*, 2017, 60, 4–46. DOI: 10.1021/acs.jmedchem.6b00538
- 4 S. Sansook, C. A. Ocasio, R. Jones, J. M. Roberts, T. G. Scott, H. Hochegger, N. Tsoureas, P. Coxhead, M. Guille, G. J. Tizzard, S. J. Coles, J. E. Bradner and J. Spencer “Pojamide: An HDAC3-Selective Ferrocene Analogue with Remarkably Enhanced Redox-Triggered Ferrocenium Activity in Cell” (In preparation for submission).

Poster presentations:

- 1 S. Sansook, R. Millet and J. Spencer “SF₅ – Substituted Oxindole-Based Kinase Inhibitors” Postgraduate Research Colloquium 2015 on 7-8 September 2015, University of Sussex, Brighton, UK.
- 2 S. Sansook, L. Lemaire, A. Tourteau, W. Tuo, A. Barzyk, X. Dezitter, F. Klupsch, N. Leleu-Chavain, R. Millet and J. Spencer “Biological Activities of Heterocyclic Compounds Containing Ferrocene Bioisosteres” 14th Ferrocene Colloquium on 21-23 February 2016, University of Konstanz, Konstanz, Germany.

Oral presentation:

- 1 S. Sansook and J. Spencer “Uses of Bioinorganic Compounds in Medicinal Chemistry” Postgraduate Research Colloquium 2016 on 5-6 September 2016, University of Sussex, Brighton, UK.

Workshop:

- 1 RSC Medicinal Chemistry Residential School China on 20-23 November 2014, Shanghai Institute of Materia Medica, Shanghai, China.